Charles University

Faculty of Science

Ph.D. study program: Physical Chemistry

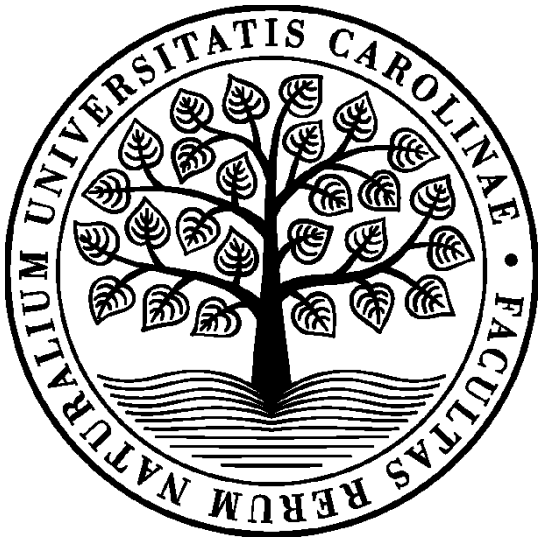

Mgr. Viktor Sinica

Molekulární mechanismy polymodální regulace TRPA1 receptoru

Molecular mechanisms of polymodal regulation of TRPA1 receptor

Doctoral thesis

Supervisor: RNDr. Viktorie Vlachová, DrSc.

Prague 2021

Prohlášení

Prohlašuji, že jsem závěrečnou práci zpracoval samostatně, a že jsem uvedl všechny použité informační zdroje a literaturu. Tato práce ani její podstatná část nebyla předložena k získání jiného nebo obdobného akademického titulu.

Declaration

I declare that I have written this thesis independently and cited all the sources I have used. I did not submit this work, or a part of it, to obtain another university degree.

V Praze dne …… ……

Viktor Sinica

Acknowledgements

I want to express my gratitude to my supervisor Viktorie Vlachová for perpetually broadening my insight into the realm of TRP channels, for her constant support in work and personal issues, and for her kind and joyful approach. I deeply thank Lucie Zímová for her straightforward approach, Lucie Máčiková for her great support, Anna Kádková for her kind patience, Kristýna Barvíková for work attitude, Ivan Dittert and Jan Krůšek for their vast technical capabilities, Magda Kuntošová for her loving care of the lab and its members, Šárka Danačíková for her support and motivation, and all the lab members I had an opportunity to meet. It has been a pleasure to work with you.

Table of contents

Abstrakt

TRPA1 kanál je univerzální buněčný nociceptivní senzor, který je aktivován celou řadou vnějších podnětů potenciálně škodlivých modalit a různých endogenních mediátorů produkovanými v důsledku patofyziologických procesů. Polymodalita TRPA1 kanálu umožňuje zesílit či zeslabit účinek aktivačního podnětu přítomností dalšího stimulu. Tento modulační efekt je zásadní pro aktivizaci ochranných buněčných a behaviorálních mechanismů, může však také vést k nežádoucím účinkům v případě chronických patofyziologických stavů způsobených nadměrnou aktivací TRPA1 kanálu. Aby bylo možné účinně a selektivně zacílit mechanismy synergických účinků TRPA1 aktivátorů a zároveň zachovat fyziologickou úlohu iontového kanálu, je nezbytné poznat mechanismy polymodální regulace TRPA1 na molekulární úrovni.

Předložená disertační práce se zabývá třemi důležitými mechanismy regulace TRPA1 kanálu: 1) regulací buněčnými signálními kaskádami a fosforylací, 2) interakcí s membránovými fosfolipidy a 3) regulací aktivity změnami okolní teploty. Výsledky uvedené v disertační práci ukazují, že účinek mediátoru zánětu bradykininu je snížen stimulací nízkofrekvenčním vysoko-indukčním elektromagnetickým polem užívaným při magnetoterapii. Identifikovali jsme serin 602, jehož fosforylace může potenciálně inhibovat aktivitu TRPA1 kanálu. Dále jsme identifikovali dvě vazebná místa pro fosfoinositidy, která jsou klíčová pro regulaci aktivace TRPA1 kanálu napětím, agonisty, vápenatými ionty a chladem. Také jsme ukázali aktivaci lidského a myšího orthologu TRPA1 teplem i chladem a odhalili specifický mód teplem vyvolané chladové aktivace těchto iontových kanálů. Naše výsledky poskytují důležitý důkaz přítomnosti regulačních center TRPA1 kanálu, která mají farmakologický potenciál ve vyhledávání nových přístupů k léčbě chronické bolesti.

Abstract

The TRPA1 channel is a universal, nociception-mediating cellular sensor activated by various environmental irritants, potentially harmful physical modalities and endogenous mediators of pathophysiological processes. The polymodality of TRPA1 channel allows the activation stimuli to further enhance or suppress each other's effect. While this modulation effect has its physiological importance in promoting the protective cellular and behavioral mechanisms, it may result into the unpleasant pain-related effects accompanying the chronical pain caused by aberrant TRPA1 channel activity. In order to effectively and selectively target the synergic properties of TRPA1 modulators, while preserving the sensitivity to the environmental threads, the knowledge of the mechanisms of polymodal regulation at the molecular level are required.

This doctoral thesis aims at the elucidation of three main mechanisms of TRPA1 regulation: 1) the regulation *via* intracellular signaling cascades and phosphorylation, 2) the interaction with membrane phospholipids and 3) the temperature-driven gating. The results presented in the thesis show that the effects of the inflammatory mediator bradykinin are decreased by the low-frequency high-induction electromagnetic field used in magnetotherapy. We have identified a residue S602 that may be involved in the phosphorylation-induced inhibition of TRPA1 channel. Furthermore, we have identified two putative binding sites for membrane phospholipids that, in a state-dependent manner, regulate the TRPA1 activation by voltage, agonists, calcium and temperature. Lastly, we demonstrated the bidirectional temperature activation of human and mouse TRPA1 orthologues and unveiled their specific mode of 'heat-induced cold activation'. Overall, our results provide valuable evidences of the regulatory domains, which have a pharmacological potential of targeting TRPA1 as a therapeutic strategy for treating chronic pain.

List of abbreviations

12-LOX	12-lipoxygenase
AA	arachidonic acid
AC	adenyl cyclase
AgTRPA1	*Anopheles gambiae* mosquito TRPA1 receptor
AITC	allyl isothiocyanate
AKAP	A-kinase anchoring protein 79/150
AMPK	AMP-activated protein kinase
AR	ankyrin repeat
ARD	ankyrin repeat domain
ATP	adenosine triphosphate
ATR-FTIR	attenuated total reflection infrared spectroscopy
A-967079	selective inhibitor of TRPA1
A-loop	activation loop within the N-terminus of TRPA1
B1, B2	bradykinin 1 and bradykinin 2 receptors
$BacNa_v$	bacterial voltage-gated sodium channel
BITC	benzyl isothiocyanate
BK	bradykinin
CaM	calmodulin
Carv	carvacrol
CC	coiled-coil
CD	circular dichroism
Cdk5	cyclin-dependent kinase 5
cDNA	complementary DNA
CHO	chinese hamster ovary cells
Cin	cinnamaldehyde
CK2	casein kinase 2
CNS	central nervous system
COX	cyclooxygenase
cryo-EM	cryo-electron microscopy
cTRPA1	chicken TRPA1 receptor
C-lobe	carboxy-lobe of calmodulin
DAG	diacylglycerol
DMSO	dimethyl sulfoxide
DRG	dorsal root ganglion
Dr-VSP	voltage-sensitive lipid 5-phosphatase from *Danio rerio*
dTRPA1	fruit fly TRPA1 receptor
EC_{50}	half maximal effective concentration
ECS	extracellular solution
EDTA	ethylenediaminetetraacetic acid
EGTA	ethylene glycol-bis(β-aminoethyl ether)-N,N,N′,N′-tetraacetic acid

EMDB	the electron microscopy data bank
FBS	fetal bovine serum
fTRPA1	frog TRPA1 receptor
GAP43	Growth Associated Protein 43
GFP	green fluorescent protein
GNE551	potent non-covalent agonist of TRPA1
GPCR	G-protein coupled receptor
G-V	conductance-voltage relationship
H1-H7	α-helices within the N-terminus of TRPA1
HCN	hyperpolarization-activated and cyclic nucleotide-gated channels
HEDTA	(2-hydroxyethyl)ethylenediaminetriacetic acid
HEK293T	human embryonic kidney cells 293T
HEPES	2-[4-(2-hydroxyethyl)-1-piperazinyl]ethanesulfonic acid
HC-030031	selective inhibitor of TRPA1
HNE	4-hydroxynonenal
hTRPA1	human TRPA1 receptor
H-T-H	helix–turn–helix motif
IA	iodoacetamide
IC_{50}	half maximal inhibitory concentration
ICS	intracellular solution
IFH	interfacial helix at the C-terminus of TRPA1
IP_3	inositol trisphosphate
IP_6	inositol hexakisphosphate
I-V	current-voltage relationship
JT010	potent electrophilic agonist of TRPA1
kDa	kilodalton
K_v	voltage-gated potassium channel
LF-EMF	high-induction low-frequency electromagnetic field
LPS	lipopolysaccharides
LUV	large unilamellar vesicles
MDS	microfluidic diffusional sizing
MDFF	molecular dynamics flexible fitting
NMM	N-methyl maleimide
mTRPA1	mouse TRPA1 receptor
MTSEA	2-aminoethyl methanethiosulfonate
N-lobe	amino-lobe of calmodulin
$p35^{-/-}$	knock-out gene for p35 protein
P1-P2	pore helices of TRPA1 channel
PBS	phosphate buffer saline
PCR	polymerase chain reaction
PDB	protein data bank
PIK	phosphatidylinositol-4-kinase
PIP_2	phosphatidylinositol-4,5-bisphosphate

PKA	protein kinase A
PKC	protein kinase C
PLA_2	phospholipase A_2
PLC	phospholipase C
pre-S1	α-helix preceding the S1 helix in TRPA1 receptor
PWR	plasmon waveguide resonance spectroscopy
RMSD	root mean square deviation
ROS	reactive oxygen species
rsTRPA1	rattlesnake TRPA1 receptor
S1-S6	transmembrane helices 1 to 6 of the TRPA1 subunit
Src	sarcoma kinase
SUV	small unilamellar vesicles
S.E.M.	standard error of mean
TG	trigeminal ganglion
TMA-OH	tetramethylammonium hydroxide
TMD	transmembrane domain
Tmem100	transmembrane protein 100
TRPA	TRP ankyrin receptor
Trpa1	gene encoding TRPA1 protein
$Trpa1^{-/-}$	knock-out gene for TRPA1 protein
TRPA1	TRP ankyrin receptor subtype 1
TRPC	TRP canonical receptor
TRPL	TRP-like helix
TRPM	TRP melastatin receptor
$Trpm8^{-/-}$	knock-out gene for TRPM8 protein
TRPML	TRP mucolipin receptor
TRPN	TRP no mechanoreceptor potential C
TRPP	TRP polycystin receptor
TRPV	TRP vanilloid receptor
V_{50}	half-maximum activation voltage
VSLD	voltage sensor-like domain
WT	wild-type

1. Introduction

The perception of pain is important sensory information through which we are able to distinguish potentially harmful events from a variety of other non-threatening ones, and to take an appropriate avoiding action afterwards. Although unpleasant, pain represents a useful tool for evaluating our condition and to sustain our life and body integrity. However, long-persisting pain without the presence of a relevant harm loses its informative purpose and impairs the quality of life.

The information about a harmful stimulus is transferred from the periphery of our body to the central nervous system (CNS) in a compressed form of a membrane potential wave *via* specialized neuronal fibers called nociceptors. Free nerve endings of nociceptors innervating the periphery of our body are covered with highly tuned receptors, which are ready to be triggered by the presence of any noxious stimuli that exceeds the threshold. The activation of such receptors has two major effects: 1) creation of action potential by locally depolarizing the plasma membrane, and 2) triggering of calcium signaling pathways by permeating calcium ions into the cell.

Transient receptor potential ankyrin 1 (TRPA1) from the Transient receptor potential (TRP) superfamily of receptor-forming ion channels is one of such pain-related receptors. It is a receptor with high polymodality – its complex protein structure is capable of detecting changes in heat, cold, pH, but also mechanical stimuli and a vast range of pungent and irritating chemical compounds of both exogenous and endogenous origin. Chemical activation of TRPA1 produces pain (Fujita et al., 2007), heat sensation (Averbeck et al., 2013), hypothermia (Gentry et al., 2015), mechanical hyperalgesia (Namer et al., 2005, Andersson et al., 2015), cold hyperalgesia (Obata et al., 2005) and many other effects (for further references see (Talavera et al., 2020)). TRPA1 is involved in the process of inflammation (Bandell et al., 2004, Bautista et al., 2006), migraine (Marone et al., 2018), diabetes (Wei et al., 2010), neuropathic pain (Nativi et al., 2013), itch (Wilson et al., 2013) and mechanic allodynia in anti-cancer drug treatment (Nassini et al., 2011), therefore it embodies a tempting target for novel analgesic and anti-inflammatory molecules. However, one should keep in mind the polymodal and allosteric nature of TRPA1 in order to specifically target the unwanted properties of TRPA1 modulation (e.g. cold allodynia and hyperalgesia as a side-effect

of anti-cancer drugs), while preserving the useful ones (e.g. sensory response to irritant compounds and noxious cold).

In recent years, the knowledge about the TRP channels remarkably increased thanks to the gradually emerging high-resolution cryo-electron microscopy (cryo-EM) structures of various TRP channels in native-like environments of lipid nanodiscs. The revelations arising from the analysis of the structures in various conformations led to the elucidation of important questions regarding the TRP channel gating and regulation mechanisms, extrapolating also to the TRPA1 channel. An increased attention is paid on TRPA1 regulation by cellular pathways and phosphorylation during the (patho)physiological conditions. The regulation of TRPA1 also involves a presence of endogenous lipids that are buried in, or bind strongly to transmembrane regions of the channel. Another important feature to be addressed is the species-specific differences in temperature activation of TRPA1 orthologues, which gives an insight into the molecular basis of temperature sensing and transduction into the channel activation.

This doctoral thesis aims at elucidating some of the aspects of the structure-function relationship and the mechanisms of polymodal regulation of the human and mouse TRPA1 channel. A special focus is put on TRPA1 regulation by cellular pathways and phosphorylation, structural mechanism of TRPA1 regulation by phospholipids and unraveling the specific mode of activation of TRPA1 by both cold and heat.

2. Literature review

2.1 Structure of TRPA1

The TRP superfamily of receptors belongs to a large group of tetrameric cation channels with six transmembrane segments (S1-S6) that also involves potassium, sodium, calcium and hyperpolarization-activated cyclic nucleotide-gated (HCN) channels. According to their amino acid sequence homology, the TRP channels are divided into seven subfamilies: TRPC (Canonical), TRPV (Vanilloid), TRPM (Melastatin), TRPP (Polycystin, also known as PKD), TRPML (Mucolipin), TRPA (Ankyrin), and TRPN (No mechanoreceptor potential C, also known as NOMPC). To this date, a total number of 28 TRP members were identified and around 136 cryo-EM TRP structures at high resolution have been determined (Huffer et al., 2020). All TRP

receptors consist of a conserved transmembrane domain (TMD) formed by S1-S4 transmembrane helices – so-called "voltage-sensor-like domain" (VSLD) as a reference to the voltage-gated channels, and the pore domain made of the S5-S6 transmembrane helices and a selective filter in between. The main structural difference between the TRP channels lies in the length and arrangement of their intracellular termini and loop regions (**Figure 1**).

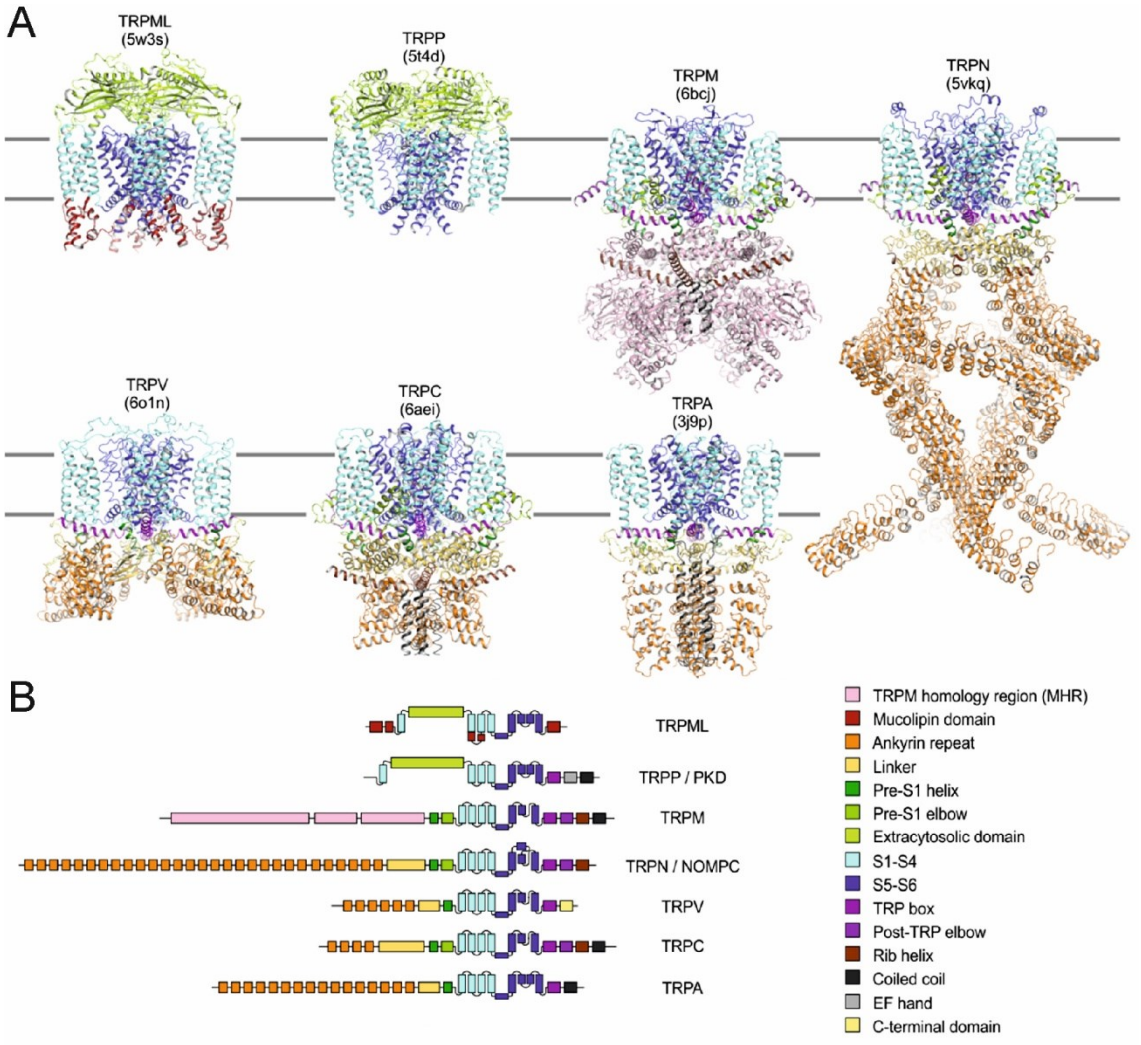

Figure 1: Structures of TRP channel subfamilies. ***(A)*** *Cartoon representation of structures of TRPML3 (5W3S), TRPP1 (5T4D), TRPM4 (6BCJ), TRPN (5VKQ), TRPV5 (6O1N), TRPC5 (6AEI), and TRPA1 (3J9P).* ***(B)*** *Schematic of domain architecture of TRP channel subunits. The structure domains are colored as in* ***(A)****. Adopted from (Huffer et al., 2020).*

TRPA1 is the only member of the TRPA subfamily in mammals, denominated according to its long ankyrin repeat domain (ARD) on its N-terminus. It was first cloned in 1999 (Jaquemar et al., 1999) and its function as a cold sensor and chemical nociceptor was discovered in 2003 (Story et al., 2003). Molecular structure of a subunit

of the human TRPA1 channel is formed by 1,119 amino acid residues of observed molecular weight 127 kDa. In the present, there are four studies providing high-resolution cryo-EM structures of TRPA1 channel (Paulsen et al., 2015, Liu et al., 2020, Suo et al., 2020, Zhao et al., 2020). The resolved structures provide invaluable insights into the architecture and arrangement of channel's subunits, glycosylation sites (Suo et al., 2020), transition from closed to open conformation of the channel (Zhao et al., 2020), binding sites for calcium ions (Zhao et al., 2020), several electrophilic and non-electrophilic agonists and antagonists (Paulsen et al., 2015, Zubcevic et al., 2016, Liu et al., 2020, Zhao et al., 2020), and regulation by membrane lipids (Liu et al., 2020, Suo et al., 2020). The topology of TRPA1 is shown in **Figure 2**.

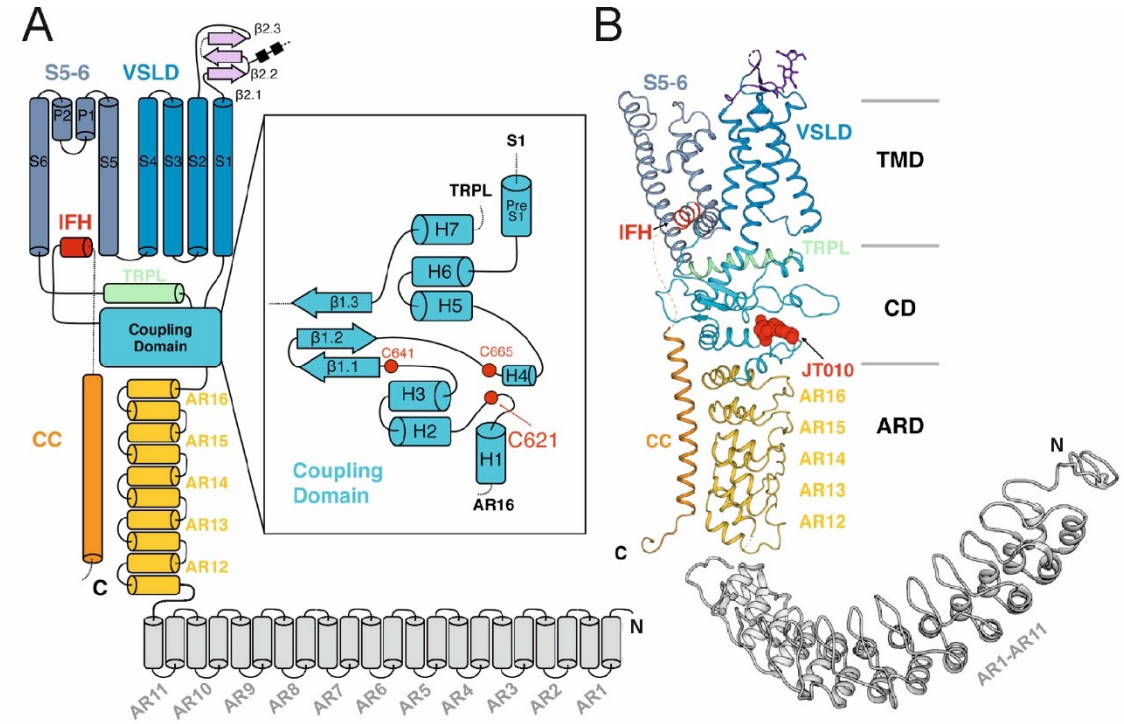

Figure 2: Overview of human TRPA1 structure. (A) *The topology of a single protomer, a voltage sensor-like domain (VSLD), pore domain (S5-S6 helices and P1-P2 pore helices), ankyrin-repeat domain (ARD; composed of AR1-AR16), interfacial helix (IFH), TRP-like helix (TRPL), coiled-coil domain (CC) and coupling domain (CD, in the inset, composed of H1-H7 helices, a three-strand β-sheet and pre-S1 helix). The cysteines important in the activation by electrophiles are highlighted.* ***(B)*** *The structure overview of TRPA1 protomer with bound electrophilic agonist JT010. A homology model of AR11-16 is shown. Adapted from (Samanta et al. 2018) and (Suo et al. 2020).*

2.1.1 **The transmembrane domain**

The transmembrane domain is composed of the voltage sensor-like domain (VSLD) and the pore domain (S5-S6 helices and a pore loop including two pore helices P1-P2) arranged in a domain-swapped manner. Four helical segments S1-S4 of VSLD form an intracellular, solvent accessible cavity. The VSLD of TRPA1 can be solvated (Zimova et al., 2018), occupied by calcium ion (Zhao et al., 2020) terpenoidic agonists (Ghosh et al., 2020) and membrane lipids (Zimova et al., 2018, Startek et al., 2019a). The calcium ion was bound to conserved polar residues E788, Q791, N805 and E808 (**Figure 3.A**); mutations of these residues resulted in a lack of both Ca^{2+}-dependent potentiation and desensitization of AITC-evoked currents (Zimova et al., 2018, Zhao et al., 2020). The calcium binding site is conserved among TRPC (Duan et al., 2018, Duan et al., 2019) and TRPM channels (Autzen et al., 2018, Huang et al., 2018, Wang et al., 2018a, Zhang et al., 2018, Diver et al., 2019, Huang et al., 2019). The role of VSLD in the modulation of TRP channels in general is also supported by the localization of phosphatidylcholine in TRPV1 (**Figure 3.B;** (Gao et al., 2016)), and by the binding of icilin and menthol inside in TRPM8 channel (Yin et al., 2019). The study presented in this thesis shows that the polar residues inside of the VSLD cavity are capable of binding regulatory phosphoinositides in a state-dependent manner.

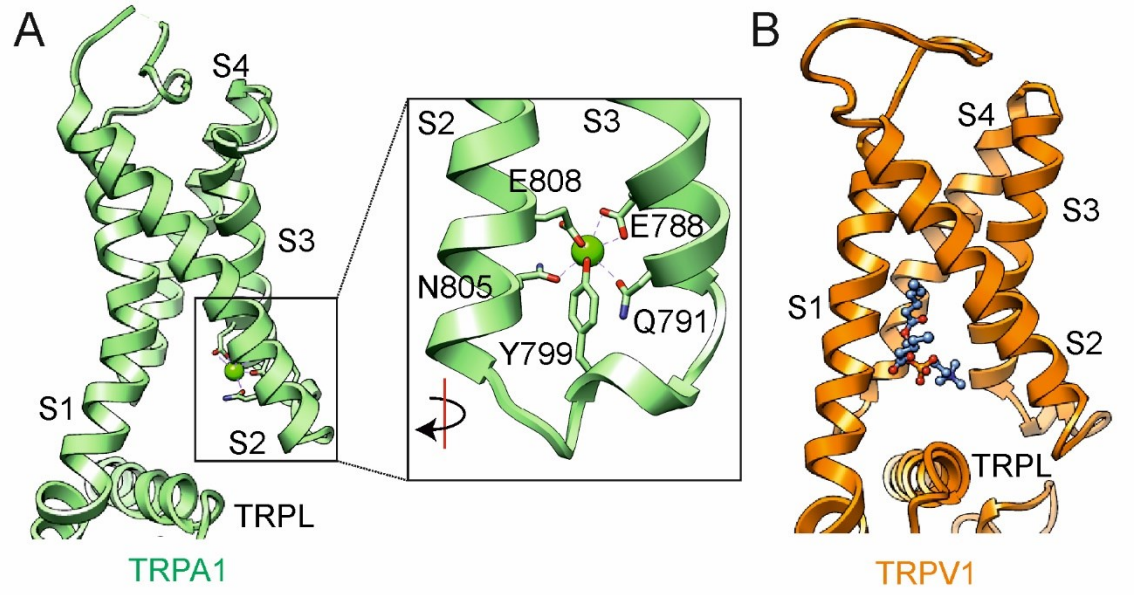

Figure 3: The intracellular voltage sensor-like domain cavity of TRP channels. (A) *A calcium ion (green) binds at the cytoplasmic end of S2–S3 helices in the voltage sensor-like domain (VSLD) of TRPA1 channel (6V9W). The inset shows the conserved residues that are involved in Ca^{2+} binding.* ***(B)*** *In TRPV1 channel, a molecule of phosphatidylcholine (blue) was localized inside of the VSLD (5IRZ).*

The extracellular loop between S1-S2 is formed by three-stranded β-sheet motif and contains a glycosylation site at the residue N747 (Suo et al., 2020). Consistent with the presence of glycosylation, mutation of N747 reduces the channel's sensitivity to various types of agonists (Egan et al., 2016) and mutation of F746 to alanine substantially affects the voltage dependence of TRPA1 (Marsakova et al., 2017).

The VSLD and the pore domain are linked by the flexible S4-S5 linker that runs parallel to the membrane. The S4-S5 linker is involved in channel gating and undergoes large rearrangements during the close-to-open transition (Liu et al., 2020). A residue N855 in hTRPA1 is a key to promote the effect of a specific inhibitor HC-030031 (Gupta et al., 2016). The channelopathy mutation N855S at the S4-S5 linker renders the channel constitutively open and causes an episodic pain syndrome characterized by bouts of debilitating upper body pain that can occasionally radiate to the abdomen and legs (Kremeyer et al., 2010).

The pore domain of TRPA1 is composed of two S5-S6 helices and a selectivity filter in between with two pore helices P1-P2, permeable for mono- and divalent cations. One of the pore helices attracts positively charged ions toward the pore of the channel and determines the Ca^{2+} permeation (Christensen et al., 2016). The central cavity in the ion permeation pathway holds two restrictions: 1) the upper gate involves diagonal interactions between opposite D915 residues at the selective filter, and 2) the lower gate of two hydrophobic seals formed by residues I957 and V961 at the S6 helix. The vicinity of S5-S6 helices shapes a binding site for several ligands (Xiao et al., 2008, Paulsen et al., 2015, Ton et al., 2017, Chernov-Rogan et al., 2019, Liu et al., 2020) and also an annular "lipid 5" (Suo et al., 2020). In the middle of the S6 helix is a single π-hinge, a feature conserved among nearly all members of the TRP channels (Zubcevic and Lee, 2019).

A comparison of the closed (TRPA1 with bound antagonist A-967079 (PDB ID: 6V9Y) and open state of TRPA1 driven by iodoacetamide (IA; PDB ID: 6V9V) revealed the gating-related transitions within the transmembrane core (**Figure 4** on page 18). The entire TMD rotates by 15° relative to the static ARD. In context of the TMD, the VSLD performs a near rigid-body rotation as well. The movements are accompanied by rotation and upward translation of the pore loop and the pore helices P1-P2, opening the upper gate of TRPA1. These transitions are in concert with the upward shift of the π-hinge in S6 and the straightening of the S4-S5 linker and S5 helix into a single α-

helix, coordinating the movement of S6 helix and pore helices to couple both the upper and lower gate (Zhao et al., 2020).

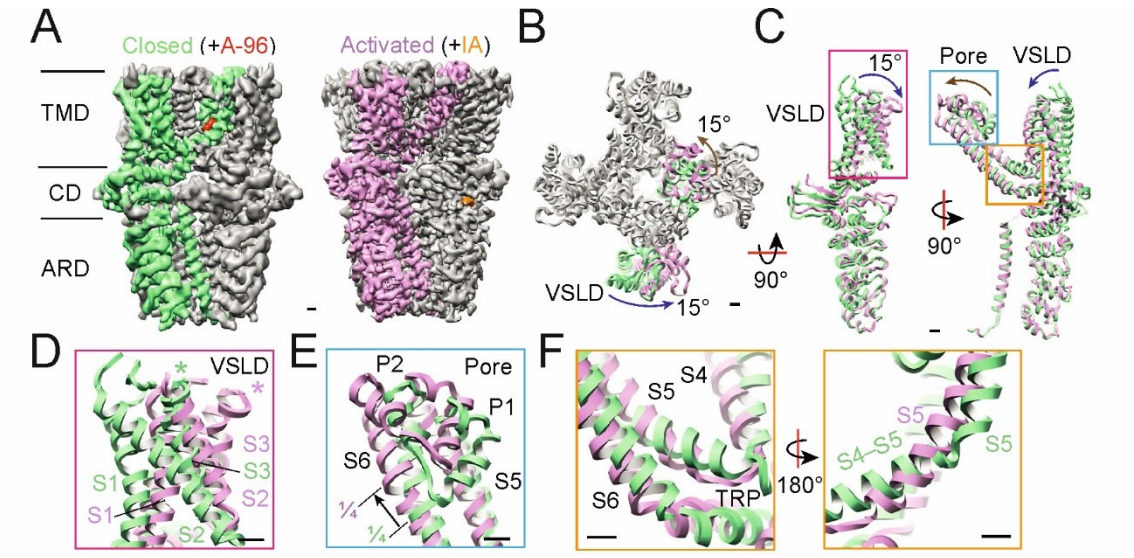

Figure 4: The close-to-open transitions of TRPA1 channel. ***(A)*** *Cryo-electron microscopy density maps of the closed (one subunit in green; 6V9Y) and open state (one subunit in purple; 6V9X) of TRPA1 channel bound to antagonist A-967079 (red) or agonist iodoacetamide (IA; orange), respectively.* ***(B)*** *The upper view of the overlaid closed and open structures.* ***(C)*** *During the opening, the VSLD and the pore domain rotates about 15° (pink inset in* ***(D)****), the pore domain twists and translates upwards together with the shift in the S6 π-helix (blue inset in* ***(E)****) and the S5 α-helix together with the S4-S5 linker straighten (orange insets in* ***(F)****). Scale bars = 10 Å. Adapted from (Zhao et al. 2020).*

2.1.2 **The N-terminus**

The N-terminal part of TRPA1 constitutes more than a half of the protein size (720 out of 1119 amino acids in a human orthologue). It is characterized by an ankyrin repeat domain (ARD), consisting of a tandem array of 16 ankyrin repeats (ARs) and a linker region connecting the ARD with the fist transmembrane segment S1. The ARD is divided into two parts – the distal part of AR1 - AR11 and the proximal part of AR12 - AR16. First eleven ARs are unresolved in all cryo-EM structures, which probably reflects their high flexibility. According to the TRPA1 electron density, the distal part is crescent-like shaped and protrudes to the inner sheet of the plasma membrane (Paulsen et al., 2015). The proximal AR12 – AR16 domain forms a structurally well-defined stem and is in a close interaction with the C-terminal coiled-coil (CC). Five ARs of TRPA1 possess a strictly conserved tetrapeptide T/SPLH motif that contributes to conformational stability and regulation of TRPA1 (Hynkova et al., 2016).

Generally, the ankyrin repeat is a common structural sequence motifs of 33 amino acids that fold into two antiparallel α-helices connected with a β-turn. The sequence of ARs tends to stack together to form a spring-like structures, which are generally important for protein-protein interactions (Gaudet, 2008). In case of metazoan TRPN channel with the total number of 29 ARs, the ARD anchors to microtubules and thus accounts for the TRPN1 mechanotransduction (Zhang et al., 2015). TRPA1 channel was a candidate for the mechanosensitive transduction channel of vertebrate hair cells where it is widely expressed (Corey et al., 2004). Contrarily, experiments with *Trpa1*$^{-/-}$ knock-out mice showed that neither TRPA1 (Kwan et al., 2006), nor any other TRP channel (Wu et al., 2016) is essential for hair-cell transduction of auditory signal. It has been reported that TRPA1 is involved in detection of mechanical stimuli in native cells including sensory neurons (Kerstein et al., 2009), Merkel cells (Soya et al., 2014), odontoblasts (Shibukawa et al., 2015) and human periodontal ligament cells (Tsutsumi et al., 2013).

In the study (Cordero-Morales et al., 2011), authors investigated the temperature-sensing properties of chimeric constructs of human and rattlesnake TRPA1 (hTRPA1 and rsTRPA1) and showed that the N-terminal ARD contains two spatially distinct thermosensory modules – the primary module (AR10 - AR15) and the enhancer module (AR3 – AR8). Both modules of rsTRPA1 show different average temperature coefficients of activation, thus they together modulate the overall thermal response properties of native rsTRPA1 channel. Insertion of the primary module of rsTRPA1 into the hTRPA1 orthologue renders the channel active to increased temperature. The authors also suggest the localization of a Ca^{2+}-sensitive module in the region around AR11. The AR12 primary sequence contains a conserved motif called “EF-hand” (D468 – L480) which is a general calcium-binding motif (Lewit-Bentley and Rety, 2000). However, mutation of negatively-charged residues in the EF-hand sequence did not result in changes in calcium-dependent modulation of the channel (Wang et al., 2008). Molecular dynamic simulations of the N-terminal ARD of TRPA1 based on channel’s cryo-EM structure in resolution of 16 Å (Cvetkov et al., 2011) showed that binding of Ca^{2+} ions to the EF-hand increases the rigidity of the ARD (Zayats et al., 2013). Another regulatory site lies in P394 in AR10, whose hydroxylation has been shown to inhibit TRPA1. Releasing TRPA1 from inhibition by decreasing the activity

of prolyl hydroxylases is a mechanism of TRPA1 activation by hypoxia (Takahashi et al., 2011).

The structural layer under the transmembrane domain forms a coupling domain. It is composed of eight short α-helices (H1 – H7 and a helix preceding S1; pre-S1), a β-sheet composed of three antiparallel β-strands, and the TRP-like (TRPL) helix at the C-terminus. Helices H2 – H3 and H5 – H6 are assembled as two helix–turn–helix motifs (H-T-H). The coupling domain possesses a binding site for a variety of pungent electrophilic compounds that activate TRPA1 *via* covalent modification of reactive cysteines and lysine (Hinman et al., 2006, Macpherson et al., 2007). The binding site is composed of two parts: a more static bottom part made of H1-H2 region, and a flexible upper part called the activation loop (A-loop) (Suo et al., 2020, Zhao et al., 2020). Depending on the size of electrophile, modification of C621 at the lower part of the binding site and a partial modification of C665 at the upper part is sufficient to reorient the conformation of A-loop upwards and establish the ion-dipole interaction between the C-terminus of TRPL helix and the residue K671 (**Figure 5**). As a result, the dipole moment of the opposite terminus of TRPL helix is enhanced and most likely promotes repulsion between TRP domains from neighboring subunits, which would ultimately lead to the opening of the lower gate (Zhao et al., 2020).

Although the N-terminus is involved in a number of activating modalities, it may not be inherently necessary for activation. The experiments on truncated human and

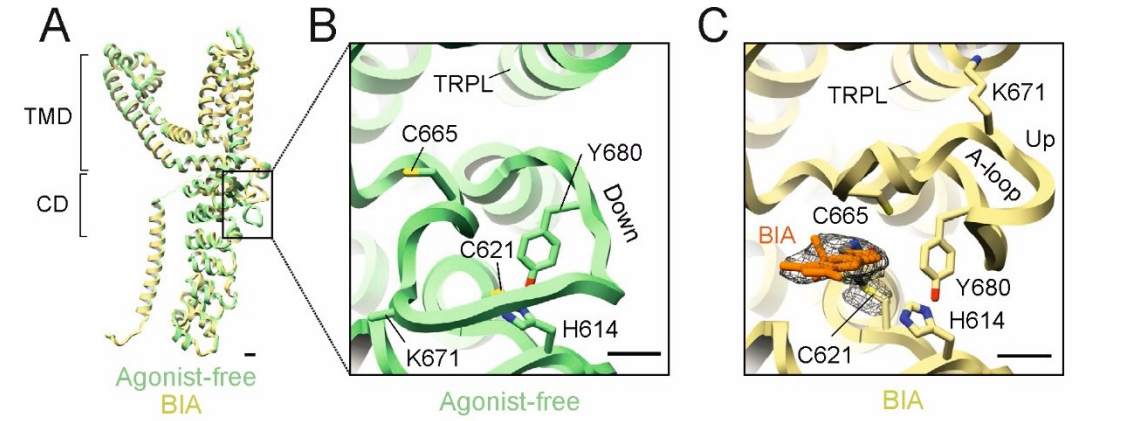

Figure 5: The structural changes underlying the binding of electrophilic activators. (A) *Aligned subunits of agonist-free TRPA1 channel (green; 6V9W) and TRPA1 with bound BODIPY-iodoacetamide (BIA) into the coupling domain (yellow; 6V9V).* ***(B)*** *The activation loop (A-loop) adopts a 'down' conformation in the agonist-free channel, partially occluding a reactive pocket containing C621.* ***(C)*** *Upon binding of BIA (orange) to C621, the A-loop transitions to an 'up' conformation, repositioning K671 to coordinate backbone carbonyl oxygens at the TRPL helix of C-terminus. Scale bars = 5 Å. Adapted from (Zhao et al., 2020)*

Anopheles gambiae mosquito TRPA1 (Δ1-688 hTRPA1, Δ1–776 AgTRPA1) with whole N-terminus deleted conducted in artificial membranes suggest that TRPA1 sustains its activation by cold, electrophiles (Moparthi et al., 2014), heat (Survery et al., 2016), calcium ions (Moparthi et al., 2020b), and even mechanical stimuli (Moparthi and Zygmunt, 2020).

2.1.3 **The C-terminus**

The resolved part of the C-terminal end of TRPA1 (A971 – E1079 of human orthologue) is composed of several structural features: a TRPL helix that runs parallel to the inner sheet of the plasma membrane, an interfacial, hydrophobic helix (IFH) partly buried in the lipid membrane, and a well-resolved tetrameric coiled-coil below the ion permeation pore, where it forms a stalk-like interaction locus for all four subunits.

The TRPL helix shows a structural similarity with an α-helical TRP-helix present in many members of the TRPM, TRPC and TRPV families, although the TRPL helix does not contain a characteristic consensus sequence motif EWKFAR (Venkatachalam and Montell, 2007). The TRPL helix sequentially follows the S6 helix of the transmembrane domain and facilitates intersubunit interactions of other regions of the channel - the S4-S5 linker, S1 helix, the second H-T-H motif of the coupling domain and also the upward conformation of A-loop. Substitutions of positively charged residues of TRPL helix (K969A, R975A, and K989A) impaired the electrophile- and also voltage-dependent activation of TRPA1 (Samad et al., 2011), confirming that the TRPL helix acts as an important element transducing distal structural changes into the channel gating, similarly to the TRP-helix in other TRP channels (Rohacs et al., 2005, Garcia-Sanz et al., 2007).

The TRPL helix is followed by a short flexible α-helix and a β-strand that together with other two N-terminal β-strands from the coupling domain form a freestanding β-sheet (Paulsen et al., 2015, Suo et al., 2020, Zhao et al., 2020). The β-sheet surrounds the pre-S1 helix and connects to the IFH that is almost buried in the inner leaflet of the membrane (**Figure 6.A** on page 22). The cryo-EM structure of TRPA1 with a benzyl isothiocyanate (BITC) molecule bound to the reactive cysteine C621 at the N-terminus reveals an annular phospholipid in an interfacial cavity formed by S4, the S4-S5 linker, pre-S1, S1, and IFH. The lipid is not present in cryo-EM structures of TRPA1-C621S without agonist (PDB ID: 6PQQ) and with the larger

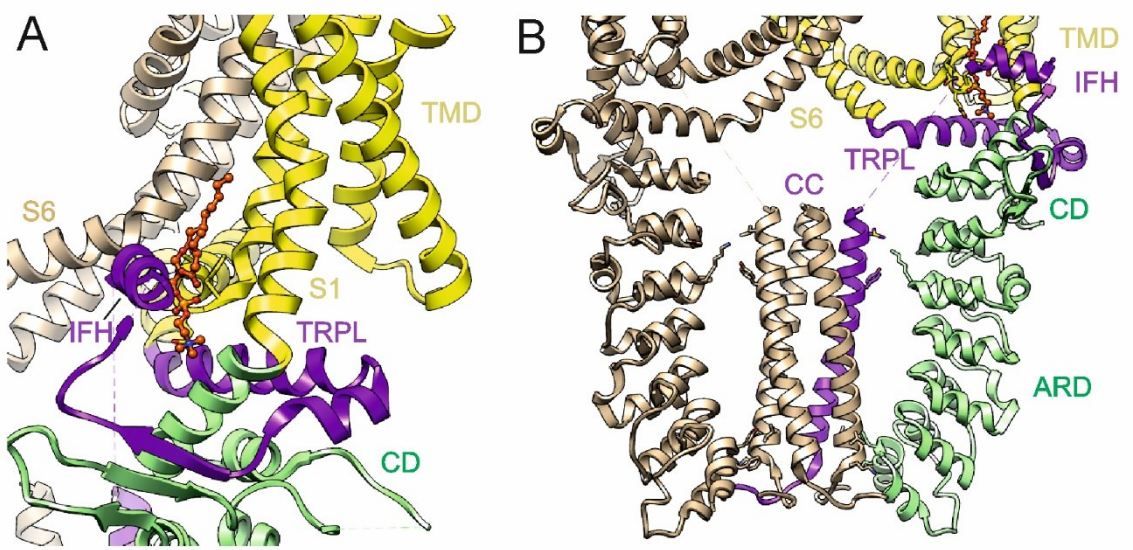

Figure 6: The C-terminus of TRPA1 channel. ***(A)*** *The proximal C-terminus (purple) surrounds the S1 of the VSLD (yellow) and pre-S1 helix of the coupling domain (CD; green). It is composed of the TRP-like helix (TRPL), a short α-helix and a β-strand, and an interfacial helix (IFH). In the apo-state, a molecule of phospholipid (orange) resides in the cavity formed by the IFH, TMD and the S6 of the adjacent subunit (tan).* ***(B)*** *The distal C-terminus forms a tetrameric coiled -coil (CC) that establishes contacts with the ARD. PDB ID: 6PQQ.*

agonist JT010 (PDB ID: 6PQO), because of the closer position of the IFH toward the VSLD and consequently reduced cavity size (Suo et al., 2020).

Three peptides that cover the primary sequence of TRPL helix (I964 – L992), short α-helix and β-strand (L992 – N1008) and the IFH (T1003 – P1034) were described in terms of binding of anionic lipids and interaction with carboxy-lobe (C-lobe) of calmodulin (CaM; (Witschas et al., 2015, Hasan et al., 2017, Macikova et al., 2019)). Results from a web server-based method for predicting the interaction between peptides and anionic lipids (Lata et al., 2007) suggest that both the TRPL helix and IFH are capable of binding lipids that may potentially regulate the channel's activity (Witschas et al., 2015). In addition, CaM binds to the peptide containing the sequence of the short α-helix and β-strand (L992 – N1008) at nanomolar concentrations of intracellular level of calcium ions, suggesting the mechanisms of Ca^{2+}-dependent potentiation and inactivation (Hasan et al., 2017). The results presented in the thesis show that the T1003-P1034 region is also important for Ca^{2+}-dependent potentiation, and that the Ca^{2+}/calmodulin complex may compete for the same or overlapping binding site with PIP_2 (Macikova et al., 2019). Whereas the C-lobe of CaM is indispensable for binding to the C-terminus of TRPA1, the amino-lobe (N-lobe) may either bridge

different domains of TRPA1 or link the channel with some different target protein(s) (Zimova et al., 2020).

The sequence following the IFH encodes a long α-helix that intermolecularly assembles into compact tetrameric coiled-coil (CC) motif (**Figure 6.B** on page 22). This structural feature is also present in TRPC and TRPM channels (reviewed in (Huffer et al., 2020)). The TRPA1 coiled-coil is distinct from canonical coiled-coils due to two polar residues inside of the structure and rather hydrophobic exposed surface that interacts with ARD (Paulsen et al., 2015). The first high-resolution cryo-EM structure (Paulsen et al., 2015) revealed an electron density of inositol hexakisphosphate (IP_6) molecule in the vicinity of positively charged coiled-coil residues (K1046 and R1050 from one coil and K1048 and K1052 from an adjacent coil), potentially elucidating the mechanism of TRPA1 stabilization by polyphosphates (Paulsen et al., 2015). However, isolated coiled-coil domains of hTRPA1 multimerize in a concentration-dependent, but IP_6- and temperature-independent manner (Martinez and Gordon, 2019, Zhao et al., 2020). Partial unfolding of coiled-coil helices occurs upon increasing the temperature to 42°C, although the multimerization remained unaffected (Martinez and Gordon, 2019).

The distal unresolved part of the C-terminus encodes an acidic cluster of residues E1077-D1082 (ETEDDD). Mutations of E1077, D1080, D1081 and D1082 to alanine had strong effects on Ca^{2+}- and voltage-dependent potentiation and/or inactivation of agonist-induced responses (Sura et al., 2012).

2.2 Activation of TRPA1

TRPA1 is a polymodal receptor that perceives various modalities of both exogenous and endogenous origin (reviewed in (Baraldi et al., 2010, Andrade et al., 2012, Giorgi et al., 2019, Talavera et al., 2020)). The receptor is sensitive to a plethora of substances including natural plant compounds (Macpherson et al., 2005, Xu et al., 2005, Xu et al., 2006), air pollutants (Andre et al., 2008), various endogenous substances (Trevisani et al., 2007, Taylor-Clark et al., 2008), noxious heat and cold (Vandewauw et al., 2018), internal calcium and zinc ions (Zurborg et al., 2007, Hu et al., 2009), mechanical stimulation (Vilceanu and Stucky, 2010) and low pH (Wang et al., 2011) (also reviewed in (Andrade et al., 2012, Talavera et al., 2020)). As the channels are expressed on a nociceptive subset of trigeminal ganglion (TG) and dorsal root ganglion (DRG) neurons, activation of TRPA1 is often perceived as pungent or

irritating (Andersson et al., 2008, Vandewauw et al., 2013). The binding sites of TRPA1 modulators are shown in **Figure 7**. Most modulators act within the transmembrane domain.

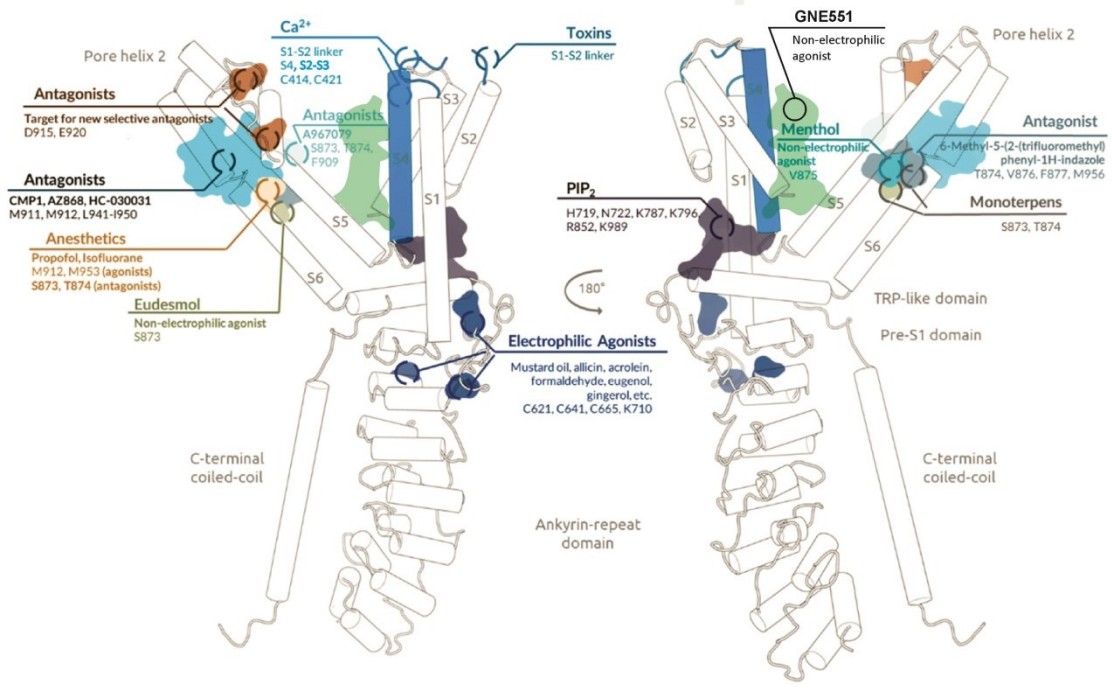

Figure 7: The binding sites of main chemical modulators of TRPA1 channel. *Adapted from (Giorgi et al. 2019).*

2.2.1 **Species-specific differences of TRPA1**

TRP channel expression patterns and functionalities vary among species, leading to intriguing evolutionary adaptations to the specific habitats and life cycles of individual organisms. Functional evolutionary divergence has presented challenges for studying TRP channels, as orthologues from different species can give conflicting experimental results. However, this diversity can also be examined comparatively to decipher the basis for functional differences.

Phylogenetical analyses of TRPA1 orthologues show that TRPA1 clade diversified from TRPA branch 500 million years ago as a chemosensory receptor for electrophilic compounds evoking pungent and irritating sensations (Kang et al., 2010). On the contrary, non-covalent modulators mostly show bimodal action, i.e. activation at lower concentrations and inhibition at higher concentrations. The EC_{50} and IC_{50} values are highly species-dependent, which accounts e.g. for divergent effects of non-covalent modulators as caffeine, menthol or nicotine on TRPA1 orthologues (Bianchi et al., 2012).

In addition to chemosensitivity, some TRPA1 orthologues also possess thermoception (reviewed in (Hoffstaetter et al., 2018)). In *Drosophila*, dTRPA1 is one of three TRPA heat-sensitive channels that are opened at temperatures between 25°C and 45°C, controlling the temperature preference (Hamada et al., 2008). Rattlesnakes can detect infrared radiation thanks to the TRPA1 channels expressed in the pit organs (Gracheva et al., 2010). TRPA1 as a noxious heat and chemical sensor is expressed in vertebrates together with TRPV1 (Story et al., 2003). The diversity in TRPA1-positive neuronal sensitization is accounted for the coexpression and heteromerization with TRPV1 (Patil et al., 2020). Conservation of TRPV1 heat sensitivity throughout vertebrate evolution could have changed functional constraints on TRPA1 and influenced the functional evolution of TRPA1 regarding temperature sensitivity, while conserving its noxious chemical sensitivity (Saito et al., 2012, Saito and Tominaga, 2017). While TRPA1 is a radiant heat sensor of snakes possessing pit organs (Gracheva et al., 2010), the ganglion-specific splicing of TRPV1 covers the analogous function in infrared sensing of vampire bats (Gracheva et al., 2011).

TRPA1 has first been considered as a cold receptor in mammals (Story et al., 2003), although later studies brought rather inconsistent results (as reviewed in (Caspani and Heppenstall, 2009, Laursen et al., 2014, Buijs and McNaughton, 2020)). Surprisingly, rodent TRPA1 has been also found to mediate a crucial physiological role in the detection of noxious heat (Hoffmann et al., 2013, Vandewauw et al., 2018). Human and mouse TRPA1 displayed activation upon noxious heat stimulation (Hynkova et al., 2016, Sinica et al., 2019). Single-channel recordings of hTRPA1 activity in the artificial membrane and measurements of intrinsic tryptophan fluorescence consolidate hTRPA1 as an intrinsic bidirectional thermosensor activated by both cold and heat (Moparthi et al., 2016). Surprisingly, nematode TRPA1 is also cold-activated (Chatzigeorgiou et al., 2010).

2.2.2 **Electrophilic agonists**

Electrophilic substances covalently modify cysteine and lysine residues by creating adducts or by oxidizing reactions, potentially impairing the protein's function. TRPA1 is a highly tuned sensor of electrophilic compounds that stands at the beginning of aversive behavior of species toward a wide range of damaging electrophiles.

Electrophilic activators of TRPA1 are structurally as diverse as their source (**Figure 8**): isothiocyanates, the pungent compounds in mustard oil, wasabi, and horseradish (Jordt et al., 2004); cinnamaldehyde from cinnamon (Bandell et al., 2004); allicin from garlic (Macpherson et al., 2005); acrolein, an irritant in vehicle exhaust fumes and tear gas (Bautista et al., 2006); reactive oxygen species (ROS) like hydrogen peroxide (Sawada et al., 2008); 4-hydroxynonenal, a product of lipid peroxidation (Trevisani et al., 2007); sulfur mustard, a chemical warfare gas (Bautista et al., 2006); JT010, a potent and site-selective TRPA1 agonist (Takaya et al., 2015); and many others.

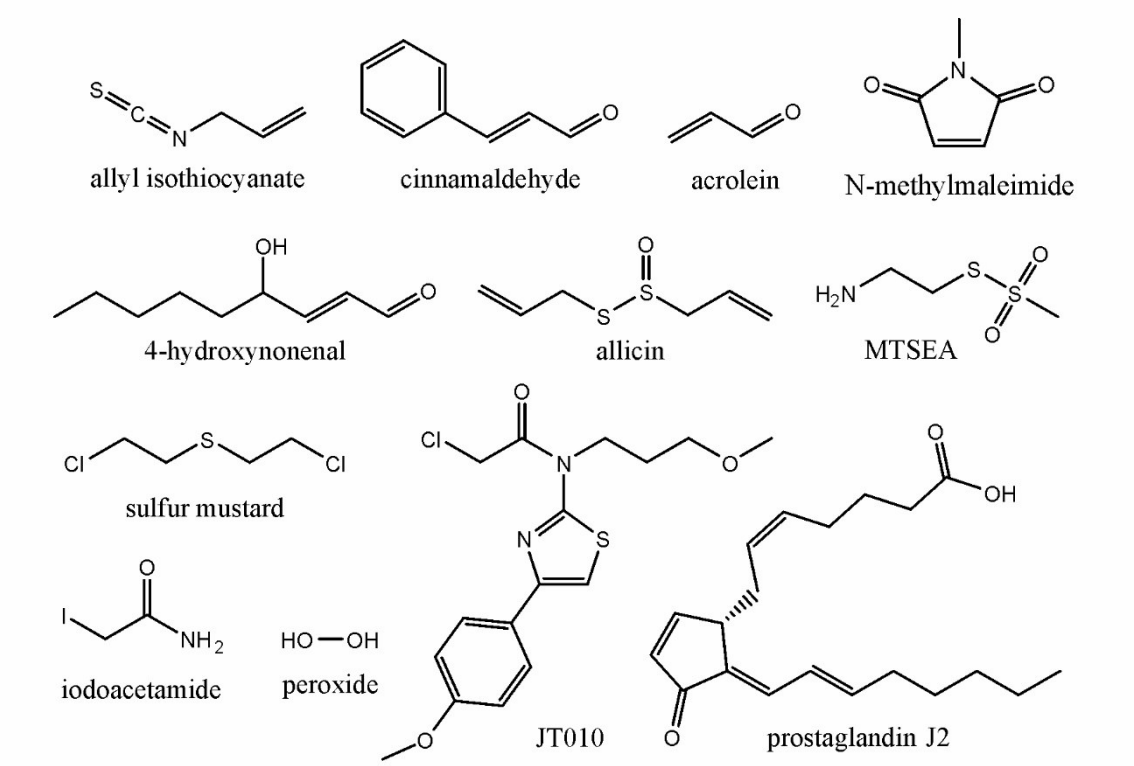

Figure 8: Electrophilic agonists of TRPA1.

There are four main reactions of electrophiles and cysteine residues (**Figure 9** on page 27). Isothiocyanates readily react with thiols to produce thiocarbamates. In Michael addition, dissociated thiol group of cysteine attacks the C_β of enols to form adduct and reduce the double bond. α-halocarbonyls as iodoacetamide (IA) are widely used for cysteine bioconjugation, where thiolate anion substitutes the halide leaving group. Cysteines also react with disulphides (allicin, 2-aminoethyl methanethiosulfonate (MTSEA)) and their oxidized forms (thiosulfinates) to form a conjugate. Among other

reactions of electrophiles with thiol group is oxidation (oxygen, peroxide) or nitrosylation (nitric oxide).

Cysteine and lysine residues, namely C414, C421, C621, C641, C665 and K710 (indexed according to hTRPA1), were proved by mass-spectrometry and electrophysiology to be essential for electrophilic modification (Hinman et al., 2006, Macpherson et al., 2007). Quadruple mutation of C621S, C665S, C641S and K710Q efficiently disrupts effects of a wide range of electrophiles on TRPA1 (Hinman et al., 2006, Trevisani et al., 2007). According to the recent cryo-EM structures, electrophiles activate TRPA1 *via* modification of key cysteines inside of a clam shell-like (A-loop) binding cavity of N-terminal coupling domain, in particular C621 and C665 (Suo et al., 2020, Zhao et al., 2020). Modification stabilizes the upward A-loop conformation which couples to TRPL helix and leads to channel gating. Bulky electrophiles stabilize active A-loop conformation by modifying C621 alone, smaller electrophiles additionally modify C665 to achieve full effect (Suo et al., 2020). A peptidergic scorpion toxin WaTx activates TRPA1 by direct interaction with the same site modified by electrophiles, providing an evidence that the binding site at the coupling domain is a

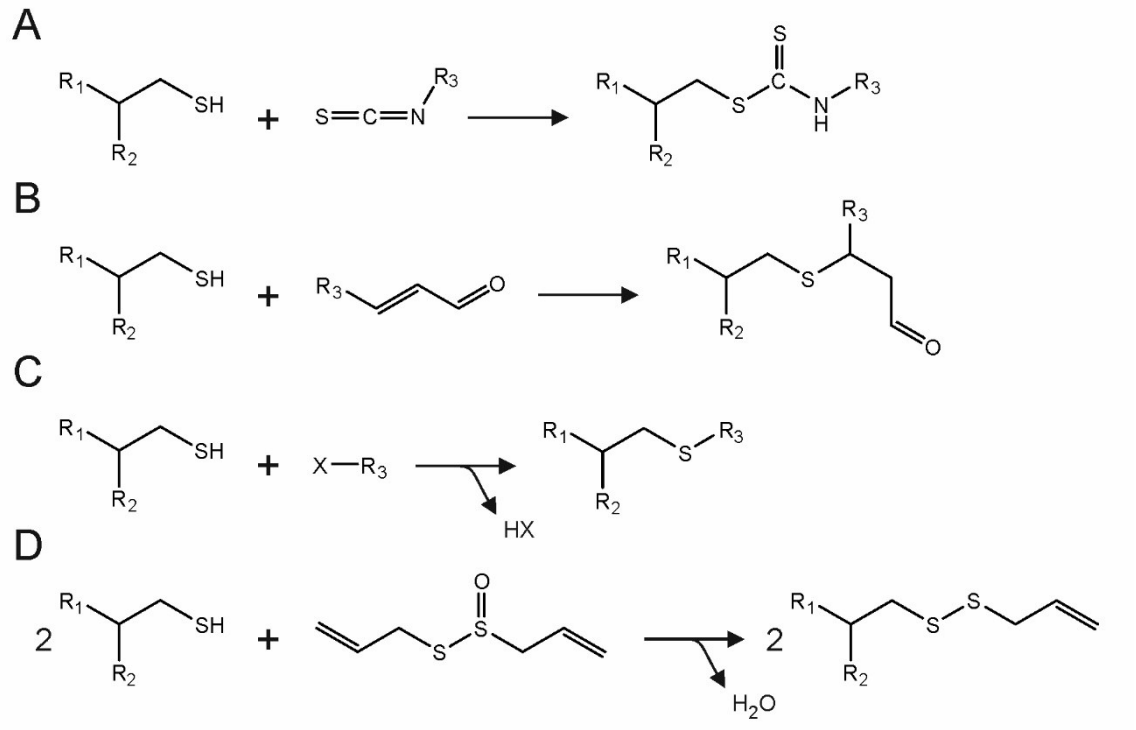

Figure 9: Thiol reactions. ***(A)*** *Reaction with isothiocyanate to produce thiocarbamate.* ***(B)*** *Michael addition with enol.* ***(C)*** *Alkylation reaction with α-halocarbonyls.* ***(D)*** *Reaction with allicin to form disulphides.*

key allosteric regulatory site targeted by both animal- and plant-derived irritants (Lin King et al., 2019).

Experiments with limited proteolysis of TRPA1 treated with N-methylmaleimide (NMM) show that electrophile binding also results in conformational rearrangements of AR11-AR15 region (Samanta et al., 2018, Moparthi et al., 2020a). Interestingly, hTRPA1 lacking the N-terminus can be activated by electrophiles even in the absence of all N-terminal cysteines (Moparthi et al., 2014). In line with this evidence, (E)-2 alkenals were able to activate TRPA1 channel even in TRPA1-3C construct (Blair et al., 2016).

2.2.3 **Non-covalent agonists**

Apart from electrophilic compounds, TRPA1 is also activated by other agonists by non-covalent interactions inside of a binding cavity (**Figure 10**). Non-covalent agonists of TRPA1 are structurally divergent and many of them exhibit species-dependent effects and bimodal action - activation at lower concentrations and inhibition at higher concentrations. Typical non-covalent activators are natural odorants and repellents from essential oils. TRPA1 mediates the pungency of menthol (Karashima et al., 2007) and other structurally similar compounds like carvacrol from oregano (Xu et al., 2006), thymol from thyme (Lee et al., 2008), but also paraben, an antibacterial agent widely used in cosmetics and food (Fujita et al., 2007), and lidocaine, a local anesthetics

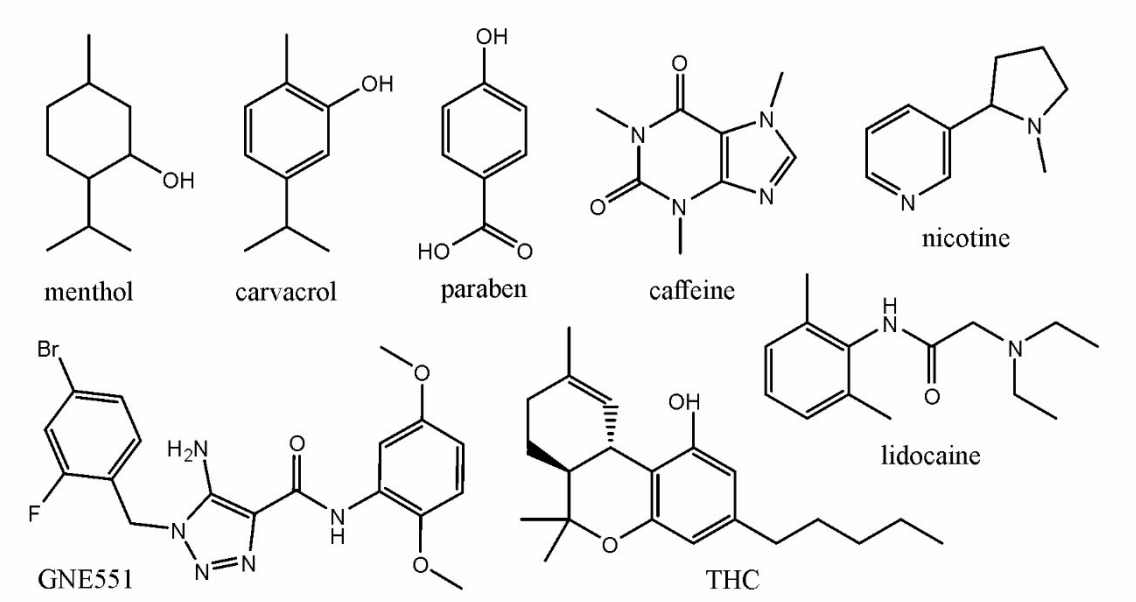

Figure 10: Non-covalent agonists of TRPA1.

(Leffler et al., 2011). Menthol is a bimodal modulator of TRPA1, activating at micromolar concentrations and blocking the channel at higher concentrations (Karashima et al., 2007). Nicotine also shows bimodal effects on TRPA1 and it interacts with the pore (Talavera et al., 2009). Caffeine activates mTRPA1 but blocks human orthologue (Nagatomo and Kubo, 2008). A single-point mutation of M268P at the distal N-terminus renders the effect of caffeine on mTRPA1 inhibitory (Nagatomo et al., 2010).

A binding pocket for menthol has been localized and functionally characterized in the TMD near the S5 helix; residues S873 and T874 in hTRPA1 are crucial for menthol activation or inhibition (Xiao et al., 2008, Chen et al., 2013). On the other hand, molecular docking simulations on carvacrol, thymol, β-myrcene and p-cymene using the hTRPA1 ion channel structure 3J9P (Paulsen et al., 2015) best fitted the compounds into the VSLD intracellular cavity with contacts to Y726, Y812, Y842, I811, S780 and S781 (Alvarenga et al., 2016, Ghosh et al., 2020).

Recently, an aminotriazole compound GNE551 from Genentech/Roche chemical library was distinguished as a highly-potent non-covalent TRPA1 agonist with $[EC_{50}] = 254$ nM for human orthologue. In contrast to electrophilic AITC, GNE551 exhibits no desensitization and provokes persisting pain that is insensitive to antagonists. The agonist binds to a groove between the S1-S4 region and the pore domain (S5-S6) of a neighboring subunit, overlapping the binding site for annular phospholipid (designated as “lipid 5” in (Suo et al., 2020)). The displacement of this lipid by ligand binding enables a conformational change in the S4–S5 linker and subsequent opening of the intracellular gate in a similar fashion as in TRPV1 channel (Gao et al., 2016).

2.2.4 **TRPA1 antagonists**

The key importance of TRPA1 in pain, inflammation and many other potential indications in acquired diseases makes it a plausible and attractive target of pharmacological treatment. Before the synthesis of selective TRPA1 antagonists, scientists used other compounds, for example ruthenium red that was developed for overcoming desensitization of capsaicin-responsive sensory fibers (Maggi et al., 1988).

The pharmaceutical companies put effort into creation of potent and selective TRPA1 antagonists (as reviewed in (Bamps et al., 2021)). In 2007, the first TRPA1

antagonist HC-030031 was synthetized **(Figure 11**; (McNamara et al., 2007)). Although commonly used as a potent TRPA1 inhibitor in a research field, HC-030031 showed low pharmacokinetics properties, high clearance and only micromolar potency (Rech et al., 2010). Chimeric studies between frog TRPA1 (fTRPA1) and hTRPA1, as well as analyses using point mutants, revealed that a single amino acid residue (N855 in hTRPA1) in the S4-S5 linker significantly contributes to the inhibitory action of HC-030031 (Gupta et al., 2016). Interestingly, a substitution by serine at position N855 is responsible for TRPA1 channelopathy in humans (Kremeyer et al., 2010).

Another potent and selective inhibitor is an oxime A-967079, which blocks human and rat TRPA1 (Chen et al., 2011), although it activates chicken TRPA1 (cTRPA1). These species-specific effects of A-967079 were utilized in a discovery of a single residue L881 in hTRPA1 that facilitates the A-967079-dependent inhibition (Banzawa et al., 2014). The binding of A-967079 into a pocket formed by S5, S6 and the first pore helix was confirmed by the cryo-EM structure (Paulsen et al., 2015).

Among antagonists with a concentration-dependent bimodal action are also non-covalent natural compounds, such as camphor derived from *Cinnamomum camphora* (Alpizar et al., 2013)

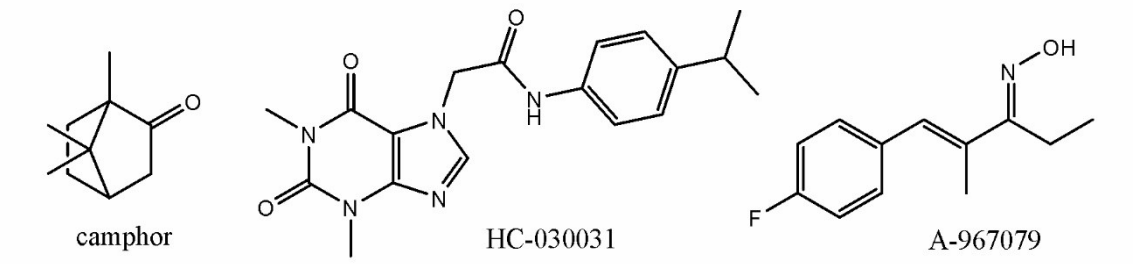

Figure 11: Antagonists of TRPA1.

2.2.5 **Activation by voltage**

TRP channels are mildly activated by depolarizing voltage due to a low gating charge, as opposed to K^+ channels with 4 arginine residues in the S4 helix (Jiang et al., 2003). The small gating charge of TRP channels is a crucial factor for the large voltage shifts induced by various stimuli (Nilius et al., 2005) and also an amplifier of thermal sensitivity (Chowdhury et al., 2014). At negative potentials, a slight inward current reflecting the basal activity of the channels is observed. The current becomes outward at potential around 0 mV and the conductance reaches its half-maximum value around 100 mV. However, the activation curve of TRPA1 is shifted to more negative potentials

by activating stimuli like intracellular Ca^{2+}, cold and agonists (Karashima et al., 2007, Zurborg et al., 2007, del Camino et al., 2010, Samad et al., 2011, Wang et al., 2013). When strongly activated, TRPA1 loses its specific rectification pattern and becomes open regardless of the membrane potential.

Prolonged stimulation at higher depolarizing potentials also inactivates mTRPA1. A conserved L906 (L903 in hTRPA1) in the first pore helix strongly impacts the voltage dependency – most substitutions at L906 converted the channel from outwardly to inwardly rectifying and also reduced its sensitivity to inhibition by TRPA1 blockers, HC-030031 and ruthenium red (Wan et al., 2014).

2.2.6 **Activation by heat**

TRPA1 orthologues from honeybees (Kohno et al., 2010), flies (Kang et al., 2010, Zhong et al., 2012), fishes (Oda et al., 2017, Oda et al., 2018), frogs (Saito et al., 2016), lizards (Saito et al., 2012), snakes (Gracheva et al., 2010), chicken (Kurganov and Tominaga, 2017), and mice (Vandewauw et al., 2018) proved to be heat-activated (**Figure 12**). Human orthologue expressed in *Xenopus laevis* oocytes was shown to be insensitive to temperatures at constant temperature 42°C, while rattlesnake TRPA1 was robustly activated above 28°C. Introduction of a part of the rsTRPA1 or dTRPA1 N-terminus into hTRPA1 was sufficient to confer heat sensitivity into the human TRPA1, emphasizing the role of the N-terminus in heat activation (Cordero-Morales et al., 2011). In accord with the study, three single-point mutations at the AR6 of mTRPA1 are individually sufficient to make the channel activated by 40°C, while leaving the sensitivity to chemicals unaffected (Jabba et al., 2014). However, mosquito

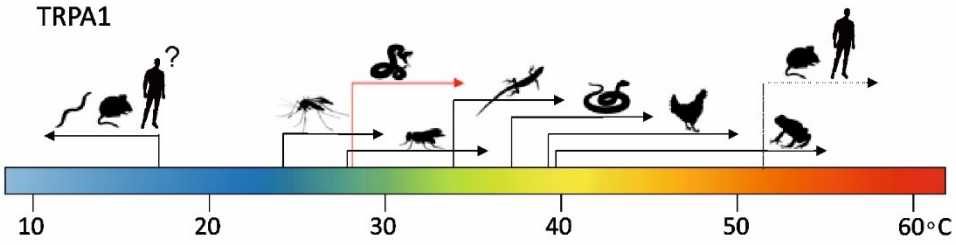

Figure 12: Species-specific temperature ranges of TRPA1. *TRPA1 apparent activation thresholds of mouse (< 17 °C), worm (< 17 °C), mosquito TRPA1- B (24.8 °C), fruit fly TRPA1-B (27.8 °C), rattlesnake (32.7 °C), green anole (33.9 °C), rat snake (37 °C), chicken (39.4 °C), and frog (39.7 °C). Mouse and human TRPA1 heat threshold is above 53 °C. Red arrow denotes specialized use of TRPA1 in snake pit organs as a radiant heat sensor. The precise cold threshold of human TRPA1 is yet to be determined. Adapted and modified from (Hoffstaetter et al., 2018).*

AgTRPA1 orthologue reconstituted in artificial membrane retains its thermosensitivity toward 35°C even if its N-terminus is deleted, suggesting that the N-terminal domain may tune the response but is not required for the activation by these stimuli (Survery et al., 2016). Introduction of mosquito-to-human point mutation in S6 helix and pore helix of dTRPA1 reverses the heat sensitivity (Wang et al., 2013). These evidences are in line with the current knowledge of TRPV activation, where the regions involved in heat activation are spread across the whole channel, including the N-terminal ARD (Laursen et al., 2016, Saito et al., 2016), membrane-proximal N-terminus TRPV3 (Yao et al., 2011, Liu and Qin, 2017), the pore domain (Grandl et al., 2010, Kim et al., 2013) and the C-terminus (Vlachova et al., 2003, Brauchi et al., 2006). Recently, both human and mouse TRPA1 expressed in HEK293T cells showed steep temperature dependence over the high temperature range of 53–59°C and 55–57°C respectively, providing evidence of a direct, rapid and reversible activation by noxious heat. (Sinica et al., 2019).

Interestingly, the noxious-heat avoidance behavior of *Drosophila* with impaired dTRPA1 can be rescued by the expression of human or heat-insensitive planarian TRPA1 (Arenas et al., 2017). The authors suggest that TRPA1 activation is mediated by H_2O_2 and ROS, early markers of tissue damage rapidly produced as a result of heat exposure. Although warm temperature suppresses rat and human TRPA1 currents evoked by ligands like AITC or menthol (Wang et al., 2012), responses to H_2O_2 are potentiated by heat in Chinese hamster ovary (CHO) cells expressing mTRPA1 (Vandewauw et al., 2018). The presence of reducing agents in the bath solution inhibited both cold and warm responses of hTRPA1 in artificial membrane (Moparthi et al., 2016), implying the importance of TRPA1 redox state in heat activation.

2.2.7 **Activation by cold**

Unlike heat sensing, activation by cold was described only in nematode, rodent and human TRPA1 channels. Rodent TRPA1 is activated by lowering temperature to 10°C both transiently expressed and in DRG neuronal culture (Bandell et al., 2004, Corey et al., 2004, del Camino et al., 2010). Cold increases the channel's open probability, slightly decreases the unitary conductance and creates a leftward shift of half-maximal activation voltage V_{50} (Sawada et al., 2007, Karashima et al., 2009, Chen et al., 2013). Human TRPA1 was also found to be activated by 12°C cooling, although to a lesser extent than mTRPA1 (Kremeyer et al., 2010, Wang et al., 2013, Moparthi et

al., 2014, Moparthi et al., 2016, Sinica et al., 2019). However, other groups did not observe any hTRPA1 cold-evoked currents upon cooling (Jordt et al., 2004, Cordero-Morales et al., 2011, Chen et al., 2013). A single residue G878 in mouse TRPA1 (V875 in hTRPA1) accounts for differences in cold sensitivity of hTRPA1 and mTRPA1 (Chen et al., 2013), and for temperature-dependent kinetics of voltage activation (Sinica et al., 2019). *TRPA1*-deficient mice were indistinguishable from wild-type littermates when examined for behavioral responses to cold (Bautista et al., 2007, Knowlton et al., 2010), probably because of the presence of other cold-activated channels (Buijs and McNaughton, 2020). In line with these findings, additional lack of TRPA1 decreases cold avoidance in *Trpm8*$^{-/-}$ mice in the temperature gradient assay (Touska et al., 2016, Winter et al., 2017).

Mild cooling markedly increases currents evoked by electrophiles and carvacrol in rat and human TRPA1, suggesting that TRPA1 is a key mediator of cold hypersensitivity (del Camino et al., 2010, Moparthi et al., 2016, Zimova et al., 2020). The TRPA1-positive neurons respond to cold only in the presence of agonist, suggesting that TRPA1 is important in pathological conditions with elevated level of proinflammatory activators, but likely plays a comparatively minor role in acute cold sensation (del Camino et al., 2010). TRPA1 has been linked with mechanical and cold allodynia accompanying nerve injury (Chen et al., 2011), inflammation (Yamaki et al., 2020), or anti-cancer treatment by oxaliplatin (Nassini et al., 2011, Park et al., 2015). Acute hypersensitivity to cold induced by oxaliplatin is mediated by human TRPA1 sensitization to ROS *via* mechanisms that are, in a dose-dependent manner, governed by the inhibition of propyl hydroxylases (Miyake et al., 2016).

2.2.8 **Mechanism of temperature activation**

In thinking about thermal sensing, it is instructive to consider how temperature induced changes alter the equilibrium between two states of a channel, such as two different conformations of a protein. The transition between two states is defined by the standard Gibbs free energy difference between the two conformations at constant pressure:

$$\Delta G^\circ = \Delta H^\circ - T\Delta S^\circ, \quad (1)$$

where ΔH and ΔS are the standard enthalpy and standard entropy changes respectively, and T is the absolute temperature. The mechanism of temperature-driven gating of TRP

channels has been associated with large changes in enthalpy and entropy upon the channel gating. Both enthalpy and entropy are temperature-dependent when a transition between two states is accompanied by a change in molar capacity, ΔC_P. The equilibrium between the open and closed state is defined by the equation:

$$lnK = \frac{\Delta S°(T_0)}{R} - \frac{\Delta C_P\left[1-\frac{T_0}{T}+ln\left(\frac{T_0}{T}\right)\right]}{R}, \quad (2)$$

where T_0 is a reference temperature set as the point of minimum K, when $\Delta H°(T_0) = 0$. The relationship has a "U-shape" with two temperatures where $lnK = 0$ i.e., the midpoint of the transition between the two states, implying that all temperature-sensitive channels can in principle behave as both cold and heat receptors, if the temperature range is acquired experimentally (Clapham and Miller, 2011). Positive heat capacity change is associated with disordering or unfolding process, which would lead to exposure of hydrophobic residues to solvent. A strong temperature dependence will not be seen unless ΔC_P is around several kcal·mol^{-1}·K^{-1}, an equivalent of "unburial" of 10 – 20 hydrophobic side chains per subunit in the tetrameric channel (Clapham and Miller, 2011). Point mutations could transform a hot-activating TRP into a cold-activating one, or vice versa, simply by shifting the melting temperature T_m along the temperature axis, similarly as in small protein GB1 (**Figure 13**; (Arrigoni and Minor, 2018)).

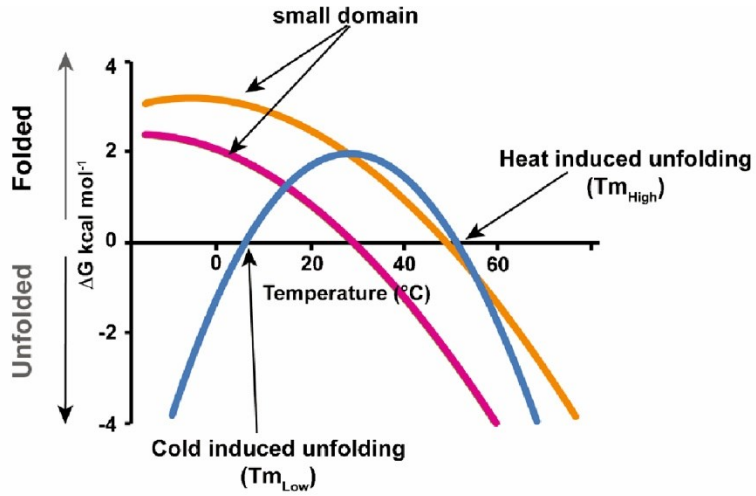

Figure 13: The curve of free energy ΔG of protein unfolding, plotted as a function of temperature. *Orange and magenta curves are for two mutants of an exemplar protein GB1 ($\Delta Cp = 624\ cal{\cdot}mol^{-1}{\cdot}K^{-1}$). The plot of these proteins exhibits a shallow 'U-shape' dependence, with the cold induced unfolding process unreachable. Note that mutations shift the U-plot along the temperature axis. The blue curve shows a protein with four times larger $\Delta Cp = 2400\ cal{\cdot}mol^{-1}{\cdot}K^{-1}$, rendering both cold- and heat- induced unfolding temperatures achievable in water solutions. Adapted from (Arrigoni and Minor, 2018).*

The heat capacity principle was proved plausible by (Chowdhury et al., 2014) who built thermosensitivity into the Shaker K_v channel by modifying the hydrophobicity of certain amino acids that undergo changes in solvation during the channel gating. So far, researchers have experimentally observed only one shoulder of the U-plot (Diaz-Franulic et al., 2020), although similar analysis has not been conducted on TRPA1, a hot/cold candidate for bimodal temperature activation. However, the folding/unfolding processes have to take part in the regions that are allosterically coupled to the channel's gate. A shining example of such coupling is the C-terminal coiled-coil of $BacNa_v$ sodium channel and TRPM8 channel: while $BacNa_v$ channel is heat-activated by partial coiled-coil unfolding (Arrigoni et al., 2016), in TRPM8 activation occurs after coiled-coil stabilization upon cooling (Diaz-Franulic et al., 2020). Similar mechanism is plausible for TRPA1 with C-terminal coiled-coil (Paulsen et al., 2015) that partially unfolds at elevated temperatures (Martinez and Gordon, 2019) and potentially undergoes changes in solvation upon channel gating (Arrigoni and Minor, 2018).

An allosteric model composed of gate and independent voltage and temperature sensors represents a more complex yet precise model of TRP channels (**Figure 14**;

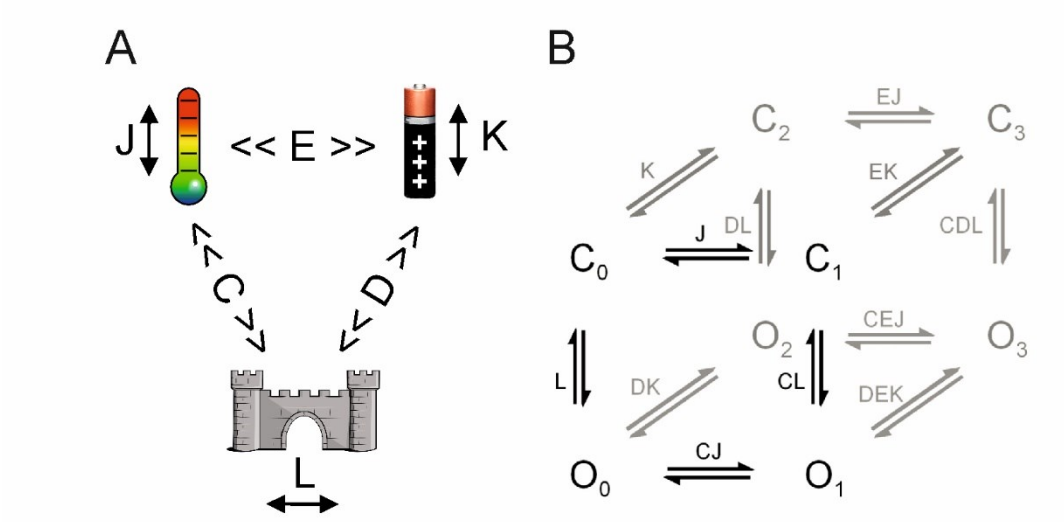

Figure 14: Allosteric model for temperature- and voltage-dependent activation of TRPA1 channel. (A) *The model consists of three elements - the channel's gate, the temperature sensor and the voltage sensor. Each has two states (closed-open, resting-activated) and the equillibrium constant (L, J, K) between these two states. The coupling constants C and D determine, whether the activation of temperature / voltage sensor will facilitate of impede the opening of the channel. The coupling constant E determines the further effect of simultaneous activation of both sensors on gating.* ***(B)*** *An eight-state allosteric model with corresponding equillibria between each states. States with deactivated voltage sensors are in black. Adapted from (Sinica et al., 2019) and (Jara-Oseguera and Islas, 2013).*

(Salazar et al., 2011)). An allosteric model implies that the channel has a gate, described by an equilibrium constant *L*, and also independent voltage and thermal sensors, both described by their own constants *J* and *K* of the temperature- and voltage-dependent transitions. The sensors allosterically couple to the channel's gate and to each other according to coupling energy terms *C*, *D* and *E* respectively. This model is capable of explaining the sensitization of an agonist-induced activation by temperature (del Camino et al., 2010), or, on the other hand, a loss of sensitivity to other stimuli at high concentrations of agonist (Matta and Ahern, 2007). Moreover, introduction of temperature-dependent coupling even give rises to channels that respond to both cooling and heating in a ΔCp-independent manner (Jara-Oseguera and Islas, 2013).

Furthermore, the results presented in this thesis provide the evidence that preceding stimulation of human and mouse TRPA1 by voltage and heat strongly enhances TRPA1-mediated cold-evoked currents (Moparthi et al., 2016, Sinica et al., 2019). Another proposed (indirect) mechanism of temperature-dependent activation is represented by ROS activation (as described above) and protein-lipid interactions (reviewed in (Zubcevic, 2020)), which were proposed to play an important role in temperature-dependent actuation (Melnick and Kaviany, 2018) .

2.3 Regulation of TRPA1

2.3.1 **Regulation by lipids**

TRPA1 channel forms both specific and non-specific interactions with membrane lipids. The mediators produced by the phospholipase A_2 (PLA_2) and phospholipase C (PLC) pathways, as well as products of oxidative stress (e.g. 4-hydroxynonenal (HNE)) activate TRPA1 directly through covalent modification of cysteines in the N-terminus (Bandell et al., 2004, Trevisani et al., 2007, Taylor-Clark et al., 2008). PLC mediates its effect by hydrolysis of phosphatidylinositol-4,5-bisphosphate (PIP_2) into inositol trisphosphate (IP_3) and diacylglycerol (DAG). Also phosphoinositides were proposed to regulate TRPA1; however, the findings in regards to the PIP_2 regulation are inconsistent (Rohacs, 2016). Preincubation with the phosphatidylinositol-4-kinase (PIK) inhibitor wortmannin reduces both constitutive TRPA1 channel activity and the response to AITC. Also other techniques using

transiently expressed PIP_2 sequestrators, Myristoylated alanine-rich C-kinase substrate (MARCKS) and Growth Associated Protein 43 (GAP43), as well as voltage-sensitive phosphatase Dr-VSP reduced the chemical activation of TRPA1, especially at negative potentials (Zimova et al., 2018, Zimova et al., 2020). PIP_2 reactivates the activity of recombinant TRPA1 in excised patches, where the channels run down (Karashima et al., 2008). Contrarily, (Kim and Cavanaugh, 2007) reported no effect of PIP_2 in excised patches. Also depletion PIP_2 with a rapamycin-inducible 5-phosphatase did not inhibit TRPA1, while it inhibited TRPM8 (Wang et al., 2008). TRPA1 retains its activity in the artificial membrane, showing that it does not need PIP_2 for activation (Moparthi et al., 2014, Moparthi et al., 2016).

The cryo-EM structures of TRPA1 in lipid nanodiscs (PDB ID: 6PQO, 6PQP, 6PQQ) revealed 6-7 annular lipids that dwelled in contact with the TMD (**Figure 15**; (Suo et al., 2020). Importantly, some sites have been shown to also serve as a binding site for ligands. It has been proposed that lipids and ligands compete for these binding sites, and that ligand binding shifts the gating equilibrium toward the open state (Zubcevic, 2020). Such site that is capable of binding 'phospholipid 5' and a non-covalent agonist GNE551 is located in between the S5-S6 helices of adjacent TRPA1 subunits (**Figure 16** on page 38). The substitution of a proximal residue E864 with bulky tryptophan resulted in the constitutively open channel, indicating that disrupted interaction with the residing lipid propagates into the opening of the channel

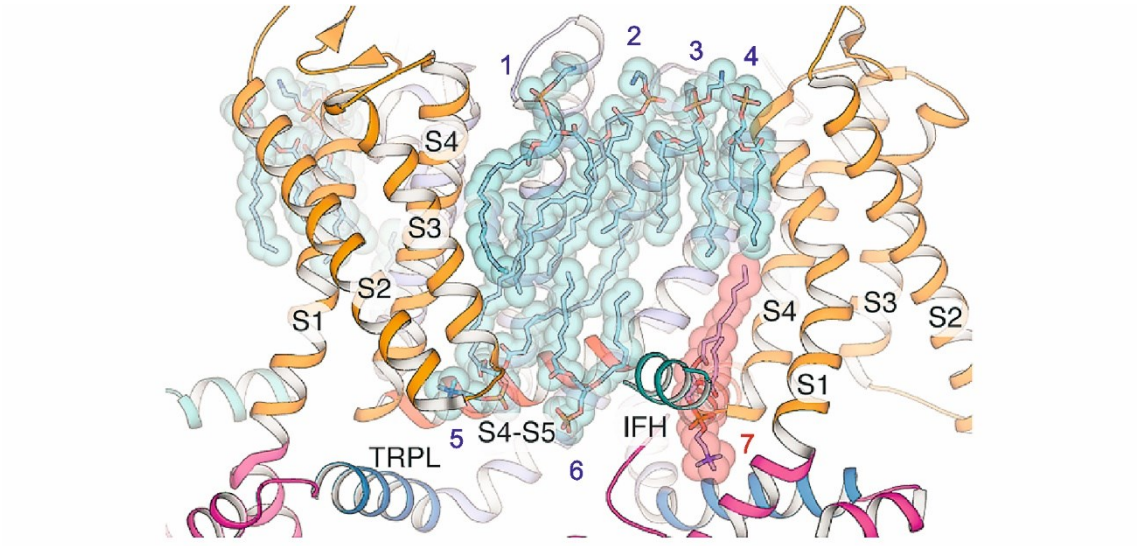

Figure 15: Annular lipids of TRPA1 channel. *Seven lipid molecules were captured by the cryo-EM (6PQQ) between two protomers of TRPA1. The 'phospholipid 7' (red) between the IFH and the VSLD was observed only in the apo state of the channel, but not in the TRPA1-JT010 bound state. Adapted from (Zubcevic, 2020).*

(Liu et al., 2020). The identical binding site of phospholipids is present in TRPV1 channels, where the displacement of lipids by vanilloid agonists or heat was proposed to be a mechanism of TRPV1 activation (Gao et al., 2016). The studies presented in this doctoral thesis investigated two potential lipid-binding sites and revealed their importance in TRPA1 regulation (Zimova et al., 2018, Macikova et al., 2019, Zimova et al., 2020).

TRP channels in general are highly sensitive to the membrane environment and compounds that can change the local physical properties of the membrane (Startek et al., 2019b). TRPA1 is modulated by compounds that shape the membrane curvature – crenation-forming amphiphilic trinitrophenol activates TRPA1, while chlorpromazine induces cup formation and inhibits TRPA1 (Hill and Schaefer, 2007). Bacterial lipopolysaccharides (LPS), one of the most potent mediators of inflammation, insert into the lipid bilayer and trigger TRPA1 activation both in cellular and artificial membranes (Startek et al., 2018). The ability to activate TRPA1 correlates with the shape of LPS: conically-shaped LPS are more active (Meseguer et al., 2014).

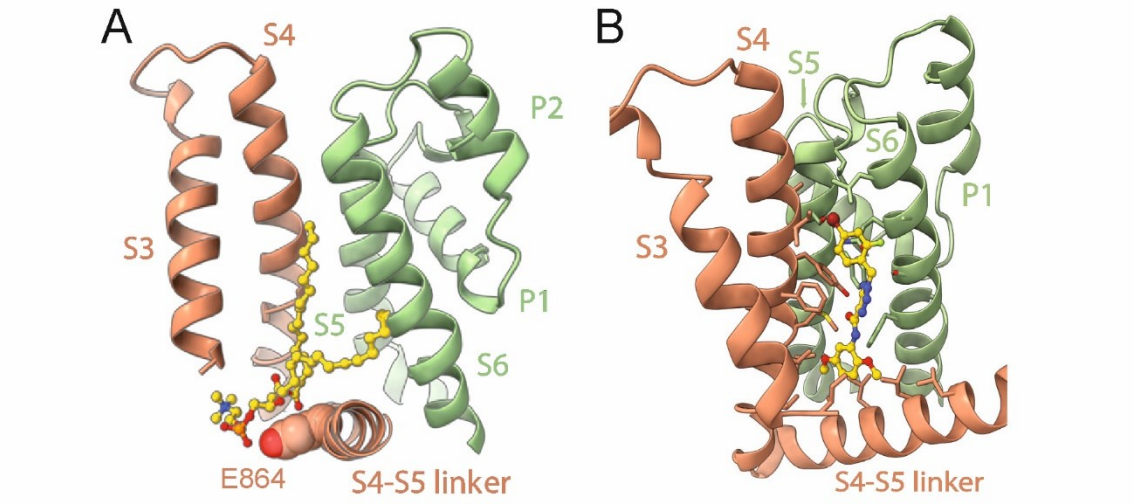

Figure 16: The binding site in the vicinity of S5-S6 helices of the TRPA1 channel. (A) *A molecule of phospholipid (yellow), located at the interface between the S4 helix and S4-S5 linker of one subunit and the pore domain of the adjacent subunit (structure 6PQQ). The interacting residue E864 is shown.* ***(B)*** *A selective non-covalent agonist GNE551 (yellow) binds into the region overlapping the binidng site of phospholipid (structure 6X2J). Adapted from (Liu et al. 2020).*

2.3.2 **Regulation by phosphorylation**

One of the most potent algogenic compounds that are involved in the development of pain and hyperalgesia upon tissue damage, inflammation and nerve injury is bradykinin (BK). The acute effect of bradykinin is mediated through the G protein-coupled receptors (GPCR) B2, initiating the G_q/phospholipase C (PLC), G_i/phospholipase A_2 (PLA_2) and G_s/adenylyl cyclase (AC) pathways (**Figure 17** on page 40; reviewed in (Petho and Reeh, 2012)). These pathways regulate the activity of TRPA1 channel by production of DAG, arachidonic acid (AA) and its metabolites that direct activate TRPA1 (Taylor-Clark et al., 2008), by elevating the intracellular level of Ca^{2+} that potentiates and inactivates TRPA1 (Bautista et al., 2006), by increasing the membrane expression of TRPA1 (Schmidt et al., 2009), and by phosphorylation (Brackley et al., 2017, Meents et al., 2017).

The AC pathway switches on the protein kinase A (PKA) that promotes acute sensitization of TRPA1 by phosphorylation. Amino acid residues S86, S317, S428, and S972 were found as the principal targets of PKA by using electrophysiology and site-directed mutagenesis (Meents et al., 2017). Additionally, protein kinase C (PKC) acting downstream of PLC pathway sensitizes TRPA1 through phosphorylation of residues S119, T281 and T529. Both the PKA and PKC kinases require the A-Kinase Anchoring Protein 79/150 (AKAP) in order to facilitate phosphorylation and sensitization of TRPA1 channel (Brackley et al., 2017). AKAP directly interacts with TRPV1 (Zhang et al., 2008) and there is an evidence based on molecular modeling that AKAP can interact with the proximal part of the N-terminus of TRPA1 (Zimova et al., 2020).

TRPA1 is also targeted by cyclin-dependent kinase 5 (Cdk5) that recognizes a structural consensus (S/T)PX(K/H/R). Cdk5 activity is dependent upon binding to one of its two regulatory proteins, p35 or p39 (Tsai et al., 1994). A residue T673 outside of the ARD was considered as the possible target of Cdk5 (Hynkova et al., 2016). In addition, immunopurified Cdk5 was observed to phosphorylate human TRPA1 peptide substrate at S448A in the AR12 *in vitro* (Hall et al., 2018, Sulak et al., 2018). *p35*$^{-/-}$ knock-out mice showed attenuated oral aversion to TRPA1 agonist AITC in a concentration dependent manner (Hall et al., 2018).

While the activity of the above mentioned kinases most likely upregulate the responses of TRPA1, activators of AMP-activated protein kinase (AMPK) negatively regulate the channel in DRG neurons by downregulation of plasma membrane

expression (Wang et al., 2018b). A study presented in this thesis shows that a residue S602 preceding the coupling domain of TRPA1 may potentially be a site for inhibitory phosphorylation of TRPA1 channel (Barvikova et al., 2020). This residue was predicted to be phosphorylated by several phosphorylation site prediction servers. The phosphomimetic mutation S602D completely abrogated channel activation, whereas the phosphonull mutations produced a fully functional channel (Barvikova et al., 2020).

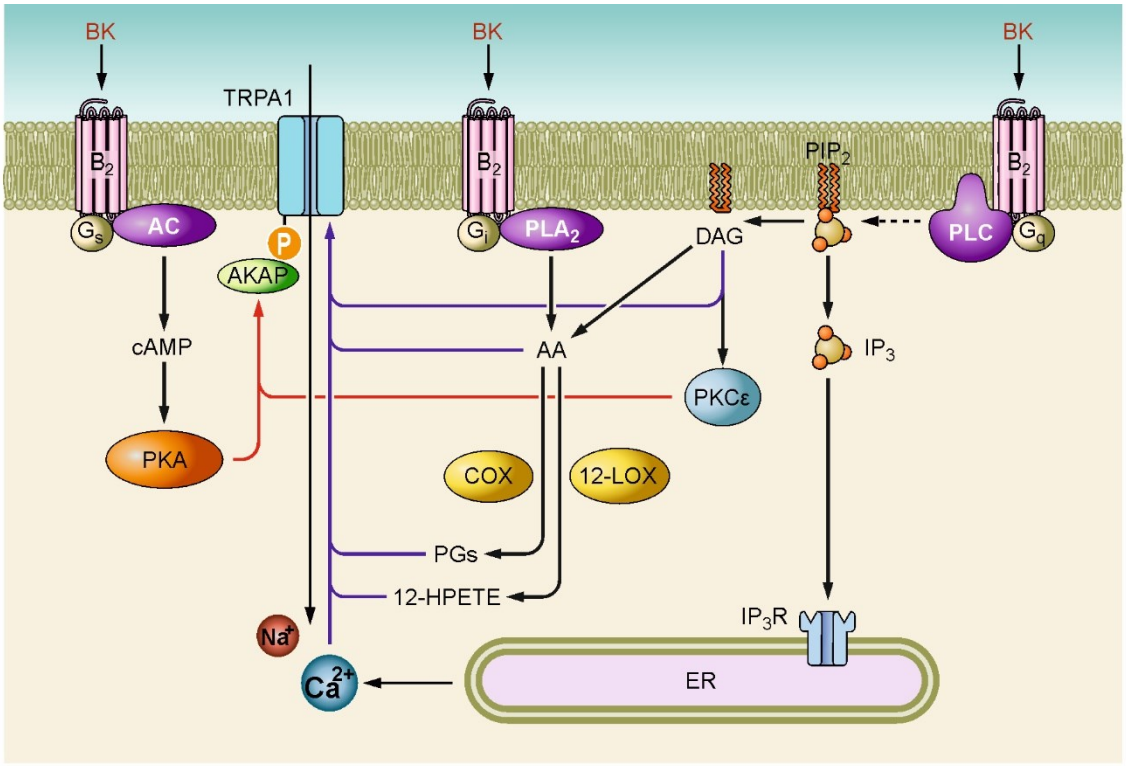

Figure 17: Sensitization of TRPA1 channel by the inflammatory mediator bradykinin. *Bradykinin (BK) triggers the phospholipase C (PLC), phospholipase A_2 (PLA_2) and adenylate cyclase (AC) pathways through binding to the bradykinin 2 receptor (B_2) with indicated G-protein subunits. PLC cleaves phosphatidylinositol bisphosphate (PIP_2) into inositol trisphosphate (IP_3) and diacylglycerol (DAG). IP_3 binds to inositol trisphosphate receptor (IP_3R) in the endoplasmatic reticulum (ER) and releases Ca^{2+} ions that directly modulate TRPA1 channel. DAG activates protein kinase Cε (PKCε), that binds to the anchoring protein AKAP79/150 and sensitizes TRPA1 by phosphorylation. In addition, DAG directly activates TRPA1. The arachidonic acid (AA) is formed by PLA_2-mediated cleavage of phospholipids, or by diacylglycerol lipase from DAG. AA is further metabolized by cyclooxygenase (COX) and lipooxygenase (12-LOX) to form prostaglandins (PGs) and 12-HPETE. Both AA and its metabolites directly activate TRPA1. The AC stimulates protein kinase A (PKA), which together with PKC binds to AKAP79/150 and sensitizes TRPA1 via phosphorylation. Adapted from (Petho and Reeh, 2012).*

3. Aims of the study

- Investigate the impact of low-frequency high-induction electromagnetic field on calcium responses induced in naïve and TRPA1-expressing cells by the inflammatory agent bradykinin.
- Explore the role of N-terminal serine residue 602 as a potential target of TRPA1 phosphorylation.
- Test the effects of AKAP79/150 on the sensitization of the TRPA1 channel.
- Characterize the involvement of polar residues facing the inside of the intracellular VSLD cavity in the modulation of TRPA1 channel by voltage, agonists and calcium ions. Explore the possibility of lipid binding inside of the VSLD cavity.
- Investigate the role of the C-terminal region (L992-P1034) forming the intersubunit crevice on the binding of phosphatidylinositol-4,5-bisphosphate. Test the involvement of this region in the regulation of TRPA1 channel in terms of modulation by voltage, agonists and calcium ions.
- Characterize and compare the temperature- and voltage-dependent properties of human and mouse TRPA1 to unravel the differences between their mechanisms of gating. Examine the mechanisms of bidirectional temperature activation of human and mouse TRPA1 channels.

4. Methods

4.1 Chemicals and solutions

All solutions were prepared using deionized water, which was for molecular biological methods further purified by Simplicity 185 device (Millipore, USA) and sterilized. If not stated otherwise, all chemicals were purchased from Sigma-Aldrich (Prague, Czech Republic).

Agonists, modulators

Allyl isothiocyanate (AITC), cinnamaldehyde (Cin) and carvacrol (Carv) solutions were prepared from a 0.1 M stock solution in DMSO. Bradykinin (BK) solution was prepared from a 0.1 mM stock solution in DMSO. All stock solutions were stored at 4°C.

Extracellular solutions (ECS)

The composition of the extracellular solutions used is listed in the **Table 1**. The ECS classic was used in **publications I, II, IV** and **V**. The ECS Zygmunt from the study (Moparthi et al., 2016) was used in **publications III, V, VI**, and **VII**. The ECS with 0 mM or 2 mM concentration of Ca^{2+} was used to determine the effect of calcium in **publications IV** and **V**. The ECS Hasan from the study (Hasan et al., 2017) was used in **publications V, VI**.

Table 1: The compositions of extracellular solutions (in mM).

ECS classic	ECS 0 Ca^{2+}	ECS 2 Ca^{2+}	ECS Zygmunt	ECS Hasan
160 NaCl	150 NaCl	150 NaCl	140 NaCl	140 NaCl
2.5 KCl			5 KCl	4 KCl
1 $CaCl_2$	2 HEDTA	2 HEDTA	5 EGTA	
2 $MgCl_2$			2 $MgCl_2$	1 $MgCl_2$
10 HEPES	10 HEPES	10 HEPES	10 HEPES	10 HEPES
10 Glucose			10 Glucose	5 Glucose
pH 7.3 NaOH	pH 7.3 NaOH	pH 7.3 NaOH	pH 7.4 TMA-OH	pH 7.4 NaOH
320 mOsm	280 mOsm	280 mOsm	300 mOsm	285 mOsm

Intracellular solutions (ICS)

The composition of the intracellular solutions used is listed in the **Table 2**. The ICS classic was used in **publications II, IV** and **V.** The ICS Zygmunt from the study (Moparthi et al., 2016) was used in temperature experiments in **publication IV, V** and **VII**. The ICS phos was used in **publication III** and **VII**. The ICS magnet was used in **publication I**. The ICS AKAP was used in **publication III**.

Table 2: The compositions of intracellular solutions (in mM).

ICS classic	ICS Zygmunt	ICS phos	ICS AKAP	ICS magnet
145 CsCl	140 KCl	125 Cs-gluconate 15 CsCl	125 Cs-glucono-δ-lactone 15 CsCl	125 K-gluconate 15 KCl
5 EGTA 3 $CaCl_2$ 10 HEPES 2 MgATP	5 EGTA 2 $MgCl_2$ 10 HEPES	5 EGTA 0.5 $CaCl_2$ 10 HEPES 2 MgATP 0.3 NaGTP	5 EGTA 0.5 $CaCl_2$ 10 HEPES 2 MgATP 0.3 NaGTP	5 EGTA 0.5 $CaCl_2$ 10 HEPES 2 MgATP 0.3 NaGTP 10 creatine phosphate
pH 7.3 CsOH	pH 7.4 KOH	pH 7.4 CsOH	pH 7.4 CsOH	pH 7.2 KOH
290 mOsm	280 mOsm	274 mOsm	275 mOsm	300 mOsm

4.2 Cell cultures, constructs, transfection

Human embryonic kidney 293T (HEK293T, CRL-3216; ATCC, Manassas, VA, USA) cells were cultured in Opti-MEM I media (Invitrogen, USA) supplemented with 5% fetal bovine serum (PAN-Biotech, Germany). The magnet-assisted transfection (IBA GmbH, Germany) technique was used to transiently cotransfect the cells in a 15.6-mm well on a 24-well plate with 200 ng of GFP plasmid (TaKaRa, Japan) and with 300 or 400 ng of cDNA plasmid encoding wild-type or mutant human TRPA1 (pCMV6- XL4 vector, OriGene Technologies, USA). In experiments with coexpression of TRPA1 channels with other proteins, 200 ng GAP43 (pCMV6-XL5 vector, OriGene Technologies, USA), 100 ng MARCKS (pCMV6-XL5 vector, OriGene Technologies, USA), 300 ng DrVSP (IRES2-EGFP vector, a gift from Yasushi Okamura, Addgene plasmid #80333) or 200 ng AKAP79/150 (pCMV6-XL4 vector, OriGene Technologies,

USA) were added into the transfection mixture. At least two independent transfections were used for each experimental group. The cells were used 24–48 h after transfection.

F11 cells (The European Collection of Authenticated Cell Cultures, ECACC 08062601, UK) cultured in Dulbecco's modified Eagle's medium supplemented with 2 mM glutamine and 10% fetal bovine serum were passaged once a week using trypsin-EDTA (Invitrogen, USA) and grown under 5% CO_2 at 37°C. One to two days before transfection, cells were plated in 24-well in 0.5 mL of medium and became confluent on the day of transfection. The cells were transiently cotransfected with 300 ng of cDNA plasmid encoding human TRPA1 (in the pCMV6-XL4 vector OriGene Technologies) and with 200 ng of GFP plasmid (TaKaRa, Japan) with the use of Lipofectamin 2000 (Invitrogen, USA) and then plated on poly-L-lysine-coated glass coverslips.

4.3 Site-directed mutagenesis

The constructs of hTRPA1 channel were made using QuikChange II XL Site-Directed Mutagenesis Kit (Agilent Technologies, USA). For each mutation the primer of length about 30 amino acids was designed and synthesized (by VBC-Biotech, Austria). As the wild-type template served human TRPA1 (in the pCMV6- XL4 vector, OriGene Technologies, USA) or mouse TRPA1 (in pcDNA5/FRT, kindly provided by Dr. Ardem Patapoutian, Scripps Research Institute, USA). The polymerase chain reaction (PCR) was performed using the mix of oligonucleotides (Invitrogen, USA) in a Thermo-cycler device (Eppendorf, Germany). After the PCR was completed, the template DNA was eliminated by enzymatic digestion with a restriction enzyme DpnI which is specific for methylated DNA. The PCR product was detected using horizontal electrophoresis with 1 % agarose gel (70 mV, 50 min). According to the above-mentioned kit manual, the XL10-Gold ultracompetent cells were transformed by 2 µl PCR product by the heat shock protocol. The cells were then cultured on agar plates (Biolife, Italy) with ampicillin or kanamycin (100 mg/l or 50 mg/l, respectively) and subsequently in Lysogeny Broth (water solution of 0.5% yeast extract, 1% peptone, 0.26 M NaCl) medium over night at 37°C in shaking incubator. The DNA from multiplied bacterial cells was isolated using Plasmid DNA Miniprep Kit (Invitrogen, USA). The presence of the intended mutation was then confirmed by DNA sequencing on ABI Prism 3100 Genetic Analyzer device (Institute of Microbiology, Academy of Sciences of the Czech Republic).

4.4 Electrophysiology

Whole-cell membrane currents were filtered at 2 kHz using the low-pass Bessel filter of the Axopatch 200B amplifier and digitized (5-10 kHz) using a Digidata 1440 unit and pCLAMP 10 software (Molecular Devices, USA). Patch electrodes were pulled from a glass tube with a 1.65-mm outer diameter by a horizontal puller P-1000 (Sutter Instrument Company, USA), the tip of the pipette was heat-polished with a Microforge MF-830 (Narishige, Japan) to a resistance of 3-6 MΩ. The glass microelectrodes were filled with intracellular solution and placed in a holder controlled by micromanipulator MP-255 (Sutter Instrument Company, USA). A silver/silver chloride (Ag/AgCl) reference electrode was submerged into the extracellular bath. Series resistance was compensated by at least 70 % in all recordings. A system for rapid superfusion of the cultured cells was used for drug application (Dittert et al. 2006). Capillary of the application system was placed at a distance of less than 100 μm from the surface of the examined cell.

4.5 Temperature stimulation

The experiments were performed at room temperature (23–25°C). For temperature experiments, a system for fast cooling and heating of solutions superfusing isolated cells under patch-clamp conditions was used as described in (Dittert et al., 2006). Briefly, experimental solutions are driven by gravity from 7 different barrels through automatically controlled valves to a manifold that consists of fused silica tubes (inner diameter of 320 μm) connected to a common outlet glass capillary through which the solutions are applied onto the cell surface. The upper part of the outlet capillary passes the solutions through a temperature exchanger driven by a miniature Peltier device that preconditions the temperature (precooling or preheating). The lower part of the capillary is wrapped with an insulated densely coiled copper wire (over a length of 5 mm, connected to a direct current source for resistive heating) that finally heats the passing solution to a chosen temperature. The Peltier device and the heating element are electrically connected to the headstage probe which is fixed on to a micromanipulator for positioning of the manifold. The temperature of the flowing solution is measured by a miniature thermocouple inserted into the common outlet capillary near to its orifice which is placed at a distance of less than 100 μm from the surface of the examined cell.

The temperature is controlled either automatically or manually by voltage commands *via* the digital-to-analogue converter of a conventional data acquisition interface (Digidata 1440, Molecular Devices, USA). The system allows the application of temperature changes within a range of 5-60°C at maximum rates of –40°C/s to ~110°C/s.

4.6 Measurement of intracellular Ca^{2+} responses

The measurements of intracellular calcium concentration were done with the use of Fura-2-AM dye. The principle using Fura-2 is based on the shift of its fluorescence excitation spectrum toward shorter wavelength upon Ca^{2+} binding. The cells were loaded with 1 M Fura-2-AM (Invitrogen) dissolved in a bath solution for 1 hr followed by a 20-min. wash in fresh bath solution. The Cell^R imaging system (Olympus Biosystems, Germany) was used to capture the fluorescence images obtained with alternating excitation at 340 and 380 nm (TILL Photonics, Germany) and emission at >510 nm. The metal xy positioning microscope stage Olympus IX81 (Olympus Biosystems, Germany) was replaced by plastic stage to prevent electromagnetic field-induced mechanical resonance that impaired the quality of image recording. Emission ratios were calculated for each 0.5-sec. interval after subtraction of the background. Spontaneous activity of cells was measured using excitation/emission wavelengths 380 nm/510 nm and sampling rate ≤500 ms. A system for rapid superfusion of the cultured cells was used for drug application (Dittert et al., 2006). The control experiments were performed for each electromagnetic exposure system during the same day for comparison.

4.7 Confocal microscopy

HEK293T cells transfected with wild-type or S602D mutant of hTRPA1 tagged with tGFP (turbo GFP; Origene Technologies, USA) were stained with the cytoplasmic membrane labeling dye CellBriteTM Fix 640 (Biotium, USA) according to the manufacturer's protocol. Briefly, the cells were incubated in phosphate-buffered saline (1 ml) containing the dye (1 µl) for 20 min at 37 C in a 5% CO_2. After treatment, the cells were washed and imaged in Opti-MEM I media (Invitrogen, USA) supplemented with 5% fetal bovine serum. The colocalization analysis was performed using the

Colocalization Finder plugin in ImageJ and fluorescence intensity profiles measured along a rectangle drawn across the cell membrane.

4.8 Biophysical techniques

All biophysical techniques used to determine the interaction of peptides encoding the C-terminal part of hTRPA1 and PIP_2 were done by Mgr. Lucie Macikova in the laboratory of Dr. Isabel D. Alves at the University of Bordeaux, France. The techniques included preparation of small unilamellar vesicles (SUV), large unilamellar vesicles (LUV), and polymer-based nanodiscs, liposome leakage assay, circular dichroism (CD), plasmon waveguide resonance spectroscopy (PWR), attenuated total reflection infrared spectroscopy (ATR-FTIR) and microfluidic diffusional sizing (MDS). All of the methods are described in (Macikova et al., 2019).

4.9 Homology modeling, molecular docking and molecular dynamics simulations

The molecular dynamics (MD) simulations and the homology modelling were done in collaboration with Dr. I. Barvik from the Faculty of Mathematics and Physics, Charles University., Prague. To obtain a model of human TRPA1 with the S1–S4 sensor domain, the structure with protein data bank (PDB) ID: 3J9P determined by cryo-EM was used (Paulsen et al., 2015). The intracellular loop connecting helices S2 and S3 was modeled using the sequence homology with the TRPP1 channel (structures with PDB IDs: 5K47 (Grieben et al., 2017), 5T4D (Shen et al., 2016), 5MKE and 5MKF (Wilkes et al., 2017)). The homology model of the S2-S3 linker of TRPA1, uploaded on the Model Archive under the accession code ma-auqu1, was created using the Swiss-Model web server (https://swissmodel.expasy.org/). This model was further used to create a model of human TRPA1 with the C-terminal region using the Swiss-Model web server. For fitting the modelled C-terminus into the original density map of human TRPA1 (EMDB ID: 6267), the Molecular Dynamics Flexible Fitting (MDFF) method for combining high-resolution structures with cryo-EM maps was applied.

AutoDock Vina (http://vina.scripps.edu/) was used for the docking of phospholipids into the S1–S4 sensor domain of TRPA1. Yasara 18.4 was used for the docking of phospholipids into the C-terminal binding pocket of TRPA1 and the docking

of the N- (L588-C608) and C-terminal (L992-N1008) peptides from TRPA1 to calmodulin (using the structure PDB ID: 6O20).

All atom structure and topology files were generated using VMD software (Schlenkrich et al., 1996). Introduction of mutations and the phosphorylated state of S602 into the structures was done using the "Mutate residue" and the "Automatic PSF Builder" plugin in VMD. Forces were computed using CHARMM27 force field for proteins, lipids, and ions (Phillips et al., 2005). All molecular dynamics (MD) simulations were produced with the aid of the software package NAMD2.13 or NAMD2.9 (Ryckaert et al., 1977) running on computers equipped with NVIDIA graphics processing units. MD trajectories were visualized with the aid of the VMD 1.9 software package (Humphrey et al., 1996). Figures were produced with the software packages UCSF Chimera (Pettersen et al., 2004), ICM (Molsoft LLC), and CorelDraw X7 (Corel Corporation).

4.10 Statistical analysis

The electrophysiological data were analyzed using pCLAMP 10 (Molecular Devices, USA), and curve fitting of currents and statistical analyses were done in SigmaPlot 10 (Systat Software Inc., USA). Current-voltage (*I-V*) relationships were obtained from steady-state whole cell currents measured at the end of voltage steps. The reversal potential V_{rev} at which the current equals zero was read from the graph and used for calculation of the conductance and construction of the conductance-voltage (*G-V*) relationship.

$$G = \frac{I}{V - V_{rev}}. \quad (3)$$

In some cases, instead of membrane currents, we used the current density obtained by the division of the membrane currents *I* by the cell capacity *C*. Voltage-dependent gating parameters, such as are the minimum and maximum whole-cell conductance G_{min} and G_{max}, the half-maximum activation voltage V_{50} and the apparent number of gating charges *z*, were estimated by fitting the *G-V* relationship as a function of the test potential V to the Boltzmann equation:

$$G = \frac{G_{max} - G_{min}}{1 + e^{\frac{-zF(V - V_{50})}{RT}}} + G_{min}, \quad (4)$$

where *F*, *R*, and *T* have their usual thermodynamic meanings. The activation and deactivation time constants (τ_{fast} and τ_{slow}) were measured directly from outward currents

by performing a double exponential Chebyshev fit to the rising phase of the activating currents and the tail currents, ignoring the initial 1.3 ms.

$$f(t) = A_{fast}e^{-t/\tau_{fast}} + A_{slow}e^{-t/\tau_{slow}} + C, \quad (5)$$

where A_{fast} and A_{slow} are the amplitudes of each component and C is a constant. For comparisons between hTRPA1 and mTRPA1, we calculated a weighted, average time constant of the fast and slow components of activation/deactivation based on the amplitude of each component:

$$\tau_W = \frac{A_{fast}}{A_{fast}+A_{slow}} \cdot \tau_{fast} + \frac{A_{slow}}{A_{fast}+A_{slow}} \cdot \tau_{slow}. \quad (6)$$

From the time constants measured at the same membrane potential V and different temperatures were, the Arrhenius plot was constructed plotting the logarithm of the rate constant $ln\frac{1}{\tau}$ against the reciprocal temperature $\frac{1}{T}$. The difference in enthalpy ΔH and entropy ΔS of the activation/deactivation process was obtained from the linear regression of the Arrhenius plot.

$$ln\left(\frac{1}{\tau}\right) = -\frac{\Delta H - \delta zFV}{R} \cdot \frac{1}{T} + \left(ln\frac{kT}{h} + \frac{\Delta S}{R}\right), \quad (7)$$

where δ is the fraction of the gating charge the fraction of the gating charge moved in the outward direction (estimated as +0.5 for the activation and -0.5 for the deactivation process), k is the Boltzmann constant, h is the Planck constant, and R is the universal gas constant. Corresponding Q_{10} value of was obtained from time constants at two different temperatures T_1 and T_2:

$$Q_{10} = \left(\frac{\tau_1}{\tau_2}\right)^{\frac{10}{T_2 - T_1}}, T_2 > T_1 \, . \quad (8)$$

Statistical significance was determined by Student's t-test or the analysis of variance, as appropriate; differences were considered significant at $P < 0.05$ where not stated otherwise. The data are presented as means ± (or +/-) S.E.M.

4.11 Kinetic modeling and simulation

All kinetic modeling were performed using Copasi 4.22 (Mendes et al., 2009) with the use of the built-in genetic algorithm. The allosteric model with the gate and a voltage sensor was used to characterize the properties of hTRPA1 channels and F1020G mutation in **publication V** (Macikova et al., 2019). The equilibrium between the open and closed state C – O with both resting temperature and voltage sensors is defined by an equilibrium constant L. Changes in voltage lead to transitions between the resting

and active voltage states of the sensor (C1 – C2) with equilibrium constant $K = K_0 \cdot exp(zFV/RT)$, where K_0 is the equilibrium constant for the transition at 0 mV, z is the apparent number of gating charges, V is the electric potential, and F, R, and T have their usual thermodynamic meanings. Note that in (Macikova et al., 2019), the voltage sensor equilibrium constants are called J and J_0. The voltage sensor is coupled to the gate by the coupling constant D. By simultaneously fitting the normalized steady-state G–V data and the time course of the activation phase of normalized conductances induced by depolarization to +200 mV, the parameters D, L, and K_0 were obtained for representative cells.

In **publication VII**, the allosteric model was adjusted by the introduction of the temperature sensor. Changes in temperature affect the transitions of the temperature sensor with equilibrium constant $J = exp[-(\Delta H° - T\Delta S°)/RT]$, where $\Delta H°$ and $\Delta S°$ are standard changes in enthalpy and entropy. The temperature sensor is coupled to gate by the coupling constant C, and also to the voltage sensor by a coupling constant E. To include the inverted coupling of the thermosensor (Jara-Oseguera and Islas, 2013) , the temperature dependence of the coupling constant C was introduced by non-zero change in enthalpy of the coupling: $C = exp[-(\Delta Hc° - T\Delta Sc°)/RT]$. Further details are described in (Sinica et al., 2019).

4.12 Stimulation of F11 cells by low-frequency high-induction electromagnetic field

Three different systems for repetitive electromagnetic stimulation were used: EMF1 (VAS-07 STRONG, constructed by EMBITRON s.r.o., Plzen, Czech Republic), EMF2 (SALUTER MOTI, constructed by EMBITRON s.r.o., Plzen, Czech Republic) and EMF3 (DIPOL SETA-D I-100, constructed by NPF Dipol, Vitebsk, Belarus). In order to line the force of alternating magnetic field, the system was oriented so that the surface of the culture dish bottom was as perpendicular as possible. Changes of temperature around the recording area were measured by a sensitive digital thermometer before and after each recording. If the temperature changed more than ~1°C, the data were discarded. Parameters of the systems and stimulation protocols are in the **Table 3** on page 51.

Table 3: Parameters of used systems of high-induction low-frequency electromagnetic field.

Magnetic field	**EMF1**	**EMF2**	**EMF3**
Model name	VAS-07 STRONG	SALUTER MOTI	DIPOL SETA-D, I-100
Magnetic field amplitude	5 mT	2 T	1 T
Intensity of the electrical field	0.2–2 $V \cdot m^{-1}$	20–200 $V \cdot m^{-1}$	20 $V \cdot m^{-1}$
Electrical current density	0.1 – 1 $A \cdot m^{-2}$	10 – 100 $A \cdot m^{-2}$	10 $A \cdot m^{-2}$
Stimulation	Positive impulse of 340 μs and negative part with lower amplitude of 4.5 ms, repetitive frequency	10-s packet of pulses at frequency 1 to 25 Hz, followed by 50 to 2 s after-pause	Rectangular pulses of 170 μs in pack of 6 bursts, delay between the pulses 500 ms, 3.5 s pause after bursts
Frequency	72 Hz	1 Hz / 25 Hz	6 pulses / 10 s

5. List of publications

Below is a list of attached publications and the description of the contribution of Mgr. Viktor Sinica (Synytsya) to the publications presented in the submitted thesis.

Publication I

Prucha, J., J. Krusek, I. Dittert, **V. Sinica**, A. Kadkova and V. Vlachova: *"Acute exposure to high-induction electromagnetic field affects activity of model peripheral sensory neurons."* Journal of Cellular and Molecular Medicine **2018**, 22: 1355-1362. **IF 4.486**, 7 citations

Contribution: Preparation of cell cultures, involvement in calcium imaging experiments, electrophysiological measurements on F11 cells.

Publication II

Kadkova, A., **V. Synytsya**, J. Krusek, L. Zimova and V. Vlachova: *"Molecular basis of TRPA1 regulation in nociceptive neurons. A review."* Physiological Research **2017**, 66: 425-439. **IF 1.655**, 22 citations

Contribution: Preparation of cell cultures, electrophysiological measurements of bradykinin-evoked F11 currents.

Publication III

Barvikova, K., I. Barvik, **V. Sinica**, L. Zimova and V. Vlachova: *"Phospho-Mimetic Mutation at Ser602 Inactivates Human TRPA1 Channel."* International Journal of Molecular Sciences **2020**, 21:7995. **IF 4.556**

Contribution: Preparation of cell cultures, involvement in electrophysiological measurements and control measurements.

Publication IV

Zimova, L., **V. Sinica**, A. Kadkova, L. Vyklicka, V. Zima, I. Barvik and V. Vlachova: *"Intracellular cavity of sensor domain controls allosteric gating of TRPA1 channel."* Science Signaling **2018**, 11:eaan8621. **IF 6.467**, 16 citations

Contribution: Shared first co-authorship, preparation of cell cultures, electrophysiological measurements of wild-type and selected TRPA1 mutants at different temperatures, data analysis, and participation in discussions about the results.

Publication V

Macikova, L., **V. Sinica**, A. Kadkova, S. Villette, A. Ciaccafava, J. Faherty, S. Lecomte, I. D. Alves and V. Vlachova: *"Putative interaction site for membrane phospholipids controls activation of TRPA1 channel at physiological membrane potentials."* The FEBS Journal **2019**, 286:3664-3683. **IF 4.392**, 3 citations

Contribution: Preparation of cell cultures, electrophysiological measurements of TRPA1 and the F1020G mutant at different conditions, data analysis, and participation in discussions about results.

Publication VI

Zimova, L., K. Barvikova, L. Macikova, L. Vyklicka, **V. Sinica**, I. Barvik and V. Vlachova: *"Proximal C-Terminus Serves as a Signaling Hub for TRPA1 Channel Regulation via Its Interacting Molecules and Supramolecular Complexes."* Frontiers in Physiology **2020**, 11:189. **IF 3.367**, 4 citations

Contribution: Preparation of cell cultures, electrophysiological measurements of TRPA1 and TRPA1 coexpressed with MARCKS or Dr-VSP at different temperatures, data analysis, and participation in discussions about the results.

Publication VII

Sinica, V., L. Zimova, K. Barvikova, L. Macikova, I. Barvik and V. Vlachova: *"Human and Mouse TRPA1 Are Heat and Cold Sensors Differentially Tuned by Voltage."* Cells **2019**, 9:57. **IF 4.366**, 7 citations

Contribution: Conceptualization of the project, preparation of cell cultures, site-directed mutagenesis, electrophysiological measurements of mouse and human TRPA1, and their mutant constructs at different temperatures, data analysis, involvement in two-state and allosteric kinetic modeling, discussions about the results, experimental procedures and project in general.

Below is a list of publications not included in the dissertation and the description of the contribution of Mgr. Viktor Sinica (Synytsya).

Publication VIII

Bernal, L., Sotelo-Hitschfeld, P., König, C., **Sinica, V.**, Wyatt, A., Winter, Z., Hein, A., Touska, F., Reinhardt, S., Tragl, A., Kusuda, R., Wartenberg, P., Sclaroff, A., Pfeifer, J.D., Ectors, F., Dahl, A., Freichel, M., Vlachova, V., Brauchi, S., Roza, C., Boehm, U., Clapham, D.E., Lennerz, J.K., Zimmermann, K.: *„Odontoblast TRPC5 channels signal cold pain in teeth“* Science Advances **2021**, 7:eabf5567. **IF = 13.117**

Contribution: preparation of the neuronal cell culture from transgenically modified mice, electrophysiological measurements of TRPC5-positive mice neurons, measurement optimization, data analysis

6. Summary of the results

6.1 Regulation of TRPA1 by cellular pathways and phosphorylation

6.1.1 Publication I - Acute exposure to high-induction electromagnetic field affects activity of model peripheral sensory neurons

Damaged, inflamed and injured neuronal tissue is a source of pain-sensation requiring pain-relief treatments. One of the approaches of pain treatment is the use of high-induction low-frequency electromagnetic field (LF-EMF). When applied peripherally over a muscle or spinal nerve roots, LF-EMF is capable of improving sensorimotor impairments and reducing acute and persistent pain (Smania et al., 2003, Lo et al., 2011, Khedr et al., 2012, Masse-Alarie et al., 2017). The understanding of the mechanisms underlying the biological effects and cellular targets of LF-EMF exposure is still limited. There is considerable evidence that LF-EMF effects are produced by the voltage-gated Ca^{2+} channels (Piacentini et al., 2008, Cui et al., 2014, Sun et al., 2016). However, LF-EMF also acts *via* upregulation of the components of inflammatory pathways, arachidonic acid (AA) and prostaglandin E2 (Ongaro et al., 2012), that further sensitize both the excitatory and inhibitory ion channels. These different mechanisms of action may underlie diverse effects of LF-EMF depending on the cell type and cell environment. In order to assure a rational and safe usage of electromagnetic stimulators in future clinical practice (Rossini et al., 2015), cellular processes affected by exposure to high-induction electromagnetic field have to be considered and appropriately characterized in a strictly cellular-specific context.

In the **publication I**, we aimed at investigating the impact of three commercially-utilized LF-EMF (EMF 1-3, see Methods 3.12) systems on calcium responses induced in naïve and transfected cells by an inflammatory agent – bradykinin (BK). As a model of peripheral neurons, we used the cell culture of F11 cells, a somatic hybrid of a rat embryonic dorsal root ganglion (DRG) and mouse neuroblastoma cell line N18TG2. The systematic functional and transcriptomic characterization (Yin et al., 2016) demonstrated that F11 cell line represents a convenient model to study the cellular mechanisms of sensory transduction and transmission in vitro – the cells endogenously express a range of receptors and ion channels with potential roles in

neuronal signaling and intracellular pathways: voltage-gated K^+ and Na^+ channels (particularly $Na_V1.6$, $Na_V1.7$ and $K_v11.1$) and also both B1 and B2 bradykinin receptors.

We measured the membrane currents in response to repeatedly applied set of 20-ms voltage pulses ranging from -40 mV to +60 mV in the absence and in the presence of 10 nM bradykinin (**Figure 18**). Bradykinin significantly increased the resting membrane current and decreased the inward currents, which are typical for voltage-gated Na^+ channels. On the other hand, the outward currents mediated by voltage-dependent K^+ channels were only slightly affected.

We examined the effects of three distinct sources of repetitive LF-EMF (EMF1, EMF2, and EMF3) on endogenous Ca^{2+} responses of F11 cells to repeated applications of 10 nM BK (**Figure 19** on page 57). We applied two subsequent BK exposures, each lasting 30 s and separated by 3 min. In the control experiments (without EMF1 or EMF2), both application of BK induced Ca^{2+} responses with the second response largely reduced. Continuous exposures to electromagnetic field affected the bradykinin responses: EMF1 and EMF2 markedly suppressed and delayed only the second BK

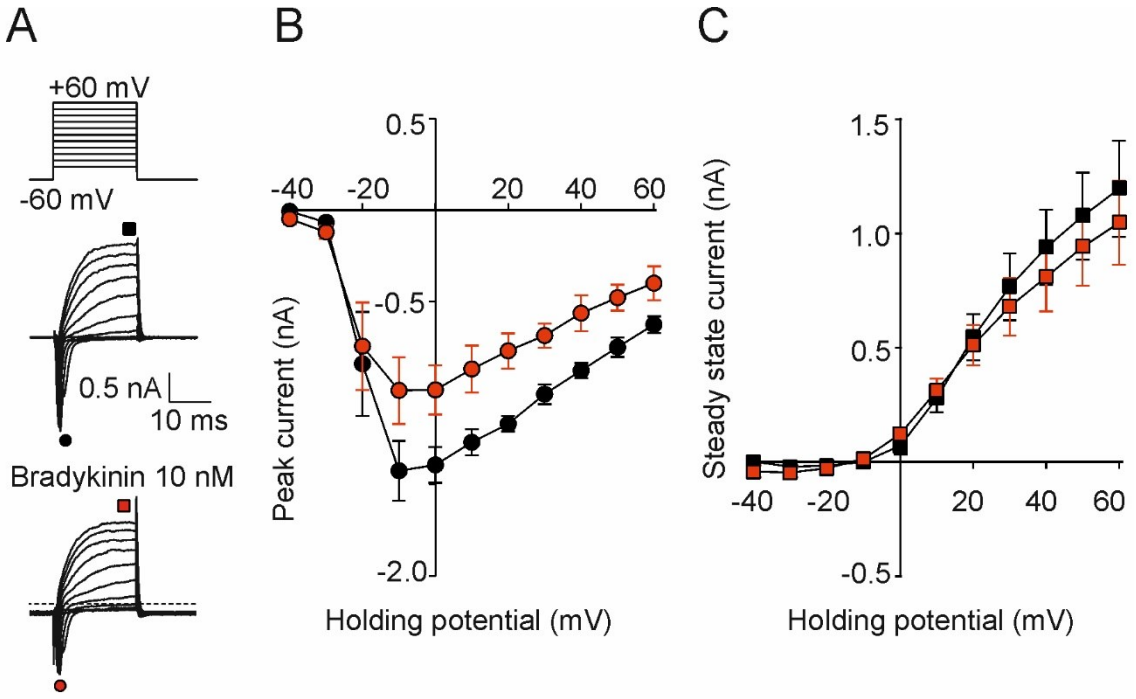

Figure 18: *Whole-cell patch-clamp recordings from a naïve F11 cell in the absence and in the presence of 10 nM bradykinin.* ***(A)*** *The currents were obtained by the voltage-step protocol above.* ***(B,C)*** *Both peak currents (circle) and steady-state currents (square) reflecting the activation of Na^+ and K^+ responses were used for the construction of the average I-V relationships (mean ± S.E.M., n = 3).*

response, while EMF3 caused a significantly delayed onset and reduction of the first BK response (**Figure 19**).

Apart from BK-evoked currents, around 19 % of F11 cells also exhibit spontaneous Ca^{2+}- activity (**Figure 20.A** on page 58). The spontaneous activity seems to be promoted by the presence of magnetic field; the EMF3 had most pronounced effects on F11 responses. We quantified the spontaneous activity evoked by EMF3 using Fast Fourier Transformation on the signal from 380 nm excitation length. The resulting average power spectra revealed a clear increase in power spectral density within the frequency range of ~0.03–0.3 Hz upon EMF3 stimulation (**Figure 20.B** on page 58).

Furthermore, we wanted to check, whether the LF-EMF itself would modulate TRPA1 channel's activation. F11 cells transiently expressing TRPA1 channels and GFP already exhibited increased basal level of intracellular calcium. Prolonged application of EMF2 did not induce any response in TRPA1 and GFP- expressing cells. However,

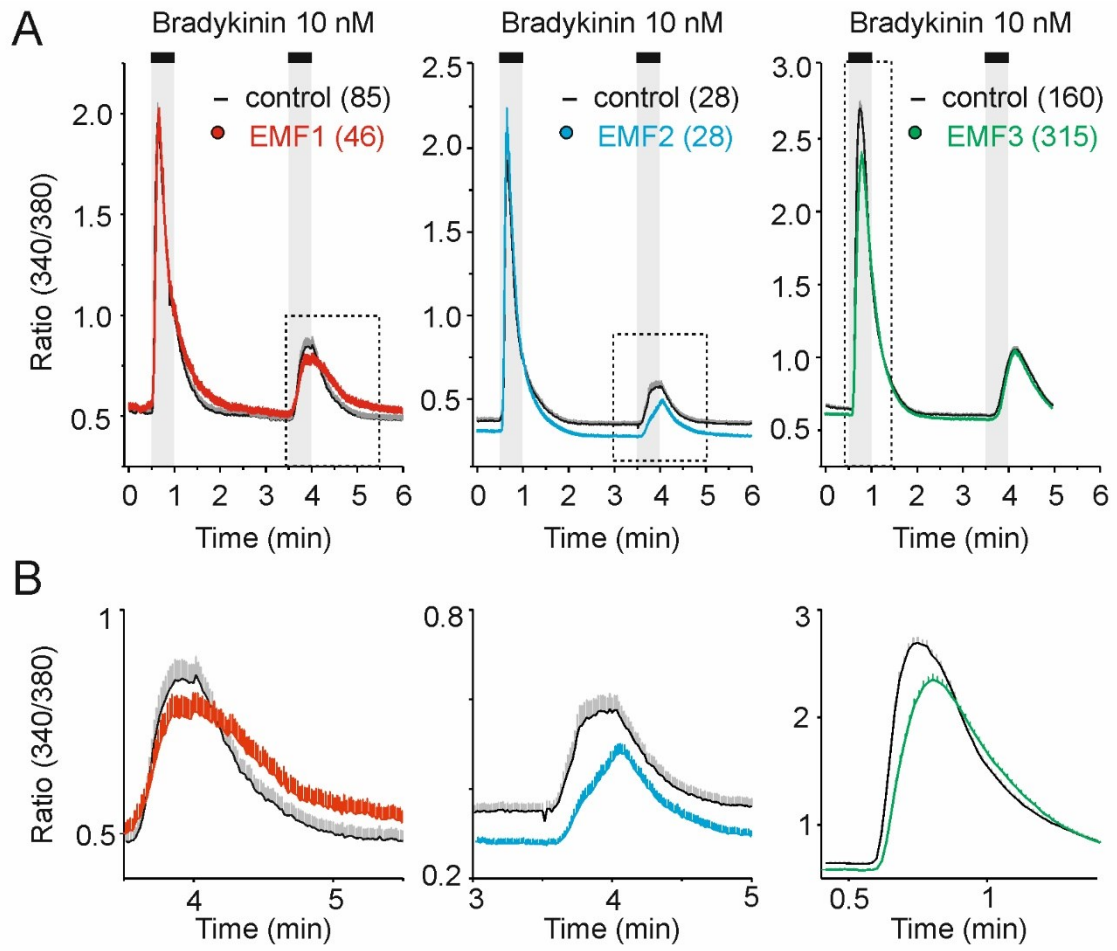

Figure 19: ***(A)*** *Average calcium responses obtained from control cells and from cells continuously exposed to three different types of electromagnetic field (EMF1, EMF2, EMF3). Continuous curves are the mean, color envelopes the +S.E.M. (n indicated in parentheses).* ***(B)*** *Bradykinin responses to bradykinin from the insets in* ***(A)***.

calcium transients occurred after discontinuation of EMF2. The same cells were activated by the second EMF2 stimulation. The cells that did not respond to second EMF2 consistently responded to application of 50 mM KCl.

Overall, the results provide evidence that electromagnetic field may directly modulate the activity of sensory neurons, and that LF-EMF can inhibit bradykinin-induced calcium responses in F11 cells.

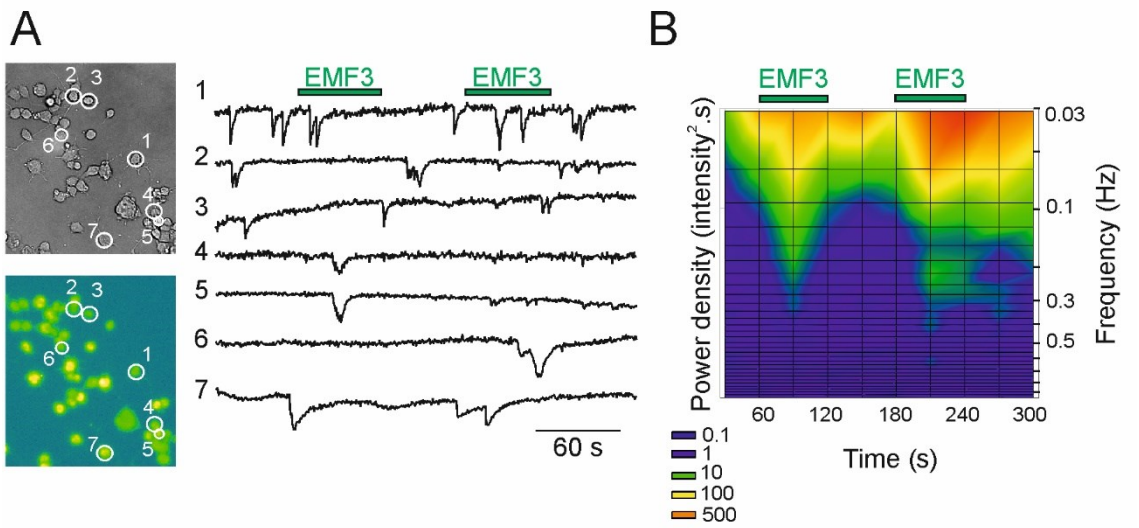

Figure 20: (A) *Spontaneous Ca^{2+} activity in seven representative Fura-2-loaded cells exposed twice to 60 sec. to EMF3, recorded using one excitation wavelength (380 nm). Brightfield image and an image taken at 510 nm emission wavelength are shown.* ***(B)*** *Average power spectrum obtained from 154 cells using Fast Fourier Transformation.*

6.1.2 Publication II - Molecular basis of TRPA1 regulation in nociceptive neurons. A review

It is known, that stimulation of B1 or B2 receptors by bradykinin can initiate either the phospholipase C pathway or activation of the AC to produce cAMP. As a final product, Ca^{2+} influx as well as the activated PKC and PKA modulates the TRPA1 channel *via* direct activation or inhibition (Ca^{2+}) or phosphorylation. The effect of phosphorylation can therefore be masked by Ca^{2+}-dependent modulation. Also the gradual agonist-induced sensitization of TRPA1 precludes from clearly differentiating the effects of kinase modulators (Meents et al., 2016). Furthermore, the use of phosphomimicking and phosphonull mutations in the investigation of phosphorylation also have some limitations (Hynkova et al., 2016).

The **publication II** aims at reviewing of the available results of site-directed mutagenesis studies regarding the posttranslational modification of TRPA1. Special attention is brought on bradykinin-evoked pathways and phosphorylation by sarcoma kinase (Src), cyclin-dependent kinase (Cdk5) and casein kinase 2 (CK2). Although the **publication II** is a review, it contains our original experimental data as well. It provides the first experimental evidence of how the transient expression of TRPA1 influences the cellular responses to membrane depolarization. When the TRPA1 channels are relatively overexpressed in F11 cells, the voltage-gated Na^+ currents were fully dampened (**Figure 21.A-B**). We also measured the endogenous Ca^{2+} responses of F11

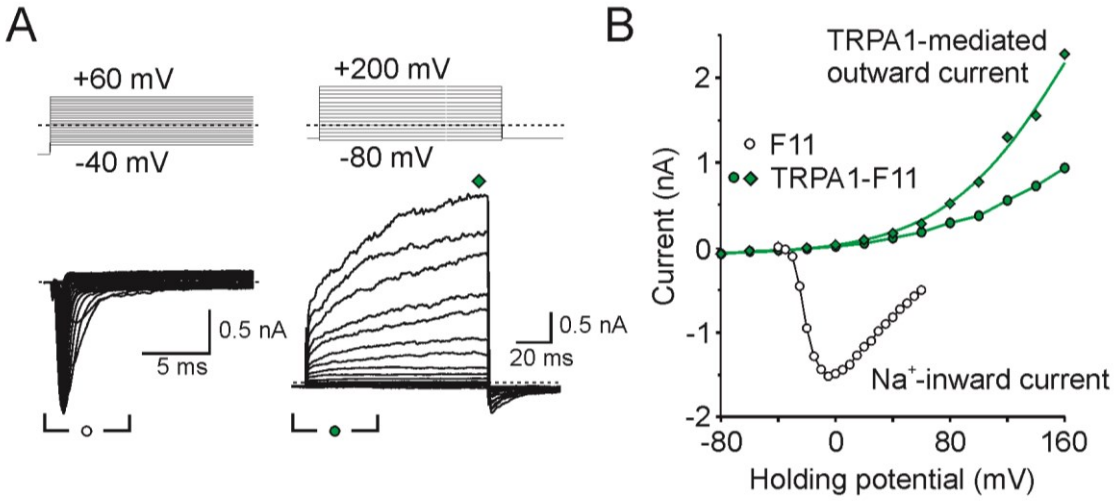

Figure 21: ***(A)*** *Whole-cell recordings of naïve F11 cells (left) and F11 cells transiently expressing TRPA1 channels (right) using the voltage step protocols (shown above).* ***(B)*** *The peak currents (circles) and steady-state currents (diamonds) were used to construct the average I-V relationship.*

cells expressing TRPA1 channels to repeated applications of 10 nM BK and AITC in order to clarify how the TRPA1 responses are modulated by the BK-mediated effects (**Figure 22.A**). TRPA1-expressing cells exhibited increased basal calcium levels likely due to constitutively opened TRPA1 channels. The response to BK slightly increased the second BK response, but the persistent increase in the basal level of intracellular calcium, which would be a sign of the TRPA1 sensitization by phosphorylation, was not present. The responses of cells preactivated by AITC were transient and partially additive (**Figure 22.B**). These results suggest that TRPA1 does not undergo long-term modulation induced by BK. It is possible that increased cellular Ca^{2+} due to the overexpression of TRPA1 makes the regulation more difficult.

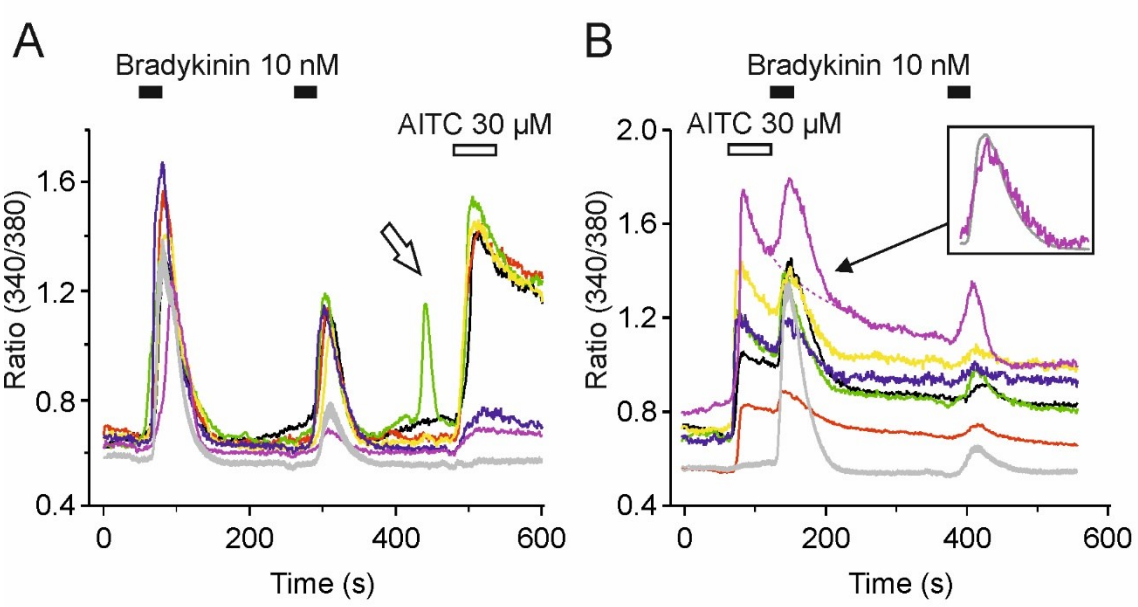

Figure 22: (A) *Calcium responses of naïve F11 cells (gray line representing mean + S.E.M. of 14 recordings) and six individual responses of F11 cells expressing TRPA1 channels to application of 10 nM bradykinin and 30 µM AITC. The white arrow denotes spontaneous calcium transient.* ***(B)*** *Calcium responses of naïve F11 (n = 19) and individual TRPA1-expressing F11 cells to concurrent application of bradykinin and AITC. The bradykinin response subtracted from the extrapolated AITC response is compared with the average response of naïve F11 cells in the inset.*

6.1.3 Publication III – Phospho-Mimetic Mutation at Ser602 Inactivates Human TRPA1 Channel

The new structural data coming from the cryo-EM structures of TRPA1 channel with bound electrophilic agonists suggest that the mechanism of electrophilic activation involves conformation rearrangements in the N-terminal coupling domain and the C-terminal TRPL helix (Suo et al., 2020, Zhao et al., 2020). These regions are structurally preceded by a serine residue S602, which has been predicted by various prediction servers to be a substrate for several protein kinases (the list of prediction servers is reviewed in (Savage and Zhang, 2020)). Because of the location, the phosphorylation of S602 may strongly impact the TRPA1 channel gating. In **Publication III**, we used site-directed mutagenesis, whole-cell electrophysiological measurements, confocal microscopy and molecular modeling in order to explore the role of this residue as a potential target of phosphorylation.

First, we measured the membrane currents of HEK293T cells expressing wild-type or mutant hTRPA1 channels with a series of depolarization pulses from -80 mV to +140 mV, followed by a repeated stimulation by voltage ramps from -100 mV to +100 mV (**Figure 23.A** on page 62). Interestingly, while the phosphonull mutation S602G exhibited similar responses as WT, the phosphomimicking mutation S602D was non-functional. Both tGFP-tagged WT and S602D TRPA1 showed qualitatively similar colocalization with a membrane-visualizing dye CellBrite^{TM} Fix 640, suggesting that the inactivity of S602D is not due to low surface-expression.

We then tested the structural role of S602 and the residues in its vicinity by the ramp stimulation in the presence of electrophilic AITC and the non-covalent agonist carvacrol (Carv). We chose K603 and R604 because of a potential salt-bridge formation with the S602D mutant, and also W605, which represents a putative consensus binding site for calmodulin and a possible phosphorylation site (Zimova et al., 2020). The S602D and both double-mutants S602D/K603 and S602D/R604 did not produce any response in the presence of agonists, while the S602N was not significantly different from WT TRPA1 channels (**Figure 23.B** on page 62). The data suggest that introduction of a negatively charged group of asparagine or the potential phosphate group may render the TRPA1 channel inactive to both chemicals and voltage.

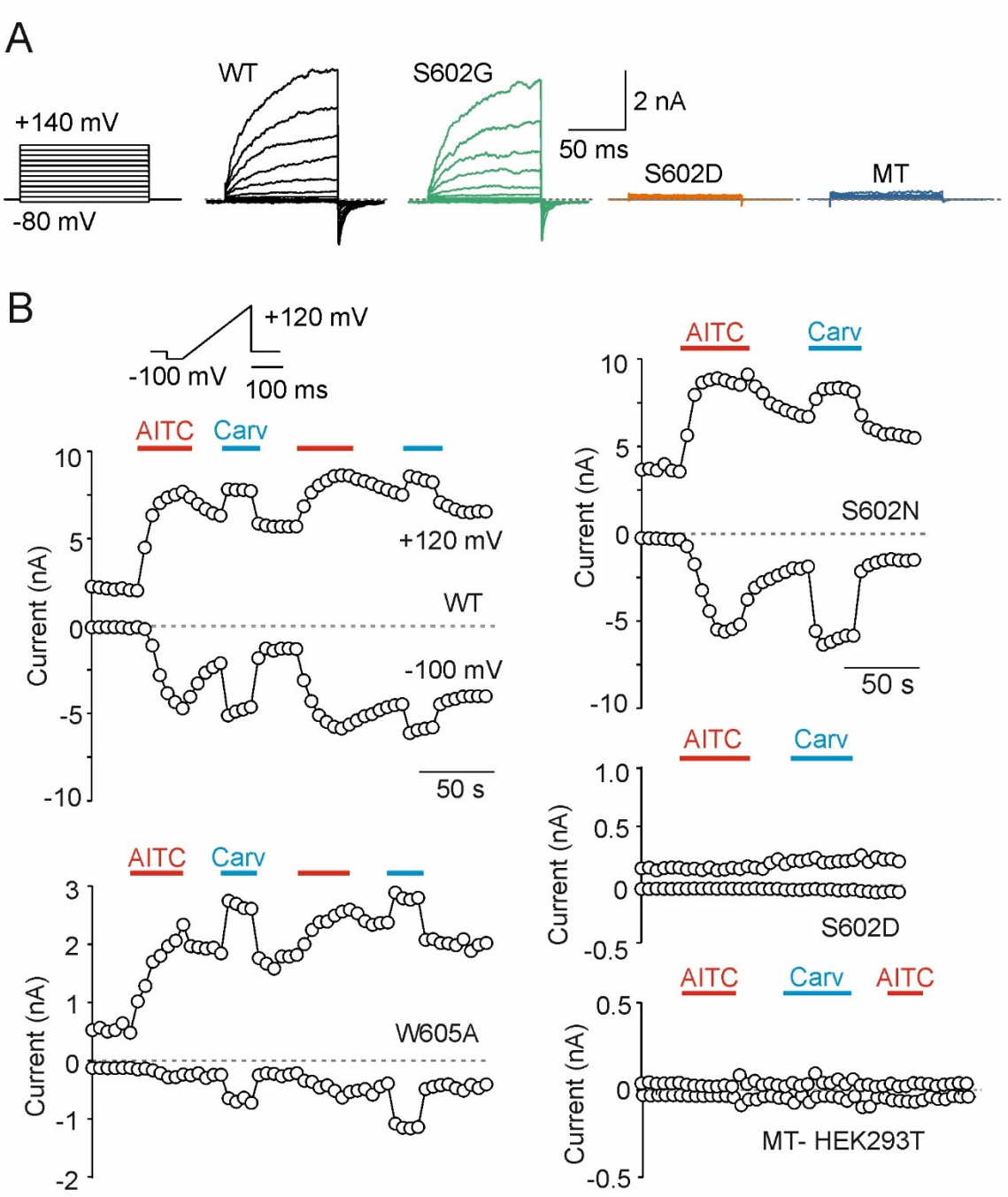

***Figure 23**: **(A)** Currents through wild-type TRPA1 (WT), S602G, and S602D channels and currents from HEK 293T cells transfected with control plasmid (MT) induced by indicated voltage-step protocol. **(B)** Time course of representative whole-cell current responses induced by a ramp protocol (shown at the top left corner) in the presence of 100 µM AITC or 50 µM carvacrol (Carv). The currents were subtracted at -100 mV and +120 mV.*

The conformational changes induced by modification of S602 were further investigated by running the 42-44 ns long MD simulations using the structure of hTRPA1 channel in the open state (PDB ID: 6V9X). The simulations were performed on the WT and structures with S602 substituted with aspartate, asparagine and

phosphoserine. WT and S602N the side chain at position 602 forms H-bonds with the carbonyl groups of T598 and I599 (**Figure 24.A**). In S602D and p-S602 the side chain is oriented to the aqueous environment (**Figure 24.B**). The cluster of bulky aromatic amino acids of W605, F640 and Y662 does not change their position in WT and S602N mutant, while the distance of F640 and Y662 is more pronounced in S602D and p-S602. Importantly, the distance between the important interacting residues K671 from the A-loop and E987 from the TRPL helix was increasing during the MD simulation in S602D mutant and p-S602 TRPA1 (**Figure 24.C,D**). The possible transduction pathway of the effect of mutation/phosphorylation into the channel's gating involves a cluster of bulky amino acids F640, W605 and Y662, which is in line with the impaired function of W605A mutant. These results suggest the possible structural mechanism of the inactivation of the TRPA1 channel by the modification of S602.

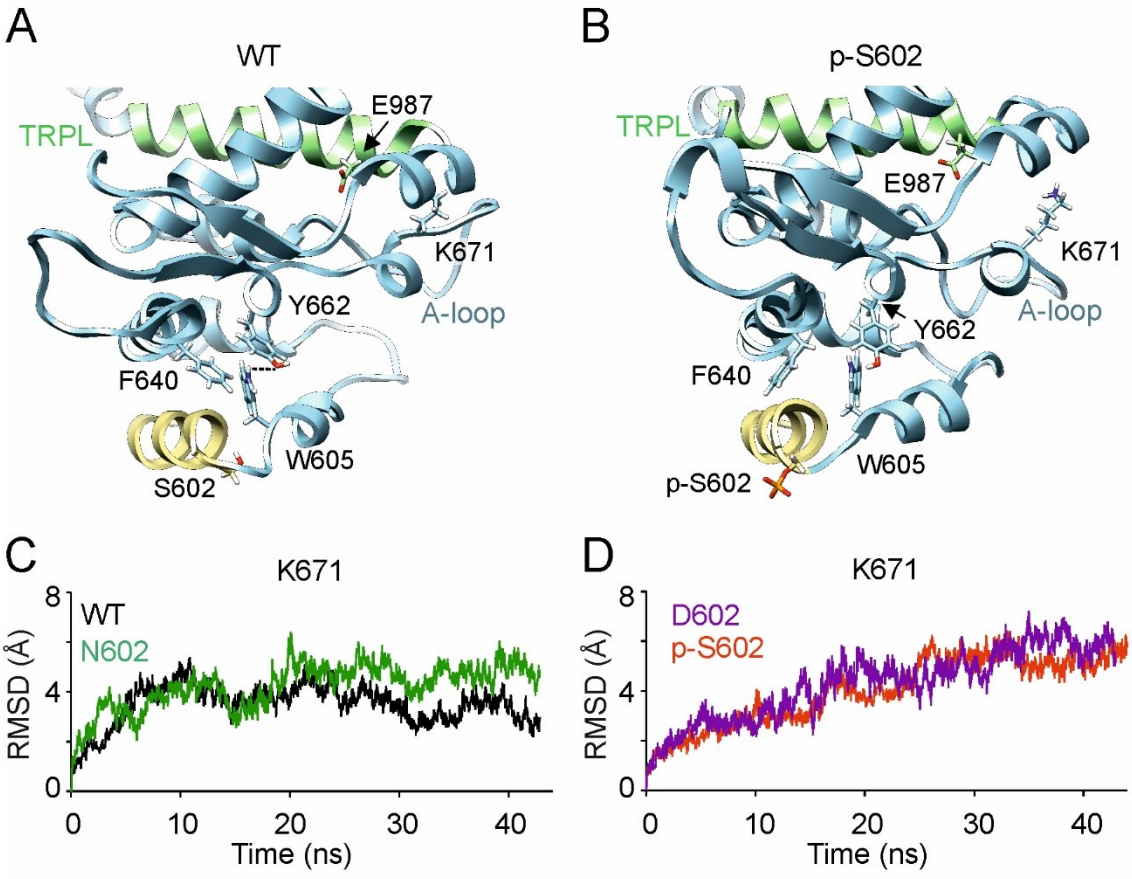

Figure 24: (A,B) *Close-up view of the cluster of amino acids F640, W605 and Y662 of TRPA1 WT and TRPA1 with phosphorylated serine 602 (p-S602).* ***(C,D)*** *Time course of the average root mean square deviation (RMSD) values for K671, measured from the indicated TRPA1 constructs*

6.2 The putative binding sites of regulatory lipids

6.2.1 Publication IV - Intracellular cavity of sensor domain controls allosteric gating of TRPA1 channel

The activation of TRPA1 channel by electrophilic agonists involves an allosteric mechanism that couples the structural changes upon the binding of an electrophile into the channel's gate. In such process, an important part is played by the intracellular cavity formed by the S1-S4 helices of the VSLD together with the TRPL helix. The comparative sequence analysis conducted on a large ensemble of K_v and TRP channel sequences shows that TRP channels differ from the K_v channels in the asymmetrical solvation of VSLD (Palovcak et al., 2015). The conserved polar residues of the TRPV1, TRPV2 and possibly TRPA1 inside of the intracellular cavity may facilitate the solvation of the region and the interaction with endogenous lipids (Liao et al., 2013, Palovcak et al., 2015, Paulsen et al., 2015, Huynh et al., 2016). In **publication IV**, we characterized the conserved polar residues facing the putative lower crevice of the sensor domain that were crucial determinants of the electrophilic, voltage, and calcium sensitivity of the TRPA1 channel. We also investigated the possibility of interaction with endogenous lipids within the VSLD cavity.

First of all, we wanted to see whether the VSLD and the TRPL helix indeed may form a hydrated cavity. For this purpose, we constructed a model of hTRPA1 using the available cryo-EM structure (PDB ID: 3J9P). The missing S1-S2 loop and the S2-S3 loop were modeled with the use of sequence homology with the TRPP2 channel. The model showed that the water molecules can permeate into the highly hydrophilic cavity with the polar residues facing inside (**Figure 25.A,D** on page 65). Because of the positive electrostatic potential in the bottom part of the cavity, we used the ligand docking and molecular dynamics (MD) simulations to test the binding of PIP_2 into the cavity. Indeed, the inositol trisphosphate head group of PIP_2 may adopt several conformations with contacts to H719, N722, K787, K796, R852 and K989 (**Figure 25.B,C,E** on page 65).

Next, we assessed the properties of polar amino acids that face the cavity according to the predicted model. We created the single point mutations of the selected polar residues and measured the voltage-dependent activation properties of the WT and

mutants expressed in HEK293T cells (**Figure 26** on page 66). The voltage step protocol ranging from -80 mV to +200 mV revealed that five of six mutants of residues involved in PIP_2 binding, namely H719A, N722A, K787A, K796A and R852A, had their voltage sensitivities shifted toward more positive voltage, and suppressed currents at both negative and positive potentials (**Figure 26.B-D** on page 66). On the other hand, the E788A, E788K, N805A, and E808A mutants exhibited significantly increased currents at positive membrane potentials and also low activity at basal currents, a feature that cannot be explained only by a shift of the voltage sensor sensitivity (**Figure 26.E-I** on page 66). The mutations of H719A, N722, K787, K796, E788 and E808 exhibited

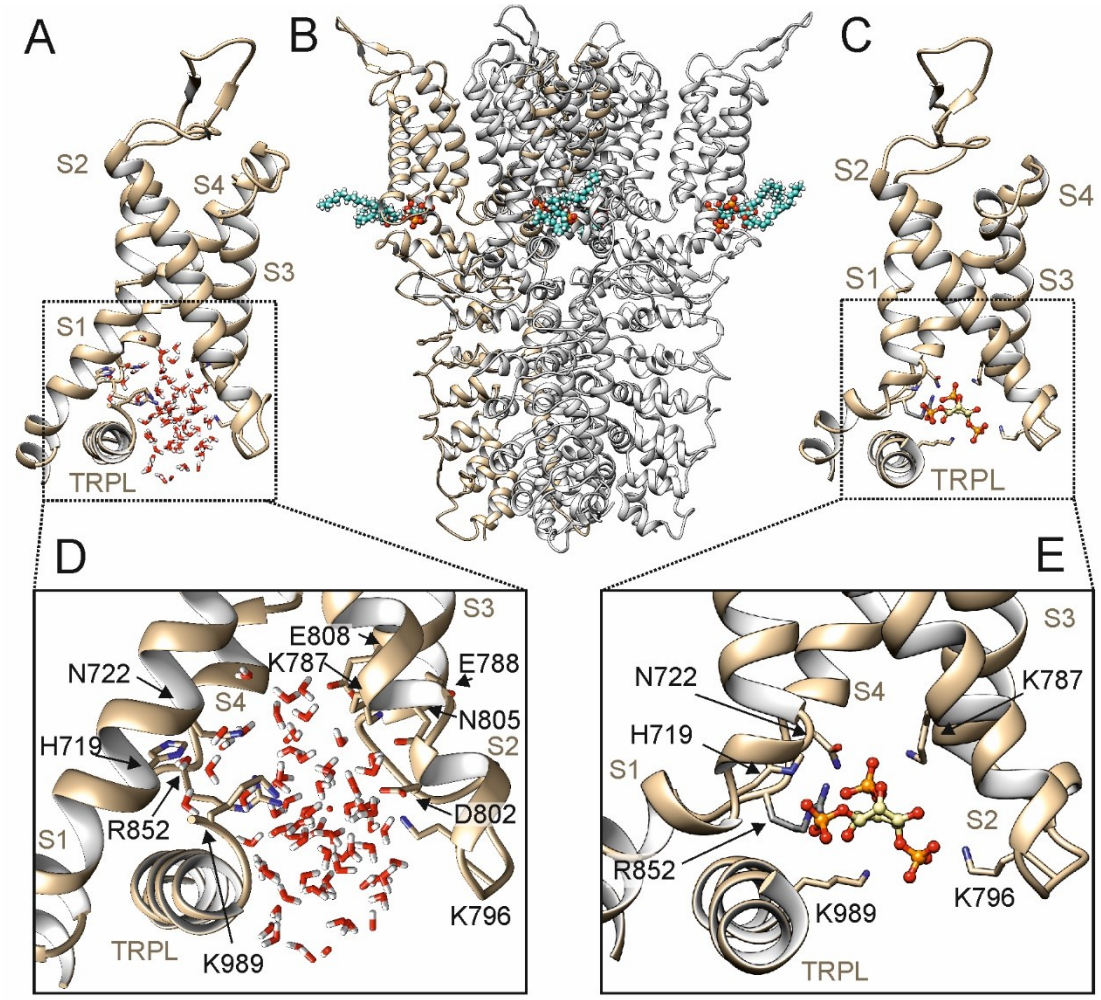

Figure 25: ***(A)*** *A structure of TRPA1 channel 3J9P completed with the model of the S1-S2 and S2-S3 linkers. The molecular dynamics (MD) simulation confirmed the solvation of the intracellular cavity of the VSLD.* ***(B)*** *The result of the MD simulation of the model of TRPA1 with four molecules of PIP_2 placed into the VSLD cavity by ligand docking. For a better view, the rest of the PIP_2 molecule was not shown* ***(C)*** *The model of the VSLD cavity with established contacts with the negatively charged inositol trisphosphate head group of PIP_2. The insets show a detail of the VSLD intracellular cavity with water molecules* ***(D)*** *or PIP_2* ***(E)*** *The best fits are shown.*

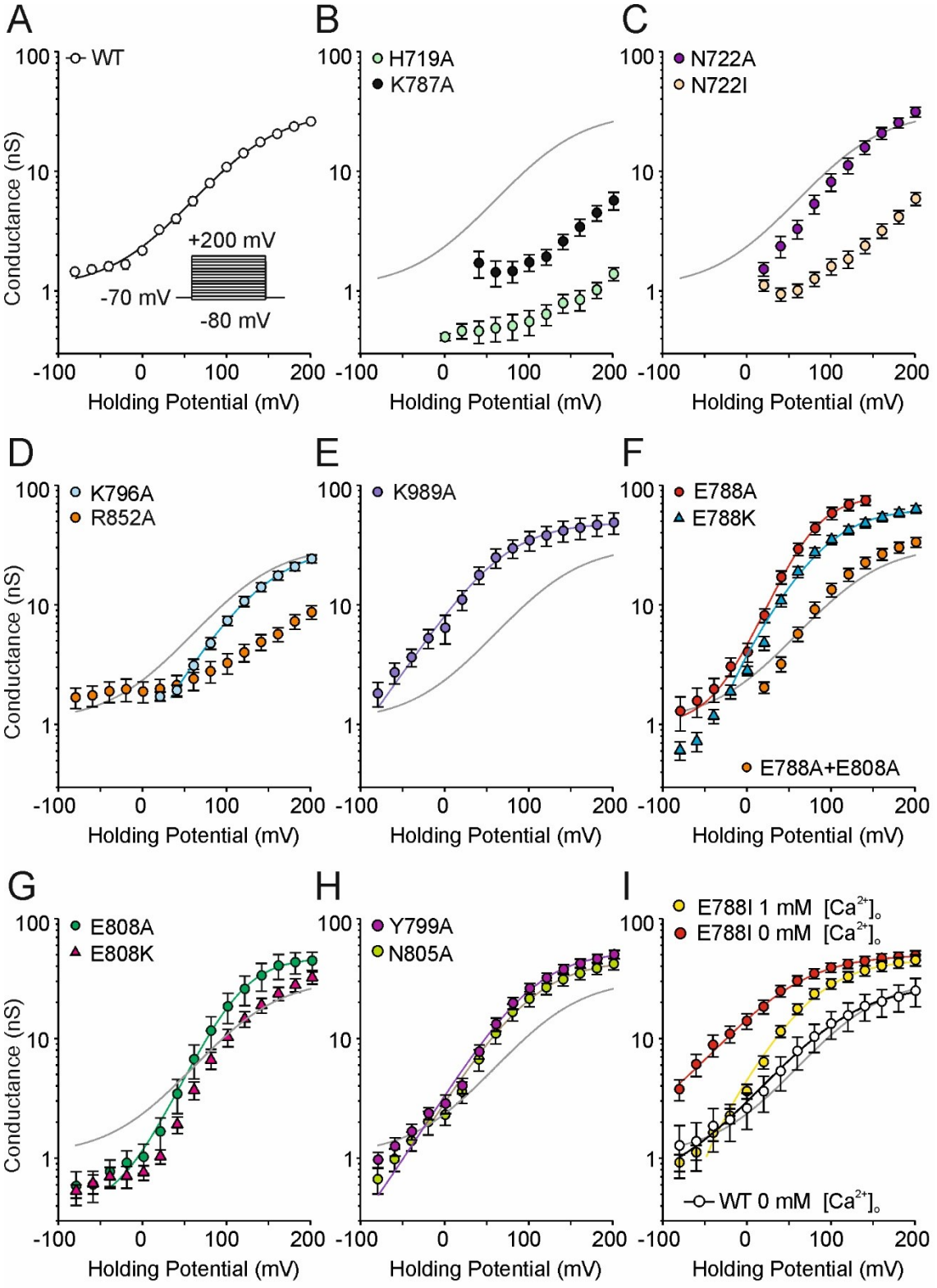

Figure 26: *Average conductances of hTRPA1 and indicated mutants, obtained at the end of each pulse of the voltage-step protocol (top left corner). Data are means ± S.E.M. (n = 132 cells for wild-type and n = 6 to 30 cells for mutants from at least two independent transfections). The lines represent the best fit to a Boltzmann function for wild-type and mutant TRPA1 (gray and colored lines). All measurements were done in the presence of 1 mM external Ca^{2+}; the measurements in* ***(I)*** *were conducted also in 0 mM Ca^{2+}.*

extremely fast deactivation kinetics upon repolarization, which is probably due to the calcium-dependent blockage – the suppressed currents of the mutant E788I at negative potentials were greatly increased in the absence of external Ca^{2+} (**Figure 26.I** on page 66).

We tested the chemical sensitivity of the mutants to electrophilic agonists of different potency, allyl isothiocyanate (AITC) and cinnamaldehyde (Cin), using the repeated ramp protocol ranging from -80 mV to +80 mV (**Figure 27** on page 68). We also investigated the potentiation and inactivation effects of 2mM Ca^{2+} on the electrophilic activation. In line with the previous measurements, mutations of residues H719, N722, K787 and R852 impaired the activation by AITC or Cin; the impairment was more pronounced at negative potentials (**Figure 27.B,C** on page 68). The gain-of-function mutants E788A and E808A displayed robust responses to Cin, reaching more than twice the maximum currents obtained from the WT-TRPA1 at +80 mV (**Figure 27.E,F** on page 68). Rapid inactivation induced by the external Ca^{2+} ions was present in the loss-of-function mutants of H719, N722, K787 and R852, but also in the gain-of-function mutants E788A and E808A, in which the inhibition was again more pronounced at negative voltage.

To further investigate the effects behind the mutations of the glutamates at positions 788 and 808, we created additional site-directed mutations at these positions, as well as the mutations of residues N805A and Y799A that according to the model of the cavity interact with those two glutamates. The charge-swapping mutation E788K displayed increased and more rapid activation by Cin equally at both negative and positive potentials, and identical responses to Ca^{2+} ions as in the WT hTRPA1. Similar results were also obtained for the E788I, N805A and Y799A mutants (**Figure 27.E,H,I** on page 68). Interestingly, the E808K and the double mutant E788A/E808A showed the contrary results – the identical activation by Cin as in WT and an immediate blockage by Ca^{2+} ions (**Figure 27.F,G** on page 68).

These results suggest an important role of the polar residues inside of the intracellular cavity of the VSLD of TRPA1 in the voltage and electrophilic activation, as well as in the modulation by calcium ions. The distinctive effects of mutations indicate that some factor other that simple electrostatic interactions between the charged residues is required to maintain the proper allosteric regulation of TRPA1. We hypothesized, that the binding of a phospholipid (such as PIP_2) inside of the cavity may

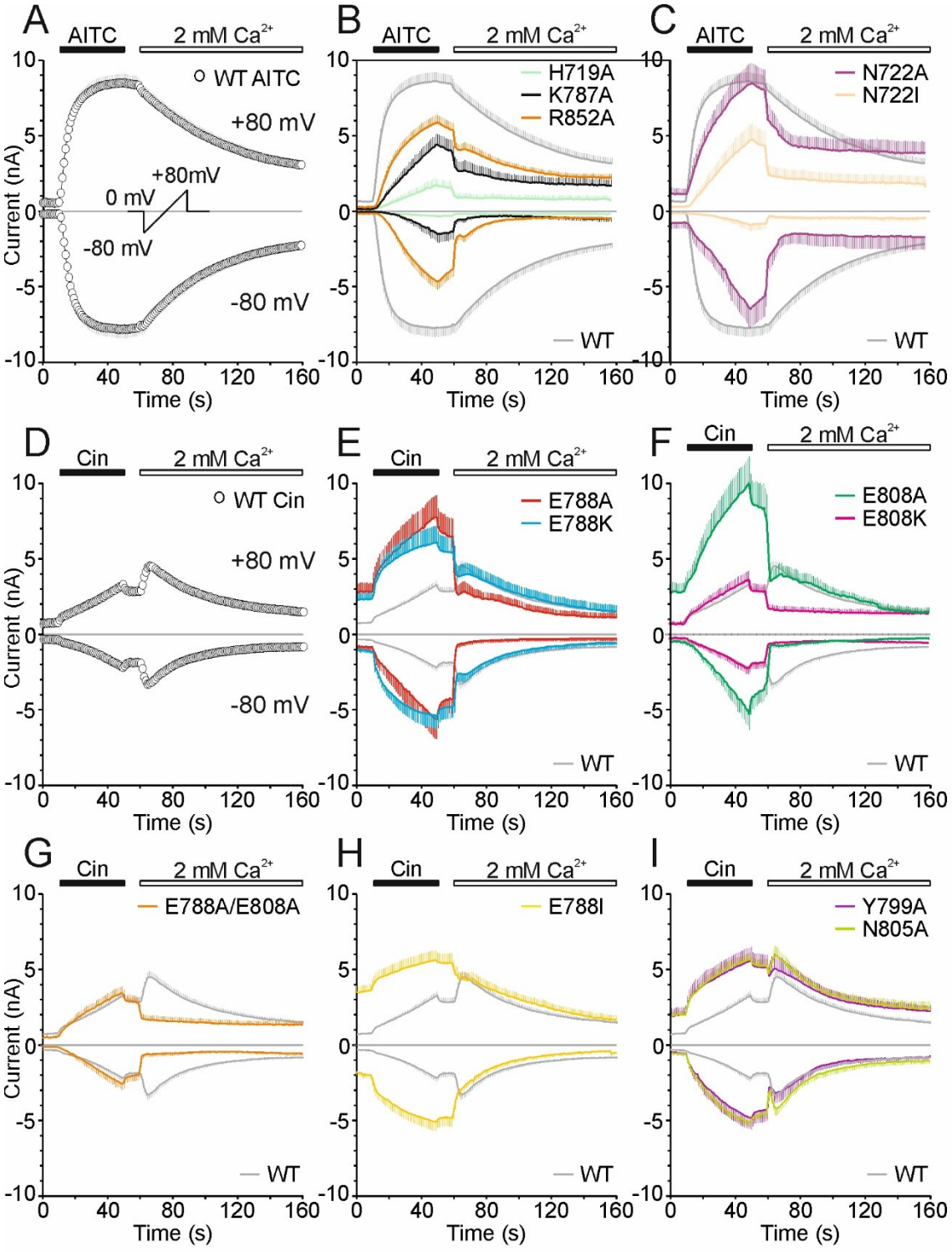

Figure 27: (A-C). *Time course of the average whole-cell currents of wild-type and indicated mutants of TRPA1 channel, measured by the ramp protocol and subtracted at -80 mV and +80 mV. During the experiment, 100 µM of AITC in 0 mM Ca^{2+} was applied (black bar), followed by the solution with 2 mM Ca^{2+} (white bar). Data are shown as circles or lines indicating mean +/- S.E.M., n = 34 for WT and 6-13 for mutants* ***(D-I)*** *The same measurements were conducted with 100 µM cinnamaldehyde (Cin; black bar). Data are shown as circles or lines indicating mean +/- S.E.M., n = 45 for WT and 7-9 for mutants.*

be such factor. The loss-of-function mutations may therefore prevent the stabilization by PIP_2, while the gain-of-function mutations may stabilize PIP_2 inside if the cavity by changing the electrostatic potential. Furthermore, the alterations within the cavity cause a calcium-dependent block. In order to examine the effects of PIP_2 binding to the TRPA1 channel, we used three different approaches to manipulate the membrane PIP_2 levels and measured responses from WT TRPA1.

First, we coexpressed TRPA1 with myristoylated alanine-rich C-kinase substrate (MARCKS), a protein that has basic domains capable of laterally sequestering membrane PIP_2 when the Ca^{2+} ions are absent (**Figure 28.A** on page 70). We observed that the sequestration of PIP_2 by MARCKS had detrimental effects on wild-type TRPA1 functioning, resembling the phenotype of mutants H719A, K787A, N722I, and K796A with responses to voltage and Cin significantly smaller than WT. Moreover, coexpression of the gain-of-function mutant E808A with MARCKS decreased the cinnamaldehyde-evoked currents to the WT level, but also pronounced the blockage evoked by extracellular calcium, resembling the E788A/E808A phenotype (**Figure 28.B** on page 70).

In the second approach, we coexpressed TRPA1 with growth-associated protein 43 (GAP43; also known as neuromodulin), which sequesters PIP_2 when the cytoplasmic Ca^{2+} concentration is increased (**Figure 28.C** on page 70). Coexpression of WT TRPA1 and GAP43 did not change the TRPA1 profiles of current responses induced by Cin in the absence of external calcium, as expected for these control measurements. We then coexpressed the WT TRPA1 with a mutant of GAP43 (R43A-GAP43) that sequestrates PIP_2 regardless of the concentration of Ca^{2+} ions, resulting in reduced current amplitudes, practically identical to those obtained with the expression of MARCKS.

In the third approach, we used a voltage-sensitive lipid 5-phosphatase from *Danio rerio* (Dr-VSP) that can be induced by depolarization greater than +50 mV and results in the hydrolysis of PIP_2 into DAG and IP_3 (**Figure 28.D** on page 70). We coexpressed Dr-VSP with TRPA1 and stimulated the cells with a 2-s depolarizing prepulse to +80 mV before each application of the standard voltage step protocol (Fig. 7E). Cotransfecion of WT with Dr-VSP and stimulation by a 2-s depolarizing pulse before the measurement resulted in a rightward shift in the *G-V* curves was similar to the effects seen with MARCKS and R43A-GAP43. The Cin-induced currents were

selectively suppressed at negative membrane potentials. Interestingly, the Ca^{2+}-dependent potentiation was pronounced compared to WT.

Overall, the results from the experiments with the modulators of PIP_2 levels suggest that the decrease of available PIP_2 in the membrane leads to a rightward shift in *G-V* characteristics. The effects of all PIP_2 modulators were obscured by the presence of the Ca^{2+} ions, indicating that PIP_2 may regulate the TRPA1 channel in a state-dependent manner and possibly compete with the Ca^{2+} ions to confer the potentiation of TRPA1.

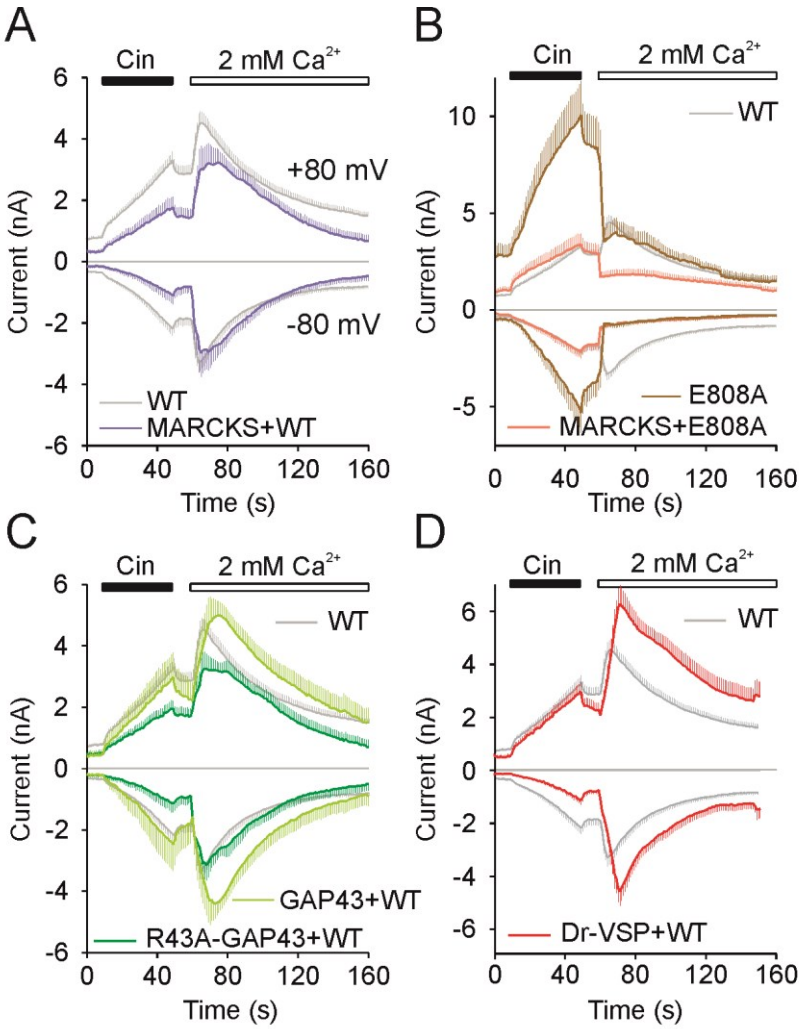

Figure 28: *The time course of average currents of TRPA1 channels, measured at -80 mV and +80 mV, as in* ***Figure 27.*** ***(A,B)*** *The wild-type or E808A mutant was coexpressed with MARCKS protein that sequestrates PIP_2 in the absence of Ca^{2+} ions.* ***(C)*** *The wild-type was coexpressed with GAP43 that sequestrates PIP_2 in the presence of the Ca_{2+} concentration, or with its mutant R43A-GAP43 that sequestrates PIP_2 regardless of the Ca^{2+}.* ***(D)*** *The wild-type was coexpressed with the voltage-sensitive Dr-VSP that cleaves PIP_2 after the induction by depolarizing voltage. Data are presented as mean +/- S.E.M., n = 7-13.*

6.2.2 Publication V - Putative interaction site for membrane phospholipids controls activation of TRPA1 channel at physiological membrane potentials

The sites at which phospholipids may interact with TRPA1 are not resolved, but most likely involve the membrane proximal regions of the N- and C- termini and inter-subunit regions near the inner leaflet of the membrane. We have previously shown, that the 29-residue peptide (I964-L992) corresponding to the TRPL helix from the C-terminus exhibits a high affinity to PIP_2-containing membranes in comparison to other lipids, suggesting that important electrostatic interactions with the negatively charged lipid head groups occur (Witschas et al., 2015). In the study, a peptide Y1006-Q1031 with even higher predicted affinity toward PIP_2 was proposed. The peptide corresponds to a short α-helix between the TRPL helix and the CC helix. According to the electron density map of the TRPA1 channel in a closed state (PDB ID: 3J9P), the unresolved helix is partially embedded into the lower leaflet of the plasma membrane. Together with the adjacent subunit, the helix forms an intracellular vestibule that may possibly accommodate a phospholipid molecule. Moreover, a Ca^{2+} sensing protein calmodulin binds even under the resting concentrations of Ca^{2+} (~100 nM) to TRPA1 within the neighboring region L992-N1008 and may compete for the same or overlapping binding site with PIP_2 or other phosphoinositides. In **publication V**, we investigated the role of both regions in the binding of a PIP_2 molecule using the electrophysiology, site-directed mutagenesis, biophysical approaches and computer modelling.

The biophysical techniques were utilized to characterize the interaction of two peptides of TRPA1 sequence (L992-N1008 and T1003-P1034) with lipids in terms of the affinity (PWR and MDS), effect in lipid membrane organization (PWR), membrane integrity (Rhodamine leakage), and peptide secondary structure (CD). All of these techniques were conducted by Mgr. Lucie Macikova in collaboration with Dr. Isabel Alves and her team at the University of Bordeaux, France. The techniques have shown that both peptides L992-N1008 and T1003-P1034 bind to the lipid membrane only in the presence of PIP_2 with high affinities (300 nM and 700 nM, respectively). The binding of peptides to PIP_2 induced weak perturbations in the lipid ordering.

Using whole-cell electrophysiology, we characterized the functional involvement of the putative short α-helix by substituting the conserved F1020 with glycine to loosen the α-helix. We measured the effect of voltage, electrophile and calcium ions for both WT hTRPA1 and F1020G mutant expressed in HEK293T cells using the same voltage-step protocol and the ramp protocol as in **publication IV** (**Figure 29**). The currents mediated through the F1020G mutant evoked by Cin were significantly smaller only at negative membrane potential and in the absence of Ca^{2+} ions, while the modulation of Cin activation by Ca^{2+} ions was not different from the WT TRPA1 channel.

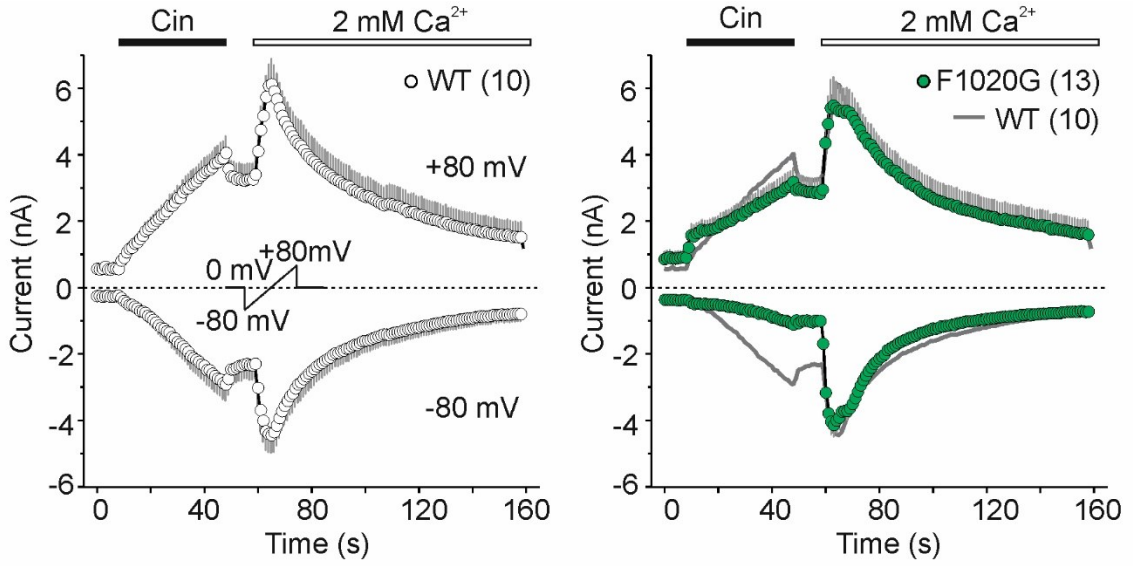

Figure 29: *Time course of the average whole-cell currents of wild-type (white circles) and F1020G mutant (green circles) of TRPA1 channel, induced by 100 µM cinnamaldehyde (Cin) in Ca^{2+}-free solution and then exposed to 2 mM Ca^{2+}. The currents were measured by the ramp protocol (indicated in the left graph) and plotted at -80 mV and +80 mV. The dotted line indicates 0 nA. Data are shown as mean +/- S.E.M., n indicated in brackets.*

The voltage-step protocols revealed that the half maximum activation voltage V_{50} was significantly shifted toward more positive voltages in F1020G mutant; this effect was more pronounced when the calcium ions were present in the extracellular solution (**Figure 30.A-D** on page 73). Also the double exponential fitting of the activation phase of voltage-induced responses and the decay of the tail currents showed significantly faster activation and deactivation kinetics of the F1020G mutant channels (**Figure 30.E-F** on page 73). For further analysis of the WT- and F1020G-mediated currents, we fitted the representative responses from of WT and the F1020 mutant to an allosteric model composed of a voltage sensor coupled to the gate (**Figure 31.A** on page 74). The results of the fitting showed that the mutation F1020G did not affect the equilibrium constant

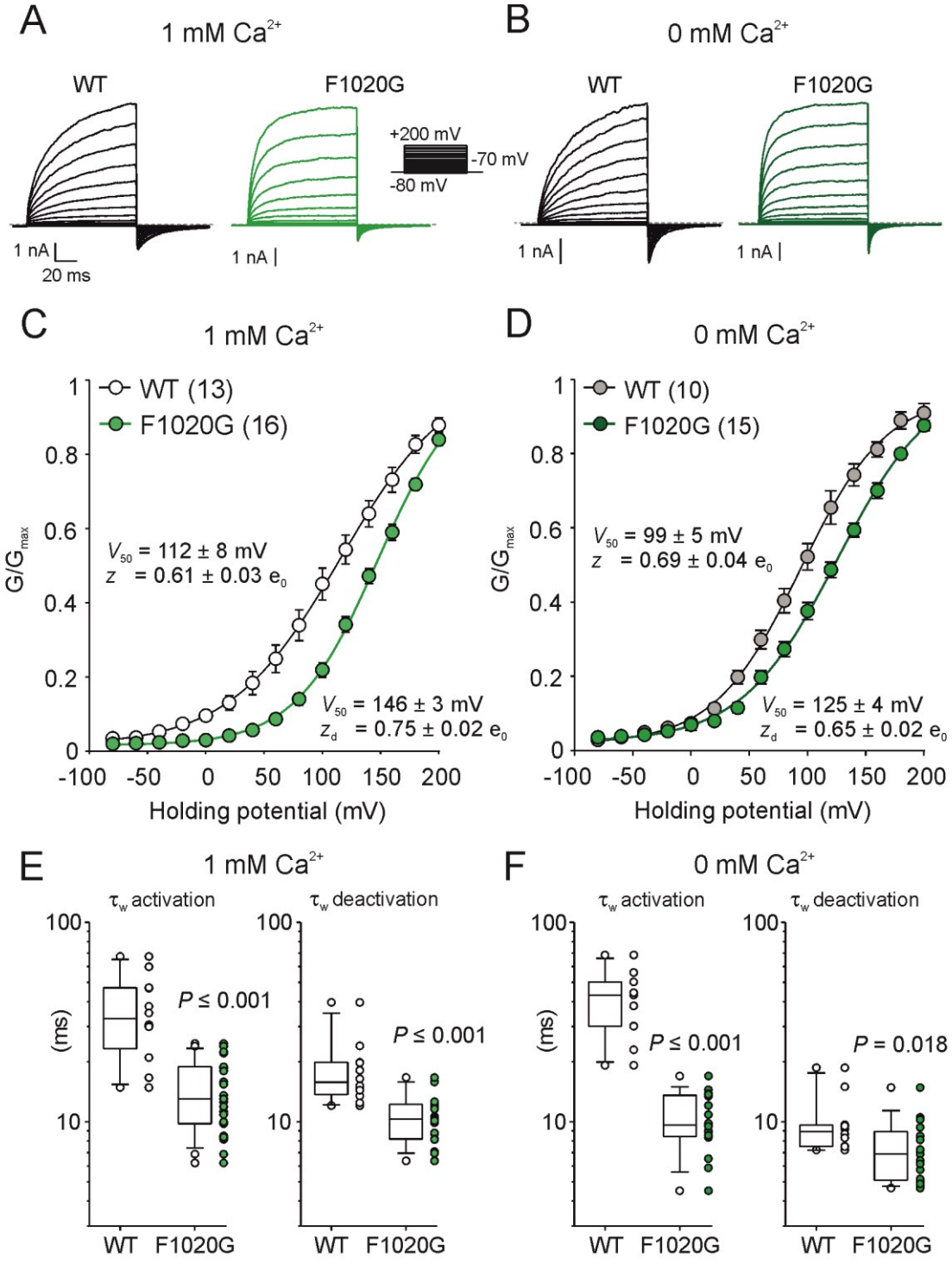

*Figure 30: **(A,B)** Representative current traces in response to voltage step protocol indicated above, recorded in solution containing 0 mM or 1 mM of Ca^{2+} ions. The currents at the end of the voltage pulses were used to generate the average conductance-voltage relationship **(C,D)** The half-maximal activation voltage V_{50} and the gating charge z were obtained by the fit to a Boltzmann function. Data are presented as mean ± S.E.M., n is indicated in brackets. **(E,F)** The activation and deactivation kinetics obtained by the bi-exponential fit of the currents evoked by depolarization from -70 mV to +200 mV, and the tail current at -70 mV elicited by stepping from +200 mV. Data are represented as vertical point plots and summary box plots. P values of statistically significant difference are indicated.*

of the gate *L* but significantly abolished the allosteric factor of coupling the voltage sensor into the gate *D* (**Figure 31.B**). The voltage sensor equilibrium J_0 of F1020G mutant was significantly increased. The absence of the Ca^{2+} increased the gating equilibrium (*L*) and the voltage sensor equilibrium J_0 only in the F1020G mutant, which favors the open state of the channel. The results indicate that the mutation F1020G induces conformation changes in a Ca^{2+}-dependent manner.

It has been shown that from nanomolar concentrations of intracellular Ca^{2+}, the Ca^{2+}/calmodulin complex binds to TRPA1 within the region L992-N1008 and potentiates the channel under resting conditions (Hasan et al., 2017). On the other hand, our results indicate that the same peptide interacts with lipid membranes if PIP_2 is

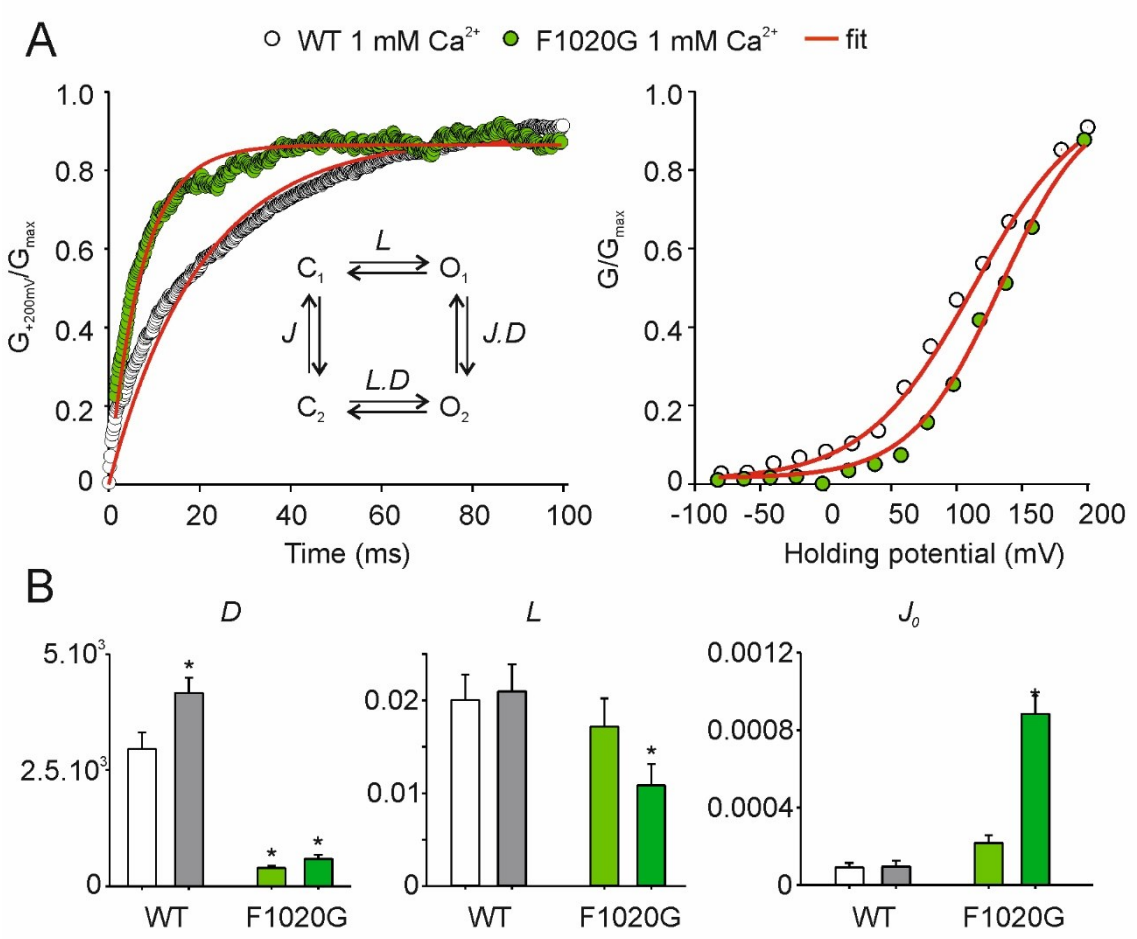

***Figure 31: (A) Left** - The time course of the normalized activation phase of wild-type TRPA1 (white circles) and F1020G mutant (light green circles) in 1 mM Ca^{2+}, induced by depolarization to +200 mV. **Right** - The normalized steady-state conductance-voltage relationship of wild-type TRPA1. Both the activation phase and the steady-state conductances were simultaneously fitted using a simple allosteric model (inset in the left graph). **(B)** Bar graphs summarizing the mean + S.E.M. of the obtained allosteric constants for WT and F1020G mutant in the presence (white, light green; n = 10 and 9) or absence (gray, dark green; n = 8 and 11) of external Ca^{2+}. Asterisks indicate a statistically significant difference from the value of WT ($P < 0.05$).*

present, and that the affinity of peptides to PIP_2 tends to decrease in the presence of calcium ions. Therefore, by introducing peptides into the patch solution, we wanted to examine whether PIP_2 and calmodulin would compete for the same binding site of TRPA1 transiently expressed in neuronal F11 cells. Using the same solutions as (Hasan et al., 2017), we measured the potentiation of the carvacrol-induced activation by calcium ions (**Figure 32**). It is known, that the binding of calmodulin to TRPA1 already occurs under the resting 100nM concentrations of Ca^{2+}. Therefore, we prolonged the

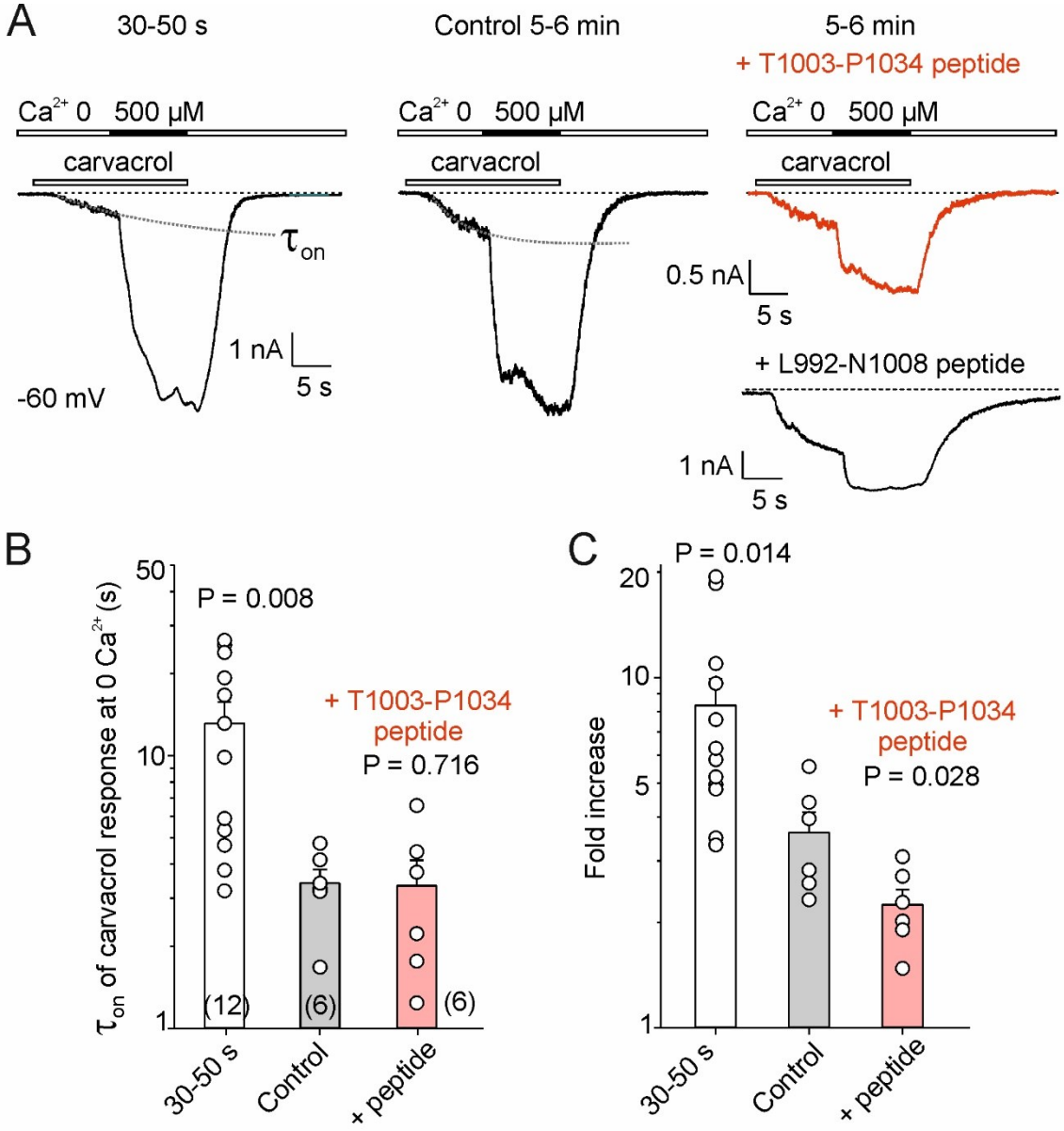

***Figure 32: (A)**, Representative recordings of TRPA1 in F11 cells measured 30-50 s after the whole-cell formation, 5-6 min after the whole cell formation and 5-6 min after the whole-cell formation with indicated peptides in the pipette solution. **(B)** Bar graphs and vertical point plots of the activation kinetics of carvacrol response in the absence of external Ca^{2+}, obtained by monoexponential fit. **(C)** Summary of TRPA1 potentiation induced by 500 µM Ca^{2+}. The data are presented as means + S.E.M., statistical significance P is indicated above the graphs.*

time between the whole-cell formation and the actual measurement to completely perfuse the cell with the intracellular solution, yielding significantly slower onset of the initial carvacrol response in 0 Ca^{2+} and a lower Ca^{2+}-mediated potentiation. Inclusion of the TRPA1-derived peptides L992-N1008 or T1003-P1034 in the intracellular solution prevented Ca^{2+}-dependent potentiation similar as in (Hasan et al., 2017), suggesting that both PIP_2 and Ca^{2+}/calmodulin complex may compete for the same or overlapping binding site.

6.2.3 Publication VI - Proximal C-terminus serves as a signaling hub for TRPA1 channel regulation *via* its interacting molecules and supramolecular complexes

The publications so far presented in this thesis were focused on two main topics regarding the regulation of TRPA1 channel: the regulation by phosphorylation pathways and the structural basis of the regulation by phospholipids. **Publication VI** addresses both of these topics and provides the evidence that further develop the findings obtained previously, as well as some perspective directions of the future research.

Publications IV-V provided the evidence that phospholipids (particularly PIP_2) may bind to at least two binding sites of TRPA1 channel – the intracellular cavity formed by the VSLD and the TRPL helix (Zimova et al., 2018), and the hydrophobic pocket formed by the interfacial helix and the adjacent pore segment of the S4-S5 linker and the pore domain (Macikova et al., 2019). This region possess a binding site for calmodulin (Hasan et al., 2017). Interestingly, a missense mutation H1018R at the IFH increases the responses to insoluble coal fly ash, suggesting its increased sensitivity to mechanic stimuli (Deering-Rice et al., 2015). We hypothesized, that H1018R mutation may alter the affinity of PIP_2 to TRPA1. The lipid displacement from the protein binding sites was proposed to be one of the mechanisms of temperature sensation in TRPV channels (Gao et al., 2016, Singh et al., 2018). We decided to investigate the effects of PIP_2 on the temperature dependence of TRPA1 channel using the ramp protocol stimulation and the non-electrophilic TRPA1 agonist carvacrol (**Figure 33** on page 78). Agonist-evoked responses in WT of hTRPA1 were potentiated by cooling the temperature of external solution from 25°C to 15°C and suppressed by heating it to 35°C. Depletion of PIP_2 by the coexpression of hTRPA1 channels with voltage-dependent phosphatase Dr-VSP used in **publication V** suppressed both basal currents and activation by carvacrol, but not the synergy between the temperature and carvacrol (**Figure 33.A** on page 78). The H1018R mutant exhibited significantly increased carvacrol responses upon cooling to 15°C (**Figure 33.B** on page 78). The voltage dependence of cold activation illustrates the opposite effects of the H1018R mutation and acute PIP_2 depletion (**Figure 33.C** on page 78). This evidence supports the role C-terminal linker in the PIP_2-mediated regulation.

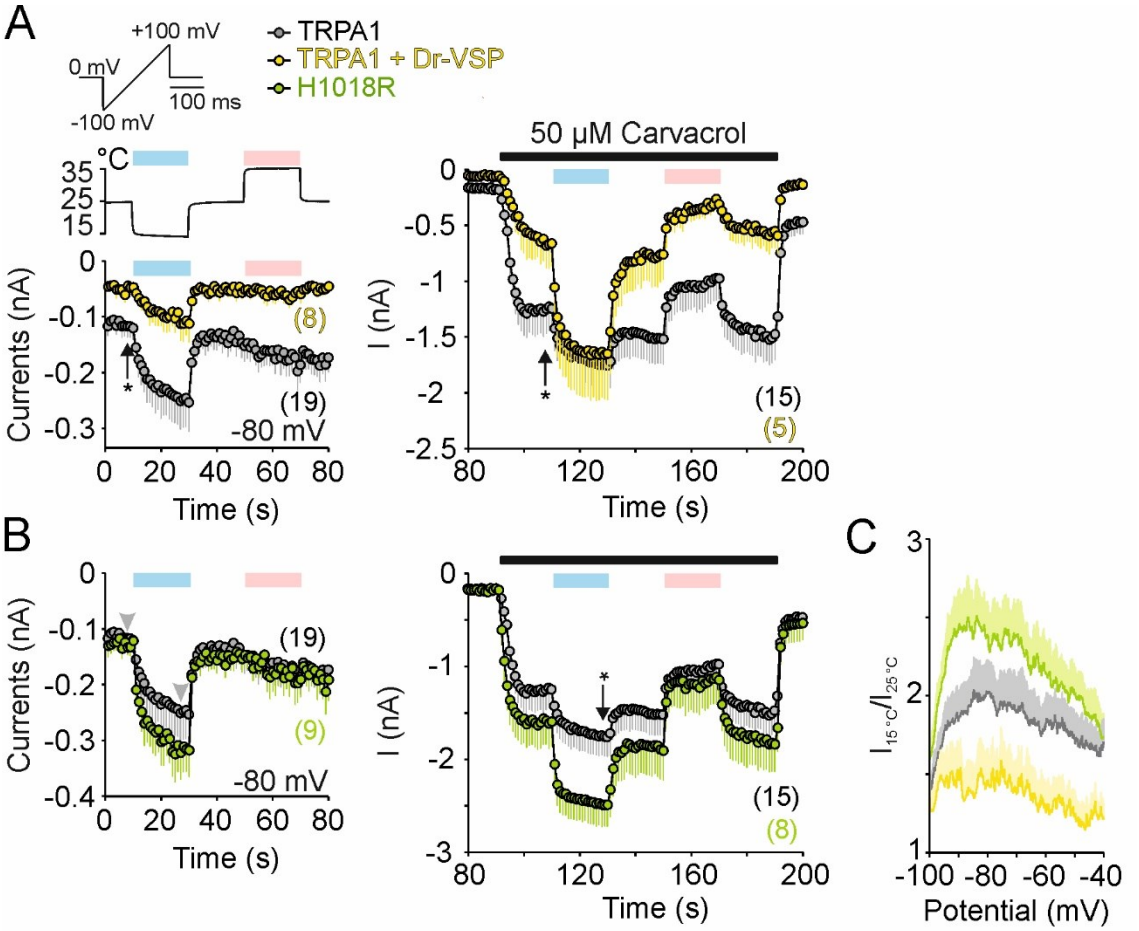

Figure 33: (A) *Time course of average whole-cell currents of human TRPA1 and TRPA1 co-expressed with Dr-VSP (yellow circles with bars indicating mean values with – S.E.M.), measured at –80 mV using the indicated voltage ramp protocol, preceeded by a 3s depolarization pulse to +80 mV to activate the Dr-VSP. The responses were measured at 25°C, 15°C (blue bar) and 35°C (pink bar) in the control solution and in the presence of 50µM carvacrol (black bar). The currents measured at -80 mV are shown.* ***(B)*** *Identical measurements were conducted for TRPA1 H1018R mutant. Data are presented as means -S.E.M., n is indicated in brackets; statistically significant differences from the WT are indicated by asterisks ($P < 0.05$).* ***(C)*** *Voltage dependence of cold activation normalized to the currents at 25°C. The currents were obtained at times indicated by gray arrowheads in* ***(B).***

The proximal C-terminus is also involved in modulation by calcium ions *via* binding of calmodulin (CaM), a protein involved in Ca^{2+}-dependent regulation of a large number of proteins. It does so in a bimodal manner so that it potentiates TRPA1 at low concentrations of cytosolic Ca^{2+} and inactivates the channel at higher Ca^{2+} concentrations. The CaM consists of two lobes – the C-lobe and N-lobe. The C-lobe of CaM binds to the C-terminal binding site of TRPA1 channel, whereas the N-lobe of CaM is capable of bridging different domains of TRPA1 or even link the channel with other target proteins. CaM may potentially act as a linker between the TRPA1 and

TRPV1 channels, as the N-lobe is also predicted to bind to the related TRPV1 channel and also to the Transmembrane protein 100 (Tmem100), which regulates the TRPA1-TRPV1 interaction (Weng et al., 2015). Moreover, the C-lobe may bind a scaffolding protein AKAP79/150 that anchors TRPA1-senzitizing protein kinases A and C, ultimately anchoring the whole signaling complex directly at the surface of the N-terminus of TRPA1 channel.

We tested the effect of AKAP79/150 on sensitization of the TRPA1 channel by voltage in HEK293T cells (**Figure 34**). In order to characterize the effect of AKAP79/150 on TRPA1 sensitization, we transiently expressed WT hTRPA1 with and without the AKAP79/150 in HEK293T cells and measured the voltage-dependence before and after the 3-minutes-long train of depolarizing pulses that sensitize the channel over time. While the train of pulses sensitized the WT currents at negative potentials, WT coexpressed with AKAP79/150 already exhibited sensitization of basal currents before the pulses. These results indicate the positive regulation of TRPA1 channels by AKAP79/150.

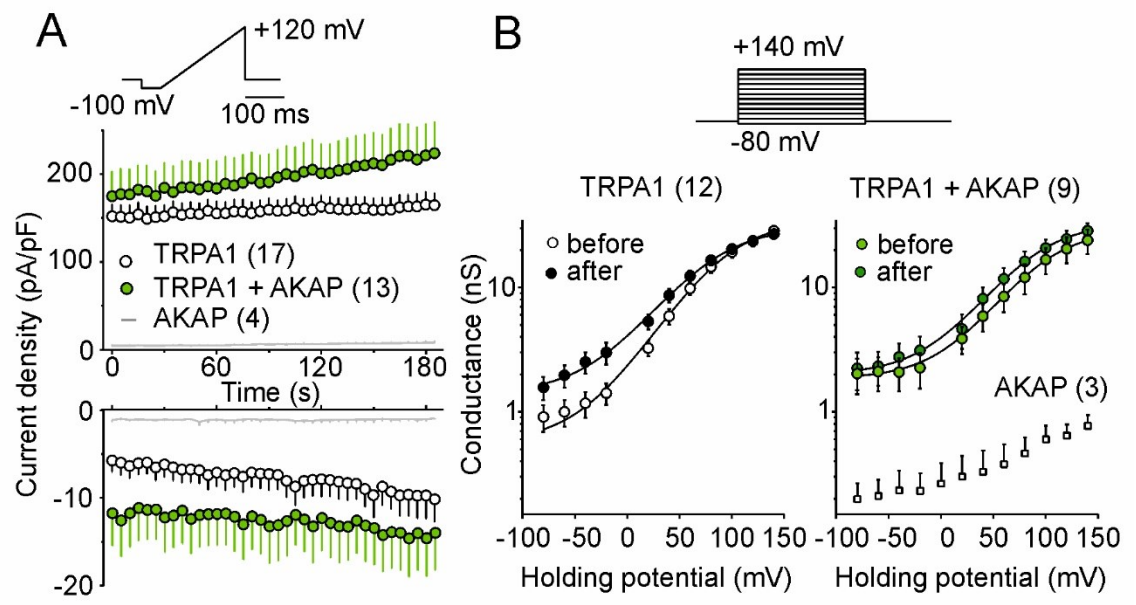

Figure 34: (A) *Average whole-cell current densities of HEK293T cells expressing TRPA1 channels (white circles), TRPA1 coexpressed with AKAP79/150 (green circles) or only AKAP79/150 (gray line), induced by repeated voltage ramps (shown above). The current densities calculated from the currents measured at -100 mV (lower graph) and +120 mV (upper graph). Data are shown as means +/- S.E.M., n in brackets.* ***(B)*** *Average G-V relationships obtained from the steady-state currents using the voltage-step protocol above. The conductances were measured before or after the train of depolarizing ramps from* ***(A)*** *Data are shown as mean ± S.E.M..*

6.3 Regulation of heat and cold dependence of TRPA1

6.3.1 Publication VII - Human and mouse TRPA1 are heat and cold sensors differentially tuned by voltage

TRPA1 has been shown to act as a receptor of heat in many species, including insects, amphibians, reptiles and birds (reviewed in (Hoffstaetter et al., 2018)). Intriguingly, the same receptor in rodent and human is activated by the opposite stimulus – cold. The activation by cold is still a matter of debate, as the studies present provide evidence either supporting (Story et al., 2003, Sawada et al., 2007, Karashima et al., 2009, del Camino et al., 2010) or denying (Jordt et al., 2004, Zurborg et al., 2007, Knowlton et al., 2010, Cordero-Morales et al., 2011, Chen et al., 2013) the activation of TRPA1 by cold or its involvement in cold perception. The sensitivity of TRPA1 to cold differs between primate and rodent species, and a single residue G878 of mTRPA1 (analogous to V875 in hTRPA1) within the S5 helix of the pore domain was proposed to account for the observed differences (Chen et al., 2013). The region around V875 is involved in the sensitivity to several TRPA1 agonists (Xiao et al., 2008) and antagonists (Paulsen et al., 2015). In addition, the region co-creates an intracellular vestibule together with the short C-terminal α-helix that was proposed to bind lipids (Macikova et al., 2019). These findings suggest that the region denoting cold sensitivity is a part of an important allosteric coupling domain. Moreover, there is evidence that the hTRPA1 can sense both heat and cold (Moparthi et al., 2016), further supported by the fact that mouse TRPA1 is one of the three TRP channels essential for *in vivo* detection of noxious heat (Vandewauw et al., 2018). In **publication VII**, we characterized and compared the temperature- and voltage-dependent properties of human and mouse TRPA1 with the aim to decipher the fundamental differences between their mechanisms of gating.

First, we compared the temperature-dependence of the voltage activation for hTRPA1 and mTRPA1 in HEK293T cells using the same voltage-step protocol as in (Karashima et al., 2009), where the authors successfully used a two-state model to describe the cold activation of mTRPA1 (**Figure 35** on page 81). The obtained *G-V* characteristics at 15°C, 25°C and 35°C under Ca^{2+}-free solution reveal that both cold and warm temperatures increased the activity of hTRPA1 and mTRPA1 at basal

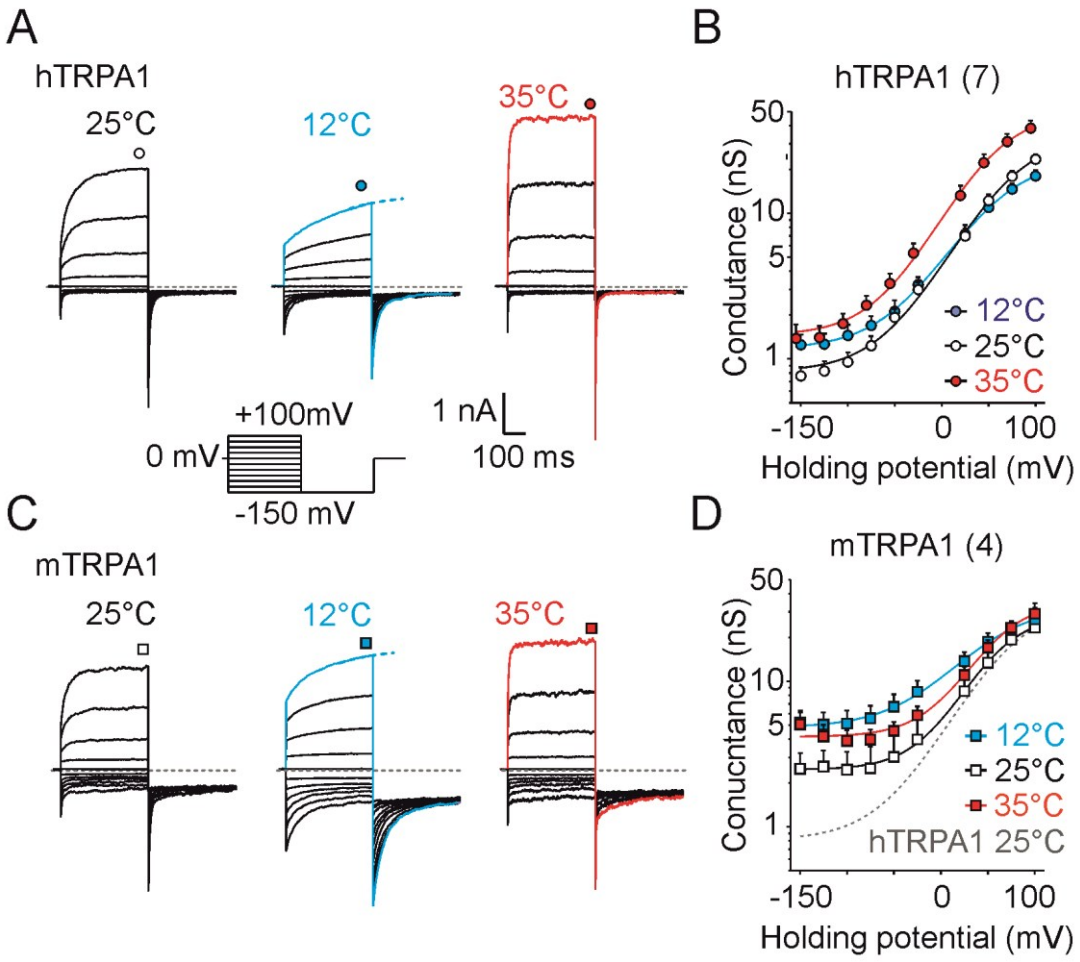

Figure 35: (A) *Representative whole-cell currents of HEK293T cells expressing human TRPA1 channels, measured by a voltage step protocol (indicated below) at three different temperatures. Steady-state currents (indicated by circle) were used to create the average conductance-voltage relationship. The last responses (colored) were used to obtain the activation and deactivation time constants and to construct the Arrhenius plot in* ***Figure 36.*** *The currents at 12°C were obtained from the exponential fit of the onsets (dashed line)* ***(B)*** *The solid lines represent the best fit to a Boltzmann function. Data are shown as means + S.E.M., n is indicated in brackets.* ***(C-D)*** *The same procedure cas conducted for HEK293T cells expressing mouse TRPA1 channel.*

(negative) membrane potentials. The mouse orthologue exhibited more pronounced increase of basal currents than hTRPA1 while maintaining similar activity at depolarizing +100 mV voltage, suggesting that mTRPA1 has the gating equilibrium more shifted toward the open state of the channel. The half-maximum activation voltage V_{50} was slightly yet significantly shifted by transition from 25°C to 35°C in hTRPA1 but not in mTRPA1, indicating the differences in the temperature-dependence of the activation and deactivation kinetics.

To address this issue, we determined the time constants of the activation and deactivation kinetics by mono- or bi-exponential fitting of the onset currents at

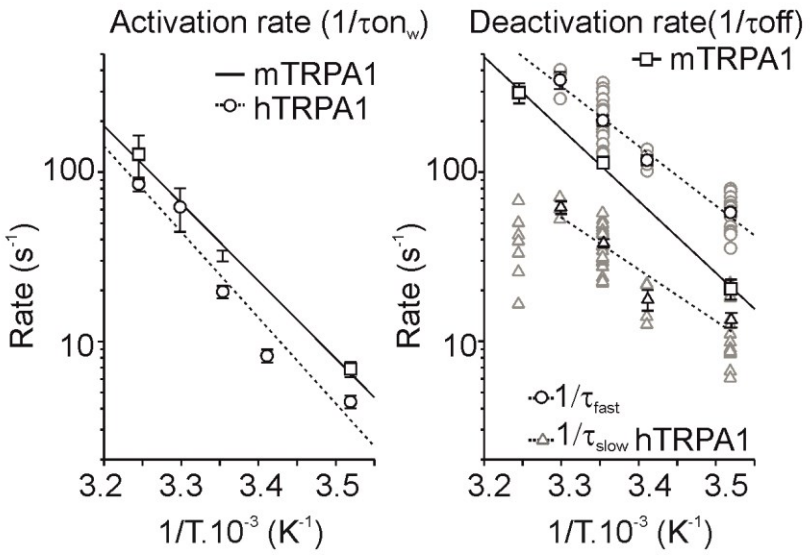

Figure 36: *Arrhenius plots of the onset (left) and deactivation (right) time constants for hTRPA1 (white circles) and mTRPA1 (white squares). The time constants of the onset were determined by mono- or bi-exponential fits of the onset currents at +100 mV, as highlighted in* ***Figure 35.A****. The time constants of the deactivation rate were determined by mono- or bi-exponential fits of the tail currents at -150 mV. Additional measurements at 30°C and 20°C were necessary to determine the rate constants of hTRPA1.*

+100 mV and the inward tail current at -100 mV for different temperatures (**Figure 36**). While both onset and offset of mTRPA1 could be successfully fitted by one exponential, currents through hTRPA1 required at least two exponential functions, where the faster component was predominant. We constructed the Arrhenius plot for both hTRPA1 and mTRPA1 to analyze the effect of temperature on the rates of activation/deactivation. Compared to hTRPA1, the mTRPA1 channel had higher activation rates and slower deactivation rates, confirming the shifted gating equilibrium of mTRPA1 toward the open state. The linear regression fits of the Arrhenius plot yielded the slopes ΔH and corresponding temperature coefficients Q_{10} (**Table 4**), indicating that the voltage-dependent activation and deactivation processes of both orthologues exhibited only mild temperature dependencies over the temperature range of 12–35°C.

Table 4: Parameters of the activation and deactivation kinetics of hTRPA1 and mTRPA1.

rate constant	mTRPA1		hTRPA1 fast		hTRPA1 slow	
value	ΔH [kJ·mol^{-1}]	Q_{10}	ΔH [kJ·mol^{-1}]	Q_{10}	ΔH [kJ·mol^{-1}]	Q_{10}
activation	87.6	3.3	95.1	3.7	77.9	2.9
deactivation	81.3	3.1	67.2	2.5	-	-

Next, we applied the same procedure and experimental conditions on HEK cells expressing hTRPA-V875G and mTRPA1-G878V to see, to what extent this residue could contribute to the temperature dependence of the voltage-induced gating. (**Figure 37**). The temperature dependence of the fast component of the deactivation rate of hTRPA1-V875G became steeper, thus resembling that of mTRPA1 (83.6 kJ·mol^{-1}; **Figure 37.D**). Likewise, the reverse mutation mTRPA1-G878V decreased the slope of the temperature dependence of the deactivation rate the less steep slope of wild-type hTRPA1 (69.6 kJ·mol^{-1}; **Figure 37.E**). However, both hTRPA1-V875G and mTRPA1-

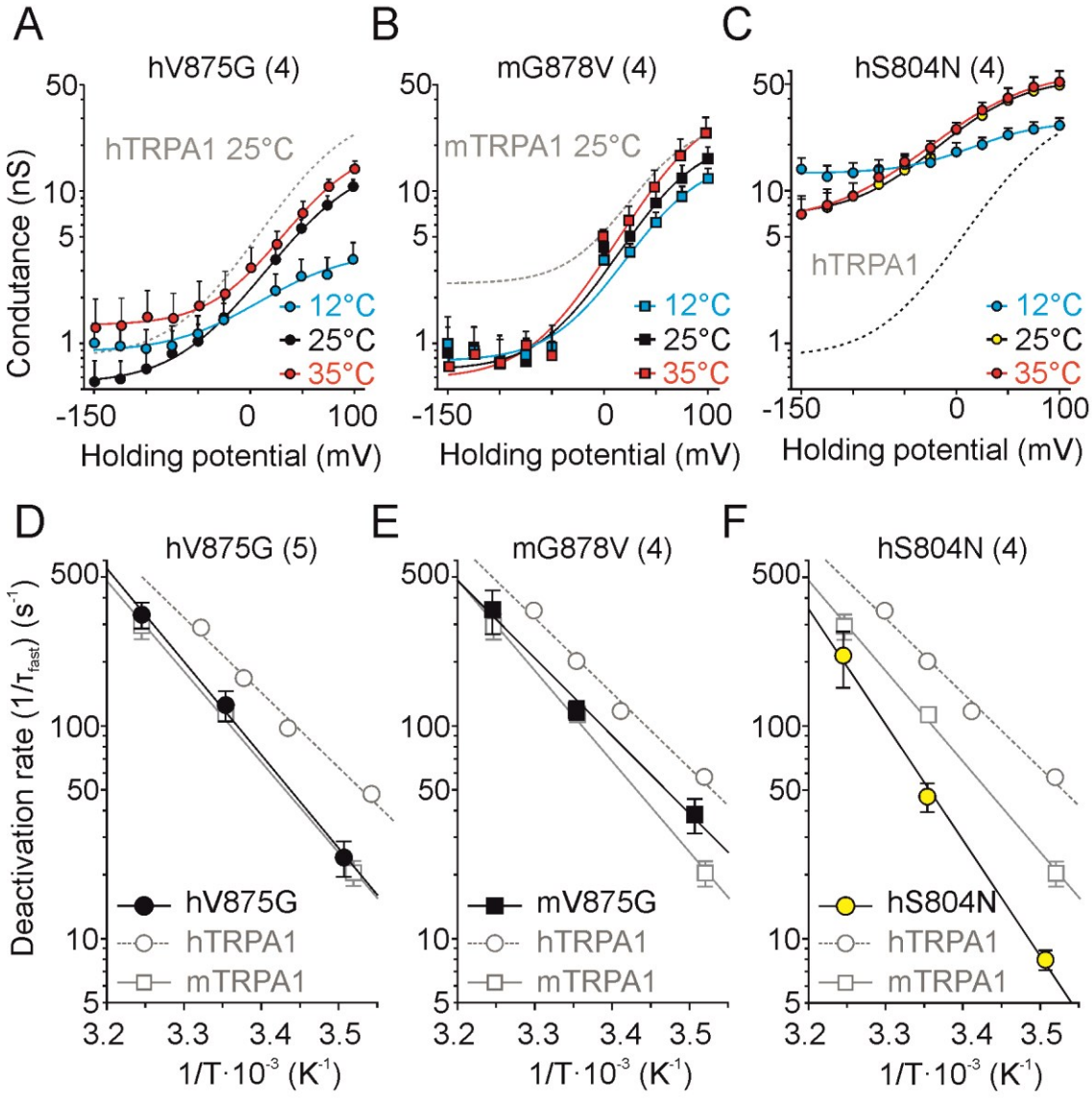

***Figure 37**: Average conductances of mutants hV875G **(A)** mG878V **(B)** and hS804N **(C)** at three different temperatures, measured by a voltage step protocol as in **Figure 35**. The fit of hTRPA1 or mTRPA1 G-V relationship to Boltzmann function is included as a dashed gray line. Data are shown as means + S.E.M. **(D-F)** Arrhenius plots of the fast deactivation time constants obtained for hTRPA1, mTRPA1 and indicated mutants. Data are shown as means ± S.E.M., n is indicated in brackets.*

G878V exhibited decreased currents, suggesting that the equilibrium of the gating was impaired (**Figure 37.A,B** on page 83). These results complement those obtained by Chen et al. (Chen et al., 2013) and emphasize the possible species-specific role of the residue V875/G878 in S5 in allosteric gating.

We wondered how the temperature signal might be conveyed to the gate and how is the allosteric coupling or gating of primate and rodent orthologues adjusted by the vicinity of V875/G878. We mapped all residues that are non-conserved between the mouse and human TRPA1 and further focused on 1) the inner part of the S1-S4 and the S4-S5 linker located close to S5 and 2) the proximal C-terminal loop that contains a hydrophobic α-helical segment (**Figure 38** on page 85; see also **publication IV, V** and **VI** described in this thesis).

We constructed and functionally analyzed a set of reverse mutants between the mouse and human orthologues (M801L, S804N, V806A, I803Y/L867F) located in the S1-S4 sensor domain. Among them, the S804N had the largest impact on the function of TRPA1, exhibiting large basal currents, significantly leftward shift of the voltage dependence and very slow activation and deactivation kinetics along with a strong voltage-independent component (**Figure 37.C,E** on page 83). The deactivation rate of S804N exhibited a steeper temperature dependence (103.8 $kJ \cdot mol^{-1}$; Q_{10} = 4.2) compared to WT channels. The neutralizing mutation S804A rendered the channel non-functional, whereas the charge-introducing S804D mutant resulted in a similar phenotype as seen in S804N. To further explore the possible mechanism of such functional impacts of mutations at S804, we performed MD simulations using the structure of hTRPA1 structure (PDB code 3J9P; (Paulsen et al., 2015)) completed with the S1-S2 and S2-S3 linkers (Zimova et al., 2018) and the S804N/D single-point mutations. According to the results from the simulations, S804 in the WT channel formed rather loose contacts with R852 or N845, while aspartate and asparagine formed tight contacts with either R852 or N845. The results reinforce the importance of the S1-S4 intracellular cavity as a regulatory and transductory site of the TRPA1 channel.

In order to explore the role of the proximal C-terminal loop (Y1006-Q1031), we used the molecular dynamics flexible fitting (MDFF) approach to refine fitting of the atomic structure into the electron density map of the hTRPA1 channel. The refined model revealed interactions between the V875 residue and the region of the interfacial helix I1019-F1022. Based on the comparison of hTRPA1 and mTRPA1 primary

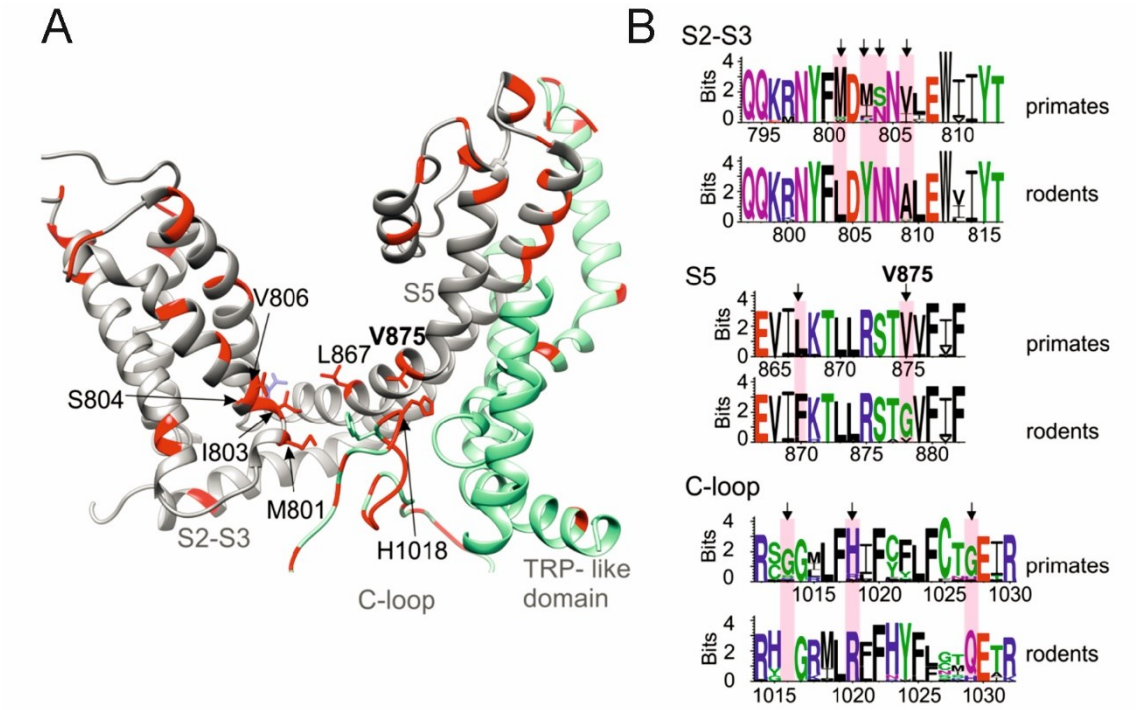

Figure 38: Screen for the non-homologous residues in the vicinity of V875. (A) *Side view of the transmembrane part of the TRPA1 model based on the structure 3J9P with modelled and fitted unresolved IFH and adjacent loops. The residues in which human and mouse orthologues differ are highlighted in red. In the C-terminal loop, side chains of H1018 and F1020 are shown.* ***(B)*** *Amino acid sequence conservation of the regions adjacent to the V875, represented as a sequence logo.The logo was calculated from primate (n = 21) and rodent (n = 27) sequences. The non-conserved residues mutated in this study are indicated by arrows.*

sequences in the context of the refined model, we constructed and analyzed three human-to-mouse mutations, H1018R, ΔG1013 and G1027Q. Out of these, ΔG1013 and H1018R mutants had significantly faster deactivation kinetics; the latter mutant exhibited slightly less steep temperature dependence. The results indicate that these residues are not key determinants of the temperature sensitivity under the experimental conditions.

The results indicate that both human and mouse TRPA1 channels might at negative membrane potentials possess so-called "U-shape" thermosensitivity, a dual cold and warm sensitivity. The fact that the kinetics of the human TRPA1 was successfully fitted by two exponential functions suggests an allosteric coupling processes rather than a simple two-state model. To explore the significance of the coupling between the voltage sensor and the temperature sensor in a wider range of temperatures, we measured the currents at the depolarizing potential of +80 mV using the 3-s temperature steps from 11°C to ~50°C (**Figure 39.A** on page 86). Both TRPA1 orthologues exhibited U-shaped outward currents with a saddle point around the room

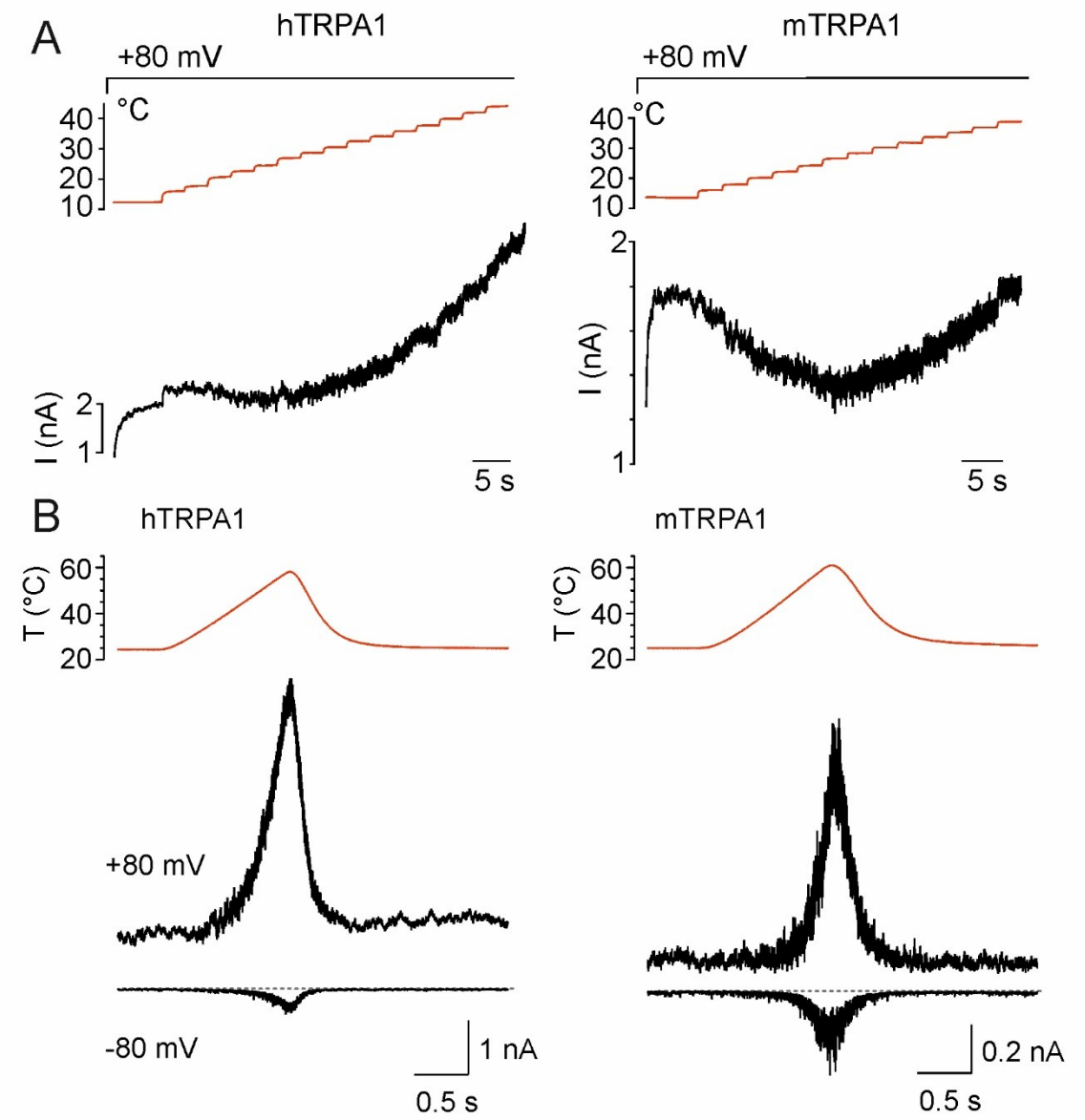

Figure 39: ***(A)*** *Representative whole-cell currents of hTRPA1 (left) and mTRPA1 (right) elicited by temperature steps ranging from ~11 to ~52 °C. The cells were held at constant depolarizing voltage +80 mV.* ***(B)*** *Representative whole-cell currents of hTRPA1 (left) and mTRPA1 (right) activated by a temperature ramp applied at a maximum speed of about 35 C/s and at constant holding potentials +80 and -80 mV.*

temperature and a potential of exhibiting the properties of a heat-activated channel at even higher temperatures. Therefore, we measured currents from hTRPA1 and mTRPA1 at both -80 mV and +80 mV using temperature ramps from 25°C up to 60°C (**Figure 39.B**). Indeed, we observed specific heat-induced currents at negative and positive membrane potentials that were rapidly reversible and exhibited steep temperature dependence over the high temperature range of 53 – 59°C for mTRPA1 and 55 – 57°C for hTRPA1. These findings provide the evidence of heat activation of both

human and mouse TRPA1 in HEK293T cells, suggesting that both mammalian orthologues possess an intrinsic heat-sensing domain.

The heat-induced currents were greater at positive potentials, suggesting an allosteric mechanism of action. We further explored the existence of allosteric coupling between the sensors. To allow the channels to fully activate and relax back to equilibrium, we applied 10-s long depolarization pulses from 70 mV to +80 mV at a constant cold temperature (~5-10°C) and then tested the effects of exposure to noxious (~ 60°C) heat (**Figure 40** on page 88). The application of noxious heat led to a strong reduction of the subsequent response to +80 mV; the reduction correlated with the maximum temperature applied, suggesting that excessive heat irreversibly impedes either the activation of voltage-sensor or its effective coupling to the gate. We also examined the concurrent stimulation by heat and the depolarization pulse. Most interestingly, when the channels were after concurrent stimulation first cooled down to 5°C and then repolarized back to -70 mV, we observed highly pronounced inward currents (**Figure 40.A-D** on page 88). The effect of cold-sensitized inward currents was not dependent on the order of applied stimuli (heat and voltage; **Figure 40.A,B,E** on page 88), but it was not seen when the reverse repolarization occurred in the presence of noxious heat (**Figure 40.F** on page 88). These striking findings indicate that noxious heat above 60°C induces substantial structural rearrangements within the channel leading to strong inward rectification at cold temperatures.

The phenomenon of the 'heat-induced cold activation' can be addressed by the inverted coupling hypothesis, according to which the activation of a TRP channel may be mediated by a heat sensor that promotes the closing of the pore gates. We applied this theory on our data and performed simulations using the eight-state allosteric kinetic model. Using the parameters $\Delta H°$ = 91 kcal·mol^{-1} and $\Delta S°$ = 0.317 kcal·mol^{-1}·K^{-1} published for TRPM8 (Jara-Oseguera and Islas, 2013) as the initial values, we estimated the K_0, L, D, E, z, $\Delta H°_C$ and $\Delta S°_C$ by fitting the average G-V curves obtained for hTRPA1 at 25°C and 12°C, assuming that the allosteric coupling factor of the temperature sensor $C = exp[-(\Delta Hc° - T\Delta Sc°)/RT]$ (**Figure 41.A-C** on page 89). A representative recording of the hTRPA1 channel was normalized to G_{max} characterized by three states: ground **state 1** with mild temperature-dependent activation by voltage and activation by noxious heat, **state 2** with impaired responses to depolarizing potentials by the exposure to excessive heat, and **state 3** with strong inward rectification

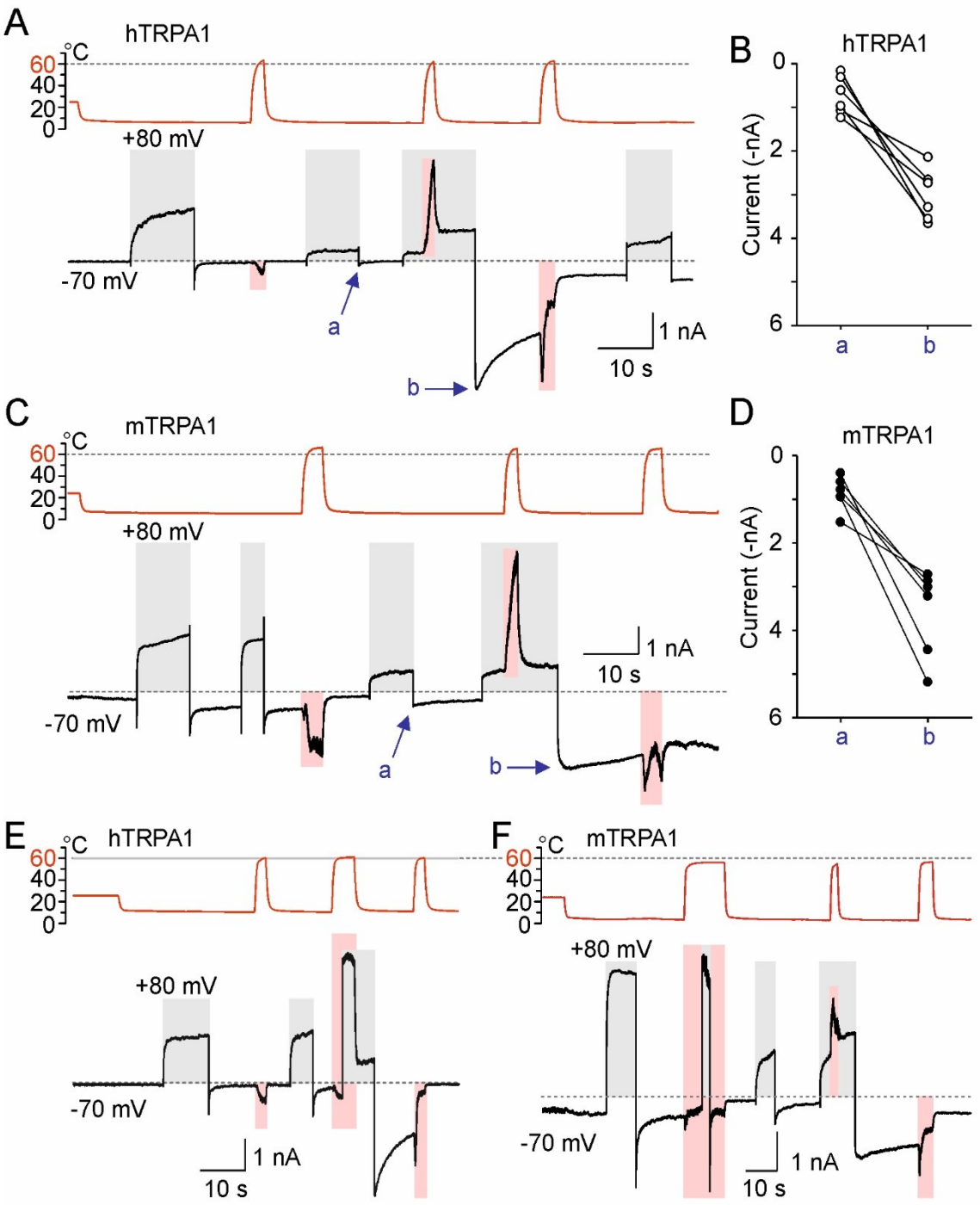

Figure 40: (A) *Representative whole-cell currents of hTRPA1 in response to temperature (shaded pink area) and voltage (shaded gray area) steps. The temperature trace is shown above the recording. Exposure to excessive heat stimulation suppresses the voltage both outward and inward (arrow a) currents. Concurrent exposure to heat and depolarization rendered the TRPA1 channels dramatically cold-activated at negative potentials (arrow b).* ***(B)*** *The increase in the inward currents for individual cells expressing hTRPA1 channels (n = 6).* ***(C,D)*** *Similar procedure was conducted on cells expressing mTRPA1 channels. The increased inward currents are present even when the heat stimulation precedes depolarization* ***(E)****, but not when repolarization to -70 mV occurs during the heating* ***(F)****.*

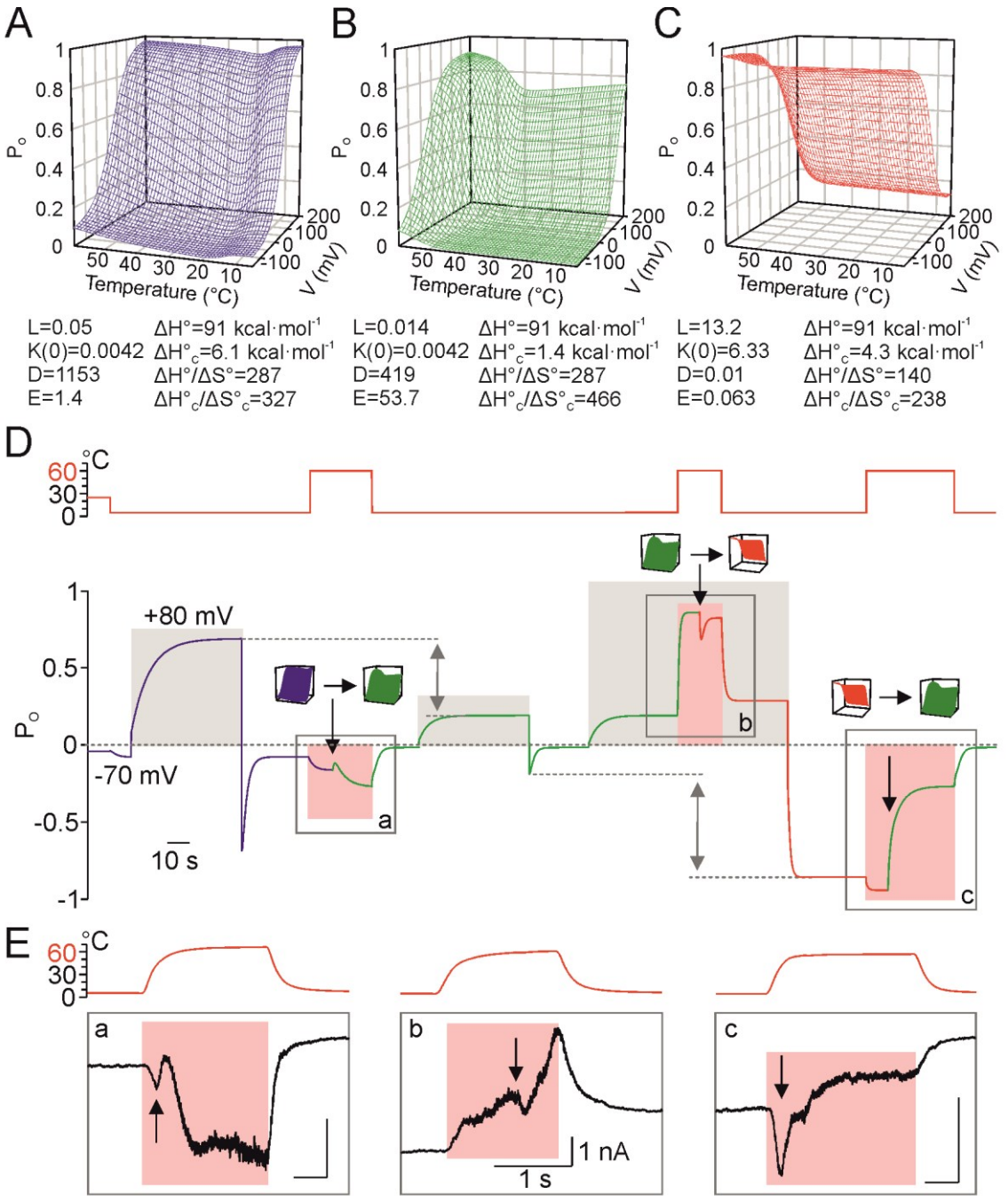

Figure 41: (A) *Open probability landscape of* ***state 1*** *obtained by calculating the open probability P_o as a function of temperature and voltage. The parameters K(0), z, L, E, D, $\Delta H°_c$ and $\Delta S°_c$ were obtained by the global fit of the G-V relationship* ***as in Figure 35.A****, normalized to maximal conductance at 25°C; the parameters $\Delta H°$ and $\Delta S°$ were set to the values published for TRPM8 channel (Jara-Oseguera and Islas, 2013). The open probability landscape was remodeled to qualitatively match the irreversible switch-after-excessive heat of the* ***state 2 (B)*** *and the heat-induced cold activation after the concurrent activation of temperature and voltage sensor in* ***state 3 (C). (D)*** *The modelled time course of P_o modelled according to* ***Figure 40.A****. Black arrows and colored pictograms indicate the transitions between the states / landscapes; grey arrows highlight the changes of P_o* ***(E)*** *Representative whole-cell currents of mTRPA1 under corresponding situations as in* ***(D)*** *(boxes a, b and c). The bars indicate 1 s and 1 nA in panels a, b, and c.*

after concurrent activation of voltage and heat sensors and their subsequent deactivation. The obtained parameters were refitted to each state individually. With these three states, we successfully recreated the time course of the experiment in the **Figure 40.A** (**Figure 41.D** on page 89), preserving the heat-dependent suppression, heat-induced cold activation and also current transients that were occurring during the temperature change (**Figure 41.E** on page 89). This further supports the modular allosteric model (rather than the two-state model) as an appropriate approximation of TRPA1 activation.

The data presented in this study demonstrate that both human and mouse TRPA1 orthologues are able to respond to noxious heat, and that their kinetics enables the activation by cold. Most importantly, our results reveal a specific mode of TRPA1 activation that can be viewed as a ‘heat-induced cold sensitivity’.

7. Discussion

7.1 Regulation of TRPA1 by cellular pathways and phosphorylation

In the **publication I**, we examined the effects of LF-EMF on the F11 cell line under the normal and inflammatory conditions induced by the potent mediator of inflammation bradykinin (BK). The measure of the activity of the F11 cells was the intracellular level of calcium, which is an important intracellular messenger and its release from the intracellular reservoirs is mediated by the PLC-dependent pathway triggered by bradykinin. The repeated application of 10 nM BK increased the levels of intracellular Ca^{2+}, confirming the efficient expression of B1 receptors in the F11 cell line. The second response to BK applied after 3 minutes was significantly reduced. This was potentially due to the chosen interval between the BK applications, since previous publication (Ambrosino et al., 2013) did not describe any desensitization of Ca^{2+} responses to BK at concentration 250 nM and with 20-min intervals between the BK applications in F11 cells. BK reduced Na^{+} inward currents and increased the resting membrane current, indicating alterations in neuronal excitability. The effect of BK is mediated by increase in the intracellular Ca^{2+} and by cleavage of PIP_2, an important cofactor for maintaining the activity of many ion channels. Thus, further experiments will be needed to distinguish between these mechanisms of BK action in F11 cells.

Exposure to LM-EMF significantly delayed and suppressed BK-induced responses and significantly potentiated the spontaneous activity of naïve F11 cells, demonstrating that LF-EMF has acute effects on calcium responses in a model of peripheral sensory neurons. In our experiments, the F11 cell line was proved to be a suitable model to study the effects of magnetic field at the cellular level. Two of three LF-EMFs impacted the second response to BK, suggesting that the LF-EMF may be involved in the desensitization process. We also examined whether TRPA1 channels could be involved in the LF-EMF-mediated responses. Transient expression of TRPA1 channels increased the sensitivity of F11 cells, most likely because of the increased basal level of intracellular Ca^{2+}.

The effect of TRPA1 expression on the cellular responses in F11 cells was further studied in **publication II**. Transient expression of TRPA1 fully dampened the Na^{+} currents, raising the possibility that both BK and TRPA1 overexpression might

affect the Na^+ currents by increasing the levels of basal calcium. BK did not further increase the persistent basal levels of Ca^{2+} in F11 cells expressing TRPA1 channels, and also did not affect the AITC-induced responses, suggesting that TRPA1 does not undergo long-term modulation (such as phosphorylation) induced by BK. BK-induced cellular pathways trigger the activity of kinases PKA and PKC that further sensitize the TRPA1 channel (Brackley et al., 2017). It is possible, that increased intracellular concentration of Ca^{2+} due to the overexpression of TRPA1 renders the regulation more difficult. Another possibility is that other factors ensuring the PKA- and PKC-dependent modulation, such as the AKAP79/150, needs to be present (Brackley et al., 2017).

The results from the **publication VI** support the involvement of AKAP79/150 in the sensitization of TRPA1 channel, as the currents of HEK293T cells expressing TRPA1 and AKAP already exhibited elevated basal currents before the train of depolarizing ramps. These results can be interpreted as 1) increased trafficking of TRPA1 protein into the plasma membrane, 2) increased activity of TRPA1 by phosphorylation, or 3) direct interaction of AKAP with TRPA1, which makes the opening of the channel easier.

The structural importance of the residue S602 predicted to be prone to phosphorylation by several kinases, including PKC, PKA and others, was examined in the **publication III**. Phosphomimicking mutation S602D rendered the TRPA1 channel inactive to depolarizing voltage and the presence of both electrophilic and non-covalent agonists of TRPA1 channel, while the mutations S602G and S602N functionally did not differ from the wild-type. Therefore, the effect of the phosphomimicking S602D mutant is probably not caused by structural changes due to the mutation of S602. The expression of S602D mutant at the surface of the cell implies that the expression and trafficking of the channels were also not structurally impaired. These results strengthen the possibility of the inhibition-causing phosphorylation of S602D. The W605A mutation in the proximity of S602 exhibited reduced activation by TRPA1 agonists. It is possible that the conformational changes with respect to the relative position of W605 and Y662 in the S602D and p-S602 MD simulations could ultimately lead to a broader conformational transition that could promote channel closure. The phosphorylation of S602 is most likely not mediated by PKA or PKC kinases, as both were previously shown to mediate sensitization of the TRPA1 channel. We predict the involvement of

some other kinase(s) with the inhibitory effects on TRPA1 channel, similarly to Src kinase (Morgan et al., 2014).

7.2 The putative binding sites of regulatory lipids

The changes in solvent accessibility during the transitions from the closed to open state were proposed to be a key thermodynamic factor that could underlie the unique bidirectional temperature dependence of the TRPA1 channel, as well as both heat- and cold- induced sensitization of TRPA1-mediated responses to chemical agonists. The structural changes occurring within the periphery of TRPA1 can be transduced into the gating movements through a putative allosteric nexus encompassing the TRPL helix, pre-S1 helix and the S4-S5 linker. The inner cavity of the VSLD is an integral part of this important region; therefore it may undergo gating-associated transitions altering the occupancy by water.

The results from **publication IV** show that the intracellular cavity can be occupied both by water or PIP_2 in state-dependent manner. Docking simulations indicate the involvement of positively charged polar residues of the lower part of the cavity in the binding of the inositol head group of PIP_2. Neutralization of the residues H719, N722, K787 and R852 contacting the inositol head group of PIP_2 impaired the voltage- and agonist-driven activation of TRPA1 channel, suggesting that hydration of these residues and/or PIP_2 binding may provide the energy required to open the channel. On the other hand, the effects of gain-of-function mutations E788A and E808A may be addressed for the enhancement of PIP_2 binding due to the increase of positive potential inside of the cavity.

Importantly, the presence of Ca^{2+} ions could bias the mutants H719A, N722 and K787, but also the gain-of-function mutants E788A and E808A toward the closed state at negative membrane potentials. The region proximal to E788 and E808 appears to be determining for the effects of the electrophilic agonists and Ca^{2+}. Mutations E788I, E788K and the proximal mutations N805A and Y799A were robustly active at both positive and negative voltages and still maintained the Ca^{2+}-dependent effects, similarly to wild-type TRPA1. In contrary, E808K and, surprisingly, the double mutation E788A/E808A resulted into an immediate inhibition of Cin-induced currents upon Ca^{2+} application, while the agonist-induced currents were similar to wild-type TRPA1. These data indicate that the intracellular cavity of TRPA1 functions as a molecular switch that

functions in a state-dependent manner. Any alteration to the polarity balance deep in the cavity causes a Ca^{2+}-dependent block of currents elicited by electrophilic agonists.

Our experiments with PIP_2 modulators further strengthen these conclusions. We found that depletion of membrane PIP_2 downregulates the wild-type TRPA1 channels in the absence of external Ca^{2+}. Most notably, depletion of PIP_2 transformed the gain-of-function mutant E808A into an identical phenotype as the E808K and E808A/E788A mutants, supporting the role of the internal sensor cavity in TRPA1 regulation. When the channel is weakly activated by depolarization or cinnamaldehyde, the intracellular cavity of the sensor domain can bind PIP_2 and then release it in response to a local increase in Ca^{2+}.

Two years after publishing of our **publication IV**, three new structural studies on TRPA1 channel emerged. One of the studies revealed a Ca^{2+} ion residing inside of the VSLD intracellular cavity, coordinated to residues E788, E808, N805, Y799 and Q791 (Zhao et al., 2020). The authors demonstrated that the regulatory actions of calcium converge on a single residue E788. These findings are fully in agreement with our results. Another study presented a structure of a closed state of TRPA1 in lipid nanodiscs and found no lipid inside of the VSLD cavity (Suo et al., 2020). This finding is not contradictory to our study, since the lipid may bind inside of the cavity in a state-dependent manner. Also the peptide I964-L992 corresponding to the TRPL helix was predicted by the AntiBP Server (http://crdd.osdd.net/raghava/antibp/index.html) to interact with negatively charged lipids; the strong interaction with membranes containing negative lipids was confirmed by subsequent biophysical studies (Witschas et al., 2015). This finding further supports the hypothesis of PIP_2 binding inside of the VSLD cavity.

TRPA1 may also possess other PIP_2 binding sites. The predicted candidate is the intersubunit crevice formed by the C-terminal interfacial helix (IFH) and the S5 helix and S4-S5 linker of the adjacent subunit. The sequence of the involved part of the C-terminus was covered by the two peptides L992-N1008 and T1003-P1034, both of which were predicted to bind anionic lipids with even higher score than the TRPL helix. In the **publication V**, we aimed to determine the extent to which this putative interaction site is involved in TRPA1 regulation. Biophysical methods showed that both peptides bind to the lipid membrane only when PIP_2 was present, exhibiting affinities of

300 nM and 700 nM. The binding is strong and superficial, inducing only small perturbation in the lipid.

Inclusion of the T1003-P1034 peptide in the pipette solution during the whole-cell experiments prevented Ca^{2+}-dependent potentiation of carvacrol-induced responses of TRPA1, similarly as previously seen in (Hasan et al., 2017). These results suggest that the T1003-P1034 region is important for Ca^{2+}-dependent potentiation, raising the possibility that calmodulin may compete with PIP_2 for the same binding site.

The mutations of a conserved residue located at the unresolved interfacial α-helix of the C-terminus of TRPA1 channel, F1020G, led to faster kinetics and rightward shift of the half-maximal activation voltage, probably due to an impaired allosteric coupling of the voltage sensor to the channel's gate. The absence of Ca^{2+} ions affected the basal-open gate equilibrium *L* in F1020G but not in wild-type channels, indicating Ca^{2+} dependence of conformational changes caused by mutation. The altered gating equilibrium of F1020G may account for the suppression of Cin-induced currents specifically at negative membrane potentials, while the Ca^{2+}-dependent potentiation remained intact. The PIP_2 depletion caused by the activity of Dr-VSP impaired the Cin-induced currents selectively at negative potentials, similarly to F1020G mutant (Zimova et al., 2018). Therefore, the TRPA1 channel may possess two PIP_2 binding sites, which, in the absence of external calcium, could modulate the electrophilic activation in a similar fashion.

In 2020, the structures of the TRPA1-C621S channel and TRPA1 with the bound agonist JT010 revealed a phospholipid residing in the intersubunit crevice, interacting with the residues W711 in the pre-S1 and E854 in the S4-S5 linker (**Figure 42** on page 96). Intriguingly, the lipid was not present in the TRPA1-BITC structure (PDB ID: 6PQP), most probably because the IFH was positioned closer to the transmembrane domain and narrowed the crevice. The IFH without lipids established contacts between the backbone of C1024 and N855 in the S4-S5 linker. These findings confirm our conclusions. The residue F1020 might play an important role in the stabilization of the closed IFH conformation as it is proximal to W711.

The channelopathy-related mutation of TRPA1 N855S induced a ~5-fold increase in inward currents upon activation by cold compared with wild-type hTRPA1 (Kremeyer et al., 2010). Thus, lipids bound inside of the intersubunit crevice might be directly involved in the activation by cold. In this context, the polymorphism mutation

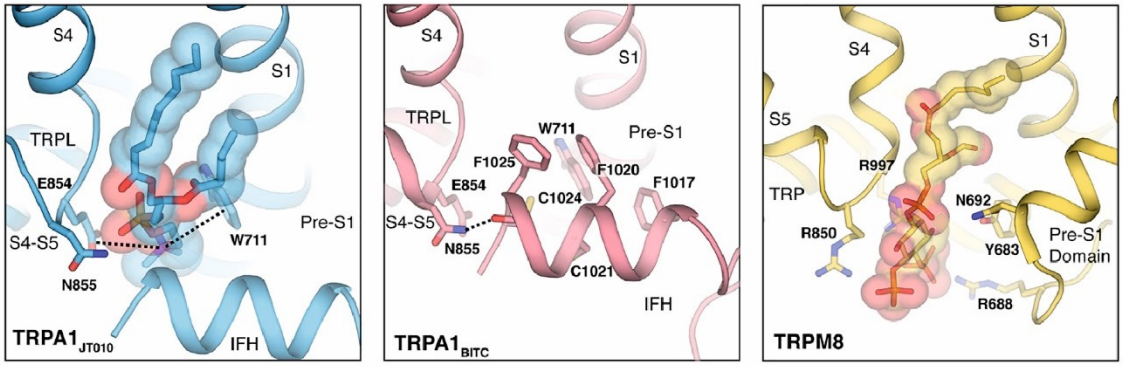

Figure 42: A close view of the interfacial cavity near the IFH. Left - *The phospholipid interacts with residues W711 in the pre-S1 and E854 in the loop connecting the S4 to the S4-S5 linker. The site of gain-of-function mutation N855 is also located at this interface.* ***Middle -*** *When the phospholipid is not present in the cavity, a direct interaction between the N855 and the backbone carbonyl of C1024 in the IFH is maintained. The aromatic residues W711, F1020 and F1025 fill the cavity.* ***Right -*** *In TRPM8, a molecule of PIP_2 is located in a position analogous to the interfacial cavity. Adapted from (Suo et al., 2020)*

H1018R studied in **publication VI** was found to play an important role in mediating the cold potentiation of carvacrol-induced responses, possibly by increasing the positive electrostatic potential that would ease the binding of PIP_2.

7.3 Regulation of the heat and cold dependence of TRPA1

The **publication VII** aimed at the comparison of human and mouse orthologues in terms of their temperature activation in order to elucidate the possibility of bidirectional temperature dependence of TRPA1 in both species. Our findings confirm that both human and mouse orthologues are activated by both cold and heat. The electrophysiological measurements indicate that both human and mouse orthologues exhibit qualitatively similar temperature- and voltage-dependent characteristics. The main difference between the orthologues may lie in the gating equilibrium, which is in mTRPA1 more shifted toward the open state. This shift in the gating equilibrium itself may account for the pronounced activation of mTRPA1 by both cold and heat. Our findings suggest a conserved molecular logic for the gating of TRPA1 across different species. According to available literature data, the majority of the TRPA1 orthologues are temperature sensitive with different thresholds. The species differences might lie not in the temperature- or voltage-sensing domains of TRPA1orthologues but rather in the mechanisms by which they are coupled to the channel gate and/or to each other.

Furthermore, human TRPA1 exhibits faster deactivation kinetics that consists of two exponential components, one of which has comparable temperature dependence as

mTRPA1. In cold-activated channels, the activation is driven by the steepness of the temperature dependence of the deactivation kinetics (as reviewed in (Voets, 2014)). The slower voltage-dependent relaxation kinetics seen in mTRPA1 and in some hTRPA1 mutants (S804D, S804N) allows these channels to dwell longer in the open state at cold temperature, producing persistent currents. These findings support the role of S804 and the VSLD as a whole in the transitions related to the channel's opening.

The excessive heat impairs the channel's voltage dependence. We cannot exclude the irreversible damage of a voltage sensor caused by excessive heat exposure. Most importantly, we have revealed a specific 'heat-induced cold sensitivity' mode of TRPA1 activation. This transition occurs after the channels are activated simultaneously by depolarizing voltage and high noxious heat and then are subsequently repolarized to the resting membrane potential at cold temperatures. This effect was shown to be reversible by another application of heat at resting membrane potential. Our simulations predict that the concurrent activation of the voltage- and heat-sensors can induce a conformational switch that leads to an increase in their energetic crosstalk, an increase in the gating equilibrium constant, and a drastic (~30,000-fold) decrease in the coupling of the voltage sensor to the channel gate. The channel becomes inward-rectifying, being opened by hyperpolarized voltage. Such effect was achieved by mutating the L906 in the first pore helix of mTRPA1 channel (corresponding to L903 in hTRPA1), creating an inward-rectifying phenotype with reduced sensitivity to TRPA1 inhibitor HC-030031 (Wan et al., 2014). The residue 903 is extremely sensitive to substitutions, thus, it is possible that the excessive heat and voltage would affect the arrangement of the pore helix. The pore helix is functionally interconnected with the S4-S5 linker, as they both undergo substantial transitions related to the channel gating.

An alternative explanation for the 'heat-induced cold sensitivity' phenomenon is an involvement of lipids, particularly the "lipid 5" residing above the S4-S5 linker in between of the subunits. The thermal displacement of the PIP_2 at the identical position in related TRPV1 channel was proposed as a mechanism of channel opening (Gao et al., 2016). In TRPA1, the E864W mutation that would clash with the residing lipid 5 resulted in a constitutively-open channel (Liu et al., 2020). It is possible, that heating and/or depolarizing voltage could displace the lipid 5 from its position. The subsequent cooling to 5°C, while still resting at the +80 mV membrane potential, would prevent the re-entry of the lipid back to its binding site, leaving the channel open after the

subsequent repolarization to -70 mV. The lipid might then slowly diffuse back to its binding site, potentially explaining why the additional heating of the channels in the ‘heat-induced, cold sensitized’ state was capable of switching back the outward rectification.

Interestingly, in experiments described by (Moparthi et al., 2016), the cold potentiation of carvacrol-induced currents in hTRPA1 was observed only when channels were pre-exposed to warm temperatures. Thus, various sources of energy, such as these derived from agonist binding or depolarization, could drive the channel opening by cooling.

8. Conclusions

- The LF-EMF has an immediate and reversible potentiating effect on neuronal spontaneous activity. TRPA1 may contribute to the LF-EMF-induced changes in the excitability of sensory neurons. The exposure of F11 cells to LF-EMF reduces calcium transients in response to bradykinin.
- The phosphomimetic mutation S602D completely abrogated channel activation by voltage and agonists, while preserving its surface expression. We propose that the phosphorylation at S602 may dampen the channel through the cluster of residues F640, W605 and Y662.
- The presence of AKAP79/150 sensitizes the TRPA1 channel at basal membrane potentials. TRPA1 can interact with AKAP79/150 to prime the channel for opening.
- The conserved polar residues inside of the VSLD intracellular cavity are crucial determinants of the electrophilic, voltage, and calcium sensitivity of TRPA1. The cavity may comprise a binding site of membrane phosphoinositides that might regulate the TRPA1 channel in a Ca^{2+} and state-dependent manner.
- The TRPA1-derived peptides L992-N1008 and T1003-P1034 strongly interact with the lipid membrane only if PIP_2 is present. The mutation F1020G inside of the C-terminal IFH exhibits faster kinetics by altering the allosteric constant that couples voltage sensing to the pore opening. Mutation H1018R affects the cold sensitivity of TRPA1. We propose that both PIP_2 and Ca^{2+}/calmodulin complex may compete for the same C-terminal site of the TRPA1 channel.
- We demonstrate that both human and mouse TRPA1 are activated by both cold and heat. The orthologues differ in their kinetical components of their voltage-dependent gating. Both orthologues can be strongly activated by cold after the concurrent application of voltage and heat.

9. References

Alpizar YA, Gees M, Sanchez A, Apetrei A, Voets T, Nilius B, Talavera K (2013) Bimodal effects of cinnamaldehyde and camphor on mouse TRPA1. Pflügers Archiv: European Journal of Physiologyiv : European Journal of Physiology 465:853-864.

Alvarenga EM, Souza LK, Araujo TS, Nogueira KM, Sousa FB, Araujo AR, Martins CS, Pacifico DM, de CBGA, Souza EP, Sousa DP, Medeiros JV (2016) Carvacrol reduces irinotecan-induced intestinal mucositis through inhibition of inflammation and oxidative damage via TRPA1 receptor activation. Chemico-Biological Interactions 260:129-140.

Ambrosino P, Soldovieri MV, Russo C, Taglialatela M (2013) Activation and desensitization of TRPV1 channels in sensory neurons by the PPAR alpha agonist palmitoylethanolamide. British Journal of Pharmacology 168:1430-1444.

Andersson DA, Filipovic MR, Gentry C, Eberhardt M, Vastani N, Leffler A, Reeh P, Bevan S (2015) Streptozotocin Stimulates the Ion Channel TRPA1 Directly: INVOLVEMENT OF PEROXYNITRITE. Journal of Biological Chemistry 290:15185-15196.

Andersson DA, Gentry C, Moss S, Bevan S (2008) Transient receptor potential A1 is a sensory receptor for multiple products of oxidative stress. Journal of Neuroscience 28:2485-2494.

Andrade EL, Meotti FC, Calixto JB (2012) TRPA1 antagonists as potential analgesic drugs. Pharmacology and Therapeutics 133:189-204.

Andre E, Campi B, Materazzi S, Trevisani M, Amadesi S, Massi D, Creminon C, Vaksman N, Nassini R, Civelli M, Baraldi PG, Poole DP, Bunnett NW, Geppetti P, Patacchini R (2008) Cigarette smoke-induced neurogenic inflammation is mediated by alpha,beta-unsaturated aldehydes and the TRPA1 receptor in rodents. Journal of Clinical Investigation 118:2574-2582.

Arenas OM, Zaharieva EE, Para A, Vasquez-Doorman C, Petersen CP, Gallio M (2017) Activation of planarian TRPA1 by reactive oxygen species reveals a conserved mechanism for animal nociception. Nature Neuroscience 20:1686-1693.

Arrigoni C, Minor DL, Jr. (2018) Global versus local mechanisms of temperature sensing in ion channels. Pflügers Archiv: European Journal of Physiology 470:733-744.

Arrigoni C, Rohaim A, Shaya D, Findeisen F, Stein RA, Nurva SR, Mishra S, McHaourab HS, Minor DL, Jr. (2016) Unfolding of a Temperature-Sensitive Domain Controls Voltage-Gated Channel Activation. Cell 164:922-936.

Autzen HE, Myasnikov AG, Campbell MG, Asarnow D, Julius D, Cheng Y (2018) Structure of the human TRPM4 ion channel in a lipid nanodisc. Science 359:228-232.

Averbeck B, Rucker F, Laubender RP, Carr RW (2013) Thermal grill-evoked sensations of heat correlate with cold pain threshold and are enhanced by menthol and cinnamaldehyde. European Journal of Pain 17:724-734.

Bamps D, Vriens J, Hoon J, Voets T (2021) TRP Channel Cooperation for Nociception: Therapeutic Opportunities. Annual Review of Pharmacology and Toxicology 61:655-677.

Bandell M, Story GM, Hwang SW, Viswanath V, Eid SR, Petrus MJ, Earley TJ, Patapoutian A (2004) Noxious cold ion channel TRPA1 is activated by pungent compounds and bradykinin. Neuron 41:849-857.

Banzawa N, Saito S, Imagawa T, Kashio M, Takahashi K, Tominaga M, Ohta T (2014) Molecular basis determining inhibition/activation of nociceptive receptor TRPA1 protein: a single amino acid dictates species-specific actions of the most potent mammalian TRPA1 antagonist. Journal of Biological Chemistry 289:31927-31939.

Baraldi PG, Preti D, Materazzi S, Geppetti P (2010) Transient Receptor Potential Ankyrin 1 (TRPA1) Channel as Emerging Target for Novel Analgesics and Anti-Inflammatory Agents. Journal of Medicinal Chemistry 53:5085–5107.

Barvikova K, Barvik I, Sinica V, Zimova L, Vlachova V (2020) Phospho-Mimetic Mutation at Ser602 Inactivates Human TRPA1 Channel. International Journal of Molecular Sciences 21:7995.

Bautista DM, Jordt SE, Nikai T, Tsuruda PR, Read AJ, Poblete J, Yamoah EN, Basbaum AI, Julius D (2006) TRPA1 mediates the inflammatory actions of environmental irritants and proalgesic agents. Cell 124:1269-1282.

Bautista DM, Siemens J, Glazer JM, Tsuruda PR, Basbaum AI, Stucky CL, Jordt SE, Julius D (2007) The menthol receptor TRPM8 is the principal detector of environmental cold. Nature 448:204-208.

Bianchi BR, Zhang XF, Reilly RM, Kym PR, Yao BB, Chen J (2012) Species comparison and pharmacological characterization of human, monkey, rat, and mouse TRPA1 channels. Journal of Pharmacology and Experimental Therapeutics 341:360-368.

Blair NT, Philipson BI, Richards PM, Doerner JF, Segura A, Silver WL, Clapham DE (2016) Naturally Produced Defensive Alkenal Compounds Activate TRPA1. Chemical Senses 41:281-292.

Brackley AD, Gomez R, Guerrero KA, Akopian AN, Glucksman MJ, Du J, Carlton SM, Jeske NA (2017) A-Kinase Anchoring Protein 79/150 Scaffolds Transient Receptor Potential A 1 Phosphorylation and Sensitization by Metabotropic Glutamate Receptor Activation. Scientific Reports 7:1842.

Brauchi S, Orta G, Salazar M, Rosenmann E, Latorre R (2006) A hot-sensing cold receptor: C-terminal domain determines thermosensation in transient receptor potential channels. Journal of Neuroscience 26:4835-4840.

Buijs TJ, McNaughton PA (2020) The Role of Cold-Sensitive Ion Channels in Peripheral Thermosensation. Frontiers in Cellular Neuroscience 14:262.

Caspani O, Heppenstall PA (2009) TRPA1 and cold transduction: an unresolved issue? Journal of General Physiology133:245-249.

Clapham DE, Miller C (2011) A thermodynamic framework for understanding temperature sensing by transient receptor potential (TRP) channels. Proceedings of the National Academy of Sciences of the United States of America 108:19492-19497.

Cordero-Morales JF, Gracheva EO, Julius D (2011) Cytoplasmic ankyrin repeats of transient receptor potential A1 (TRPA1) dictate sensitivity to thermal and chemical stimuli. Proceedings of the National Academy of Sciences of the United States of America 108:E1184-1191.

Corey DP, Garcia-Anoveros J, Holt JR, Kwan KY, Lin SY, Vollrath MA, Amalfitano A, Cheung EL, Derfler BH, Duggan A, Geleoc GS, Gray PA, Hoffman MP, Rehm HL, Tamasauskas D, Zhang DS (2004) TRPA1 is a candidate for the

mechanosensitive transduction channel of vertebrate hair cells. Nature 432:723-730.
Cui Y, Liu X, Yang T, Mei YA, Hu C (2014) Exposure to extremely low-frequency electromagnetic fields inhibits T-type calcium channels via AA/LTE4 signaling pathway. Cell Calcium 55:48-58.
Cvetkov TL, Huynh KW, Cohen MR, Moiseenkova-Bell VY (2011) Molecular architecture and subunit organization of TRPA1 ion channel revealed by electron microscopy. Journal of Biological Chemistry 286:38168-38176.
Deering-Rice CE, Shapiro D, Romero EG, Stockmann C, Bevans TS, Phan QM, Stone BL, Fassl B, Nkoy F, Uchida DA, Ward RM, Veranth JM, Reilly CA (2015) Activation of Transient Receptor Potential Ankyrin-1 by Insoluble Particulate Material and Association with Asthma. American Journal of Respiratory Cell and Molecular Biology 53:893-901.
del Camino D, Murphy S, Heiry M, Barrett LB, Earley TJ, Cook CA, Petrus MJ, Zhao M, D'Amours M, Deering N, Brenner GJ, Costigan M, Hayward NJ, Chong JA, Fanger CM, Woolf CJ, Patapoutian A, Moran MM (2010) TRPA1 contributes to cold hypersensitivity. Journal of Neuroscience 30:15165-15174.
Diaz-Franulic I, Raddatz N, Castillo K, Gonzalez-Nilo FD, Latorre R (2020) A folding reaction at the C-terminal domain drives temperature sensing in TRPM8 channels. Proceedings of the National Academy of Sciences of the United States of America 117:20298-20304.
Dittert I, Benedikt J, Vyklicky L, Zimmermann K, Reeh PW, Vlachova V (2006) Improved superfusion technique for rapid cooling or heating of cultured cells under patch-clamp conditions. Journal of Neuroscience Methods 151:178-185.
Diver MM, Cheng Y, Julius D (2019) Structural insights into TRPM8 inhibition and desensitization. Science 365:1434-1440.
Duan J, Li J, Chen GL, Ge Y, Liu J, Xie K, Peng X, Zhou W, Zhong J, Zhang Y, Xu J, Xue C, Liang B, Zhu L, Liu W, Zhang C, Tian XL, Wang J, Clapham DE, Zeng B, Li Z, Zhang J (2019) Cryo-EM structure of TRPC5 at 2.8-A resolution reveals unique and conserved structural elements essential for channel function. Science Advances 5:eaaw7935.
Duan J, Li J, Zeng B, Chen GL, Peng X, Zhang Y, Wang J, Clapham DE, Li Z, Zhang J (2018) Structure of the mouse TRPC4 ion channel. Nature Communications 9:3102.
Egan TJ, Acuna MA, Zenobi-Wong M, Zeilhofer HU, Urech D (2016) Effects of N-Glycosylation of the human cation channel TRPA1 on agonist-sensitivity. Bioscience Reports 36:e00390.
Fujita F, Moriyama T, Higashi T, Shima A, Tominaga M (2007) Methyl p-hydroxybenzoate causes pain sensation through activation of TRPA1 channels. British Journal of Pharmacology 151:153-160.
Gao Y, Cao E, Julius D, Cheng Y (2016) TRPV1 structures in nanodiscs reveal mechanisms of ligand and lipid action. Nature 534:347-51.
Garcia-Sanz N, Valente P, Gomis A, Fernandez-Carvajal A, Fernandez-Ballester G, Viana F, Belmonte C, Ferrer-Montiel A (2007) A role of the transient receptor potential domain of vanilloid receptor I in channel gating. Journal of Neuroscience 27:11641-11650.
Gaudet R (2008) A primer on ankyrin repeat function in TRP channels and beyond. Molecular BioSystems 4:372-379.
Gentry C, Andersson DA, Bevan S (2015) TRPA1 mediates the hypothermic action of acetaminophen. Scientific Reports 5:12771.

Ghosh M, Schepetkin IA, Ozek G, Ozek T, Khlebnikov AI, Damron DS, Quinn MT (2020) Essential Oils from Monarda fistulosa: Chemical Composition and Activation of Transient Receptor Potential A1 (TRPA1) Channels. Molecules 25:4873.

Giorgi S, Nikolaeva-Koleva M, Alarcon-Alarcon D, Butron L, Gonzalez-Rodriguez S (2019) Is TRPA1 Burning Down TRPV1 as Druggable Target for the Treatment of Chronic Pain? International Journal of Molecular Sciences 20:2906.

Gracheva EO, Cordero-Morales JF, Gonzalez-Carcacia JA, Ingolia NT, Manno C, Aranguren CI, Weissman JS, Julius D (2011) Ganglion-specific splicing of TRPV1 underlies infrared sensation in vampire bats. Nature 476:88-91.

Gracheva EO, Ingolia NT, Kelly YM, Cordero-Morales JF, Hollopeter G, Chesler AT, Sanchez EE, Perez JC, Weissman JS, Julius D (2010) Molecular basis of infrared detection by snakes. Nature 464:1006-1011.

Grandl J, Kim SE, Uzzell V, Bursulaya B, Petrus M, Bandell M, Patapoutian A (2010) Temperature-induced opening of TRPV1 ion channel is stabilized by the pore domain. Nature Neuroscience 13:708-714.

Grieben M, Pike AC, Shintre CA, Venturi E, El-Ajouz S, Tessitore A, Shrestha L, Mukhopadhyay S, Mahajan P, Chalk R, Burgess-Brown NA, Sitsapesan R, Huiskonen JT, Carpenter EP (2017) Structure of the polycystic kidney disease TRP channel Polycystin-2 (PC2). Nature Structural & Molecular Biology 24:114-122.

Gupta R, Saito S, Mori Y, Itoh SG, Okumura H, Tominaga M (2016) Structural basis of TRPA1 inhibition by HC-030031 utilizing species-specific differences. Scientific Reports 6:37460.

Hall BE, Prochazkova M, Sapio MR, Minetos P, Kurochkina N, Binukumar BK, Amin ND, Terse A, Joseph J, Raithel SJ, Mannes AJ, Pant HC, Chung MK, Iadarola MJ, Kulkarni AB (2018) Phosphorylation of the Transient Receptor Potential Ankyrin 1 by Cyclin-dependent Kinase 5 affects Chemo-nociception. Scientific Reports 8:1177.

Hamada FN, Rosenzweig M, Kang K, Pulver SR, Ghezzi A, Jegla TJ, Garrity PA (2008) An internal thermal sensor controlling temperature preference in Drosophila. Nature 454:217-220.

Hasan R, Leeson-Payne AT, Jaggar JH, Zhang X (2017) Calmodulin is responsible for Ca2+-dependent regulation of TRPA1 Channels. Scientific Reports 7:45098.

Hill K, Schaefer M (2007) TRPA1 is differentially modulated by the amphipathic molecules trinitrophenol and chlorpromazine. Journal of Biological Chemistry 282:7145-7153.

Hinman A, Chuang HH, Bautista DM, Julius D (2006) TRP channel activation by reversible covalent modification. Proceedings of the National Academy of Sciences of the United States of America 103:19564-19568.

Hoffmann T, Kistner K, Miermeister F, Winkelmann R, Wittmann J, Fischer MJ, Weidner C, Reeh PW (2013) TRPA1 and TRPV1 are differentially involved in heat nociception of mice. European Journal of Pain 17:1472-1482.

Hoffstaetter LJ, Bagriantsev SN, Gracheva EO (2018) TRPs et al.: a molecular toolkit for thermosensory adaptations. Pflügers Archiv: European Journal of Physiologyiv : European Journal of Physiology 470:745-759.

Hu H, Bandell M, Petrus MJ, Zhu MX, Patapoutian A (2009) Zinc activates damage-sensing TRPA1 ion channels. Nature Chemical Biology 5:183-190.

Huang Y, Roth B, Lu W, Du J (2019) Ligand recognition and gating mechanism through three ligand-binding sites of human TRPM2 channel. eLife 8:e50175.

Huang Y, Winkler PA, Sun W, Lu W, Du J (2018) Architecture of the TRPM2 channel and its activation mechanism by ADP-ribose and calcium. Nature 562:145-149.
Huffer KE, Aleksandrova AA, Jara-Oseguera A, Forrest LR, Swartz KJ (2020) Global alignment and assessment of TRP channel transmembrane domain structures to explore functional mechanisms. eLife 9:e58660.
Humphrey W, Dalke A, Schulten K (1996) VMD: Visual molecular dynamics. Journal of Molecular Graphics 14:33-38.
Huynh KW, Cohen MR, Jiang J, Samanta A, Lodowski DT, Zhou ZH, Moiseenkova-Bell VY (2016) Structure of the full-length TRPV2 channel by cryo-EM. Nature Communications 7:11130.
Hynkova A, Marsakova L, Vaskova J, Vlachova V (2016) N-terminal tetrapeptide T/SPLH motifs contribute to multimodal activation of human TRPA1 channel. Scientific Reports 6:28700.
Chatzigeorgiou M, Yoo S, Watson JD, Lee WH, Spencer WC, Kindt KS, Hwang SW, Miller DM, 3rd, Treinin M, Driscoll M, Schafer WR (2010) Specific roles for DEG/ENaC and TRP channels in touch and thermosensation in C. elegans nociceptors. Nature Neuroscience 13:861-868.
Chen J, Joshi SK, DiDomenico S, Perner RJ, Mikusa JP, Gauvin DM, Segreti JA, Han P, Zhang XF, Niforatos W, Bianchi BR, Baker SJ, Zhong C, Simler GH, McDonald HA, Schmidt RG, McGaraughty SP, Chu KL, Faltynek CR, Kort ME, Reilly RM, Kym PR (2011) Selective blockade of TRPA1 channel attenuates pathological pain without altering noxious cold sensation or body temperature regulation. Pain 152:1165-1172.
Chen J, Kang D, Xu J, Lake M, Hogan JO, Sun C, Walter K, Yao B, Kim D (2013) Species differences and molecular determinant of TRPA1 cold sensitivity. Nature Communications 4:2501.
Chernov-Rogan T, Gianti E, Liu C, Villemure E, Cridland AP, Hu X, Ballini E, Lange W, Deisemann H, Li T, Ward SI, Hackos DH, Magnuson S, Safina B, Klein ML, Volgraf M, Carnevale V, Chen J (2019) TRPA1 modulation by piperidine carboxamides suggests an evolutionarily conserved binding site and gating mechanism. Proceedings of the National Academy of Sciences of the United States of America 116:26008-26019.
Chowdhury S, Jarecki BW, Chanda B (2014) A molecular framework for temperature-dependent gating of ion channels. Cell 158:1148-1158.
Christensen AP, Akyuz N, Corey DP (2016) The Outer Pore and Selectivity Filter of TRPA1. PLoS One 11:e0166167.
Jabba S, Goyal R, Sosa-Pagan JO, Moldenhauer H, Wu J, Kalmeta B, Bandell M, Latorre R, Patapoutian A, Grandl J (2014) Directionality of temperature activation in mouse TRPA1 ion channel can be inverted by single-point mutations in ankyrin repeat six. Neuron 82:1017-1031.
Jaquemar D, Schenker T, Trueb B (1999) An ankyrin-like protein with transmembrane domains is specifically lost after oncogenic transformation of human fibroblasts. Journal of Biological Chemistry 274:7325-7333.
Jara-Oseguera A, Islas LD (2013) The role of allosteric coupling on thermal activation of thermo-TRP channels. Biophysical Journal 104:2160-2169.
Jiang Y, Ruta V, Chen J, Lee A, MacKinnon R (2003) The principle of gating charge movement in a voltage-dependent K+ channel. Nature 423:42-48.
Jordt SE, Bautista DM, Chuang HH, McKemy DD, Zygmunt PM, Hogestatt ED, Meng ID, Julius D (2004) Mustard oils and cannabinoids excite sensory nerve fibres through the TRP channel ANKTM1. Nature 427:260-265.

Kang K, Pulver SR, Panzano VC, Chang EC, Griffith LC, Theobald DL, Garrity PA (2010) Analysis of Drosophila TRPA1 reveals an ancient origin for human chemical nociception. Nature 464:597-600.

Karashima Y, Damann N, Prenen J, Talavera K, Segal A, Voets T, Nilius B (2007) Bimodal action of menthol on the transient receptor potential channel TRPA1. Journal of Neuroscience 27:9874-9884.

Karashima Y, Prenen J, Meseguer V, Owsianik G, Voets T, Nilius B (2008) Modulation of the transient receptor potential channel TRPA1 by phosphatidylinositol 4,5-biphosphate manipulators. Pflügers Archiv: European Journal of Physiology 457:77-89.

Karashima Y, Talavera K, Everaerts W, Janssens A, Kwan KY, Vennekens R, Nilius B, Voets T (2009) TRPA1 acts as a cold sensor in vitro and in vivo. Proceedings of the National Academy of Sciences of the United States of America 106:1273-1278.

Kerstein PC, del Camino D, Moran MM, Stucky CL (2009) Pharmacological blockade of TRPA1 inhibits mechanical firing in nociceptors. Molecular Pain 5:19.

Khedr EM, Ahmed MA, Alkady EA, Mostafa MG, Said HG (2012) Therapeutic effects of peripheral magnetic stimulation on traumatic brachial plexopathy: clinical and neurophysiological study. Neurophysiologie Clinique 42:111-118.

Kim D, Cavanaugh EJ (2007) Requirement of a soluble intracellular factor for activation of transient receptor potential A1 by pungent chemicals: role of inorganic polyphosphates. Journal of Neuroscience 27:6500-6509.

Kim SE, Patapoutian A, Grandl J (2013) Single residues in the outer pore of TRPV1 and TRPV3 have temperature-dependent conformations. PLoS One 8:e59593.

Knowlton WM, Bifolck-Fisher A, Bautista DM, McKemy DD (2010) TRPM8, but not TRPA1, is required for neural and behavioral responses to acute noxious cold temperatures and cold-mimetics in vivo. Pain 150:340-350.

Kohno K, Sokabe T, Tominaga M, Kadowaki T (2010) Honey bee thermal/chemical sensor, AmHsTRPA, reveals neofunctionalization and loss of transient receptor potential channel genes. Journal of Neuroscience 30:12219-12229.

Kremeyer B, Lopera F, Cox JJ, Momin A, Rugiero F, Marsh S, Woods CG, Jones NG, Paterson KJ, Fricker FR, Villegas A, Acosta N, Pineda-Trujillo NG, Ramirez JD, Zea J, Burley MW, Bedoya G, Bennett DL, Wood JN, Ruiz-Linares A (2010) A gain-of-function mutation in TRPA1 causes familial episodic pain syndrome. Neuron 66:671-680.

Kurganov E, Tominaga M (2017) Dependence of heat-evoked TRPA1 activation on extracellular Ca(2). Channels (Austin) 11:271-272.

Kwan KY, Allchorne AJ, Vollrath MA, Christensen AP, Zhang DS, Woolf CJ, Corey DP (2006) TRPA1 contributes to cold, mechanical, and chemical nociception but is not essential for hair-cell transduction. Neuron 50:277-289.

Lata S, Sharma BK, Raghava GP (2007) Analysis and prediction of antibacterial peptides. BMC Bioinformatics 8:263.

Laursen WJ, Bagriantsev SN, Gracheva EO (2014) TRPA1 channels: chemical and temperature sensitivity. Current Topics in Membranes 74:89-112.

Laursen WJ, Schneider ER, Merriman DK, Bagriantsev SN, Gracheva EO (2016) Low-cost functional plasticity of TRPV1 supports heat tolerance in squirrels and camels. Proceedings of the National Academy of Sciences of the United States of America 113:11342-11347.

Lee SP, Buber MT, Yang Q, Cerne R, Cortes RY, Sprous DG, Bryant RW (2008) Thymol and related alkyl phenols activate the hTRPA1 channel. British Journal of Pharmacology 153:1739-1749.
Leffler A, Lattrell A, Kronewald S, Niedermirtl F, Nau C (2011) Activation of TRPA1 by membrane permeable local anesthetics. Molecular Pain 7:62.
Lewit-Bentley A, Rety S (2000) EF-hand calcium-binding proteins. Current Opinion in Structural Biology 10:637-643.
Liao M, Cao E, Julius D, Cheng Y (2013) Structure of the TRPV1 ion channel determined by electron cryo-microscopy. Nature 504:107-112.
Lin King JV, Emrick JJ, Kelly MJS, Herzig V, King GF, Medzihradszky KF, Julius D (2019) A Cell-Penetrating Scorpion Toxin Enables Mode-Specific Modulation of TRPA1 and Pain. Cell 178:1362-1374 e1316.
Liu B, Qin F (2017) Single-residue molecular switch for high-temperature dependence of vanilloid receptor TRPV3. Proceedings of the National Academy of Sciences of the United States of America 114:1589-1594.
Liu C, Reese R, Vu S, Rouge L, Shields SD, Kakiuchi-Kiyota S, Chen H, Johnson K, Shi YP, Chernov-Rogan T, Greiner DMZ, Kohli PB, Hackos D, Brillantes B, Tam C, Li T, Wang J, Safina B, Magnuson S, Volgraf M, Payandeh J, Zheng J, Rohou A, Chen J (2020) A Non-covalent Ligand Reveals Biased Agonism of the TRPA1 Ion Channel. Neuron 109:273-284.e4.
Lo YL, Fook-Chong S, Huerto AP, George JM (2011) A randomized, placebo-controlled trial of repetitive spinal magnetic stimulation in lumbosacral spondylotic pain. Pain Medicine 12:1041-1045.
Macikova L, Sinica V, Kadkova A, Villette S, Ciaccafava A, Faherty J, Lecomte S, Alves ID, Vlachova V (2019) Putative interaction site for membrane phospholipids controls activation of TRPA1 channel at physiological membrane potentials. The FEBS Journal 286:3664-3683.
Macpherson LJ, Dubin AE, Evans MJ, Marr F, Schultz PG, Cravatt BF, Patapoutian A (2007) Noxious compounds activate TRPA1 ion channels through covalent modification of cysteines. Nature 445:541-545.
Macpherson LJ, Geierstanger BH, Viswanath V, Bandell M, Eid SR, Hwang S, Patapoutian A (2005) The pungency of garlic: activation of TRPA1 and TRPV1 in response to allicin. Current Biology 15:929-934.
Maggi CA, Patacchini R, Santicioli P, Giuliani S, Geppetti P, Meli A (1988) Protective action of ruthenium red toward capsaicin desensitization of sensory fibers. Neuroscience Letters 88:201-205.
Marone IM, De Logu F, Nassini R, De Carvalho Goncalves M, Benemei S, Ferreira J, Jain P, Li Puma S, Bunnett NW, Geppetti P, Materazzi S (2018) TRPA1/NOX in the soma of trigeminal ganglion neurons mediates migraine-related pain of glyceryl trinitrate in mice. Brain : A Journal of Neurology 141:2312-2328.
Marsakova L, Barvik I, Zima V, Zimova L, Vlachova V (2017) The First Extracellular Linker Is Important for Several Aspects of the Gating Mechanism of Human TRPA1 Channel. Frontiers in Molecular Neuroscience 10:16.
Martinez GQ, Gordon SE (2019) Multimerization of Homo sapiens TRPA1 ion channel cytoplasmic domains. PLoS One 14:e0207835.
Masse-Alarie H, Beaulieu LD, Preuss R, Schneider C (2017) Repetitive peripheral magnetic neurostimulation of multifidus muscles combined with motor training influences spine motor control and chronic low back pain. Clinical Neurophysiology 128:442-453.

Matta JA, Ahern GP (2007) Voltage is a partial activator of rat thermosensitive TRP channels. The Journal of Physiology 585:469-482.
McNamara CR, Mandel-Brehm J, Bautista DM, Siemens J, Deranian KL, Zhao M, Hayward NJ, Chong JA, Julius D, Moran MM, Fanger CM (2007) TRPA1 mediates formalin-induced pain. Proceedings of the National Academy of Sciences of the United States of America 104:13525-13530.
Meents JE, Fischer MJ, McNaughton PA (2016) Agonist-induced sensitisation of the irritant receptor ion channel TRPA1. The Journal of Physiology 594:6643-6660.
Meents JE, Fischer MJ, McNaughton PA (2017) Sensitization of TRPA1 by Protein Kinase A. PLoS One 12:e0170097.
Melnick C, Kaviany M (2018) Thermal actuation in TRPV1: Role of embedded lipids and intracellular domains. Journal of Theoretical Biology 444:38-49.
Mendes P, Hoops S, Sahle S, Gauges R, Dada J, Kummer U (2009) Computational modeling of biochemical networks using COPASI. Methods in Molecular Biology 500:17-59.
Meseguer V, Alpizar YA, Luis E, Tajada S, Denlinger B, Fajardo O, Manenschijn JA, Fernandez-Pena C, Talavera A, Kichko T, Navia B, Sanchez A, Senaris R, Reeh P, Perez-Garcia MT, Lopez-Lopez JR, Voets T, Belmonte C, Talavera K, Viana F (2014) TRPA1 channels mediate acute neurogenic inflammation and pain produced by bacterial endotoxins. Nature Communications 5:3125.
Miyake T, Nakamura S, Zhao M, So K, Inoue K, Numata T, Takahashi N, Shirakawa H, Mori Y, Nakagawa T, Kaneko S (2016) Cold sensitivity of TRPA1 is unveiled by the prolyl hydroxylation blockade-induced sensitization to ROS. Nature Communications 7:12840.
Moparthi L, Kichko TI, Eberhardt M, Hogestatt ED, Kjellbom P, Johanson U, Reeh PW, Leffler A, Filipovic MR, Zygmunt PM (2016) Human TRPA1 is a heat sensor displaying intrinsic U-shaped thermosensitivity. Scientific Reports 6:28763.
Moparthi L, Kjellstrom S, Kjellbom P, Filipovic MR, Zygmunt PM, Johanson U (2020a) Electrophile-Induced Conformational Switch of the Human TRPA1 Ion Channel Detected by Mass Spectrometry. International Journal of Molecular Sciences 21:6667.
Moparthi L, Moparthi SB, Wenger J, Zygmunt PM (2020b) Calcium activates purified human TRPA1 with and without its N-terminal ankyrin repeat domain in the absence of calmodulin. Cell Calcium 90:102228.
Moparthi L, Survery S, Kreir M, Simonsen C, Kjellbom P, Hogestatt ED, Johanson U, Zygmunt PM (2014) Human TRPA1 is intrinsically cold- and chemosensitive with and without its N-terminal ankyrin repeat domain. Proceedings of the National Academy of Sciences of the United States of America 111:16901-16906.
Moparthi L, Zygmunt PM (2020) Human TRPA1 is an inherently mechanosensitive bilayer-gated ion channel. Cell Calcium 91:102255.
Morgan K, Sadofsky LR, Crow C, Morice AH (2014) Human TRPM8 and TRPA1 pain channels, including a gene variant with increased sensitivity to agonists (TRPA1 R797T), exhibit differential regulation by SRC-tyrosine kinase inhibitor. Bioscience Reports 34:e00131.
Nagatomo K, Ishii H, Yamamoto T, Nakajo K, Kubo Y (2010) The Met268Pro mutation of mouse TRPA1 changes the effect of caffeine from activation to suppression. Biophysical Journal 99:3609-3618.

Nagatomo K, Kubo Y (2008) Caffeine activates mouse TRPA1 channels but suppresses human TRPA1 channels. Proceedings of the National Academy of Sciences of the United States of America 105:17373-17378.

Namer B, Seifert F, Handwerker HO, Maihofner C (2005) TRPA1 and TRPM8 activation in humans: effects of cinnamaldehyde and menthol. NeuroReport 16:955-959.

Nassini R, Gees M, Harrison S, De Siena G, Materazzi S, Moretto N, Failli P, Preti D, Marchetti N, Cavazzini A, Mancini F, Pedretti P, Nilius B, Patacchini R, Geppetti P (2011) Oxaliplatin elicits mechanical and cold allodynia in rodents via TRPA1 receptor stimulation. Pain 152:1621-1631.

Nativi C, Gualdani R, Dragoni E, Di Cesare Mannelli L, Sostegni S, Norcini M, Gabrielli G, la Marca G, Richichi B, Francesconi O, Moncelli MR, Ghelardini C, Roelens S (2013) A TRPA1 antagonist reverts oxaliplatin-induced neuropathic pain. Scientific Reports 3:2005.

Nilius B, Talavera K, Owsianik G, Prenen J, Droogmans G, Voets T (2005) Gating of TRP channels: a voltage connection? The Journal of Physiology 567:35-44.

Obata K, Katsura H, Mizushima T, Yamanaka H, Kobayashi K, Dai Y, Fukuoka T, Tokunaga A, Tominaga M, Noguchi K (2005) TRPA1 induced in sensory neurons contributes to cold hyperalgesia after inflammation and nerve injury. Journal of Clinical Investigation 115:2393-2401.

Oda M, Kubo Y, Saitoh O (2018) Sensitivity of Takifugu TRPA1 to thermal stimulations analyzed in oocytes expression system. Neuroreport 29:280-285.

Oda M, Saito K, Hatta S, Kubo Y, Saitoh O (2017) Chemical and thermal sensitivity of medaka TRPA1 analyzed in heterologous expression system. Biochemical and Biophysical Research Communications 494:194-201.

Ongaro A, Varani K, Masieri FF, Pellati A, Massari L, Cadossi R, Vincenzi F, Borea PA, Fini M, Caruso A, De Mattei M (2012) Electromagnetic fields (EMFs) and adenosine receptors modulate prostaglandin E(2) and cytokine release in human osteoarthritic synovial fibroblasts. Journal of Cellular Physiology 227:2461-2469.

Palovcak E, Delemotte L, Klein ML, Carnevale V (2015) Comparative sequence analysis suggests a conserved gating mechanism for TRP channels. Journal of General Physiology146:37-50.

Park JH, Chae J, Roh K, Kil EJ, Lee M, Auh CK, Lee MA, Yeom CH, Lee S (2015) Oxaliplatin-Induced Peripheral Neuropathy via TRPA1 Stimulation in Mice Dorsal Root Ganglion Is Correlated with Aluminum Accumulation. PLoS One 10:e0124875.

Patil MJ, Salas M, Bialuhin S, Boyd JT, Jeske NA, Akopian AN (2020) Sensitization of small-diameter sensory neurons is controlled by TRPV1 and TRPA1 association. FASEB Journal 34:287-302.

Paulsen CE, Armache JP, Gao Y, Cheng Y, Julius D (2015) Structure of the TRPA1 ion channel suggests regulatory mechanisms. Nature 520:511-517.

Petho G, Reeh PW (2012) Sensory and signaling mechanisms of bradykinin, eicosanoids, platelet-activating factor, and nitric oxide in peripheral nociceptors. Physiological Reviews 92:1699-1775.

Pettersen EF, Goddard TD, Huang CC, Couch GS, Greenblatt DM, Meng EC, Ferrin TE (2004) UCSF Chimera--a visualization system for exploratory research and analysis. Journal of Computational Chemistry 25:1605-1612.

Phillips JC, Braun R, Wang W, Gumbart J, Tajkhorshid E, Villa E, Chipot C, Skeel RD, Kale L, Schulten K (2005) Scalable molecular dynamics with NAMD. Journal of Computational Chemistry 26:1781-1802.

Piacentini R, Ripoli C, Mezzogori D, Azzena GB, Grassi C (2008) Extremely low-frequency electromagnetic fields promote in vitro neurogenesis via upregulation of Ca(v)1-channel activity. Journal of Cellular Physiology 215:129-139.

Rech JC, Eckert WA, Maher MP, Banke T, Bhattacharya A, Wickenden AD (2010) Recent advances in the biology and medicinal chemistry of TRPA1. Future Medicinal Chemistry 2:843-858.

Rohacs T (2016) Phosphoinositide signaling in somatosensory neurons. Advances in Biological Regulation 61:2-16.

Rohacs T, Lopes CM, Michailidis I, Logothetis DE (2005) PI(4,5)P(2) regulates the activation and desensitization of TRPM8 channels through the TRP domain. Nature Neuroscience 8:626-634.

Rossini PM, Burke D, Chen R, Cohen LG, Daskalakis Z, Di Iorio R, Di Lazzaro V, Ferreri F, Fitzgerald PB, George MS, Hallett M, Lefaucheur JP, Langguth B, Matsumoto H, Miniussi C, Nitsche MA, Pascual-Leone A, Paulus W, Rossi S, Rothwell JC, Siebner HR, Ugawa Y, Walsh V, Ziemann U (2015) Non-invasive electrical and magnetic stimulation of the brain, spinal cord, roots and peripheral nerves: Basic principles and procedures for routine clinical and research application. An updated report from an I.F.C.N. Committee. Clinical Neurophysiology 126:1071-1107.

Ryckaert JP, Ciccotti G, Berendsen HJC (1977) Numerical Integration of the Cartesian Equations of Motion of a System with Constraints: Molecular Dynamics of n-Alkanes. Journal of Computational Physics 23:327-341.

Saito S, Nakatsuka K, Takahashi K, Fukuta N, Imagawa T, Ohta T, Tominaga M (2012) Analysis of transient receptor potential ankyrin 1 (TRPA1) in frogs and lizards illuminates both nociceptive heat and chemical sensitivities and coexpression with TRP vanilloid 1 (TRPV1) in ancestral vertebrates. Journal of Biological Chemistry 287:30743-30754.

Saito S, Ohkita M, Saito CT, Takahashi K, Tominaga M, Ohta T (2016) Evolution of Heat Sensors Drove Shifts in Thermosensation between Xenopus Species Adapted to Different Thermal Niches. Journal of Biological Chemistry 291:11446-11459.

Saito S, Tominaga M (2017) Evolutionary tuning of TRPA1 and TRPV1 thermal and chemical sensitivity in vertebrates. Temperature 4:141-152.

Samad A, Sura L, Benedikt J, Ettrich R, Minofar B, Teisinger J, Vlachova V (2011) The C-terminal basic residues contribute to the chemical- and voltage-dependent activation of TRPA1. Biochemical Journal 433:197-204.

Samanta A, Kiselar J, Pumroy RA, Han S, Moiseenkova-Bell VY (2018) Structural insights into the molecular mechanism of mouse TRPA1 activation and inhibition. Journal of General Physiology150:751-762.

Savage SR, Zhang B (2020) Using phosphoproteomics data to understand cellular signaling: a comprehensive guide to bioinformatics resources. Clinical Proteomics 17:27.

Sawada Y, Hosokawa H, Hori A, Matsumura K, Kobayashi S (2007) Cold sensitivity of recombinant TRPA1 channels. Brain Research 1160:39-46.

Sawada Y, Hosokawa H, Matsumura K, Kobayashi S (2008) Activation of transient receptor potential ankyrin 1 by hydrogen peroxide. European Journal of Neuroscience 27:1131-1142.

Shen PS, Yang X, DeCaen PG, Liu X, Bulkley D, Clapham DE, Cao E (2016) The Structure of the Polycystic Kidney Disease Channel PKD2 in Lipid Nanodiscs. Cell 167:763-773 e711.

Shibukawa Y, Sato M, Kimura M, Sobhan U, Shimada M, Nishiyama A, Kawaguchi A, Soya M, Kuroda H, Katakura A, Ichinohe T, Tazaki M (2015) Odontoblasts as sensory receptors: transient receptor potential channels, pannexin-1, and ionotropic ATP receptors mediate intercellular odontoblast-neuron signal transduction. Pflügers Archiv: European Journal of Physiology 467:843-863.

Schlenkrich M, Brickmann J, MacKerell J, A. D., Karplus M (1996) An Empirical Potential Energy Function for Phospholipids: Criteria for Parameter Optimization and Applications In: Biological Membranes: A Molecular Perspective from Computation and Experiment(Roux, K. M. M. a. B., ed), pp 31-81 Boston Birkhauser

Schmidt M, Dubin AE, Petrus MJ, Earley TJ, Patapoutian A (2009) Nociceptive signals induce trafficking of TRPA1 to the plasma membrane. Neuron 64:498-509.

Singh AK, McGoldrick LL, Sobolevsky AI (2018) Structure and gating mechanism of the transient receptor potential channel TRPV3. Nature Structural & Molecular Biology 25:805-813.

Sinica V, Zimova L, Barvikova K, Macikova L, Barvik I, Vlachova V (2019) Human and Mouse TRPA1 Are Heat and Cold Sensors Differentially Tuned by Voltage. Cells 9:57.

Smania N, Corato E, Fiaschi A, Pietropoli P, Aglioti SM, Tinazzi M (2003) Therapeutic effects of peripheral repetitive magnetic stimulation on myofascial pain syndrome. Clinical Neurophysiology 114:350-358.

Soya M, Sato M, Sobhan U, Tsumura M, Ichinohe T, Tazaki M, Shibukawa Y (2014) Plasma membrane stretch activates transient receptor potential vanilloid and ankyrin channels in Merkel cells from hamster buccal mucosa. Cell Calcium 55:208-218.

Startek JB, Boonen B, Lopez-Requena A, Talavera A, Alpizar YA, Ghosh D, Van Ranst N, Nilius B, Voets T, Talavera K (2019a) Mouse TRPA1 function and membrane localization are modulated by direct interactions with cholesterol. eLife 8:e46084.

Startek JB, Boonen B, Talavera K, Meseguer V (2019b) TRP Channels as Sensors of Chemically-Induced Changes in Cell Membrane Mechanical Properties. International Journal of Molecular Sciences 20:371.

Startek JB, Talavera K, Voets T, Alpizar YA (2018) Differential interactions of bacterial lipopolysaccharides with lipid membranes: implications for TRPA1-mediated chemosensation. Scientific Reports 8:12010.

Story GM, Peier AM, Reeve AJ, Eid SR, Mosbacher J, Hricik TR, Earley TJ, Hergarden AC, Andersson DA, Hwang SW, McIntyre P, Jegla T, Bevan S, Patapoutian A (2003) ANKTM1, a TRP-like channel expressed in nociceptive neurons, is activated by cold temperatures. Cell 112:819-829.

Sulak MA, Ghosh M, Sinharoy P, Andrei SR, Damron DS (2018) Modulation of TRPA1 channel activity by Cdk5 in sensory neurons. Channels (Austin) 12:65-75.

Sun ZC, Ge JL, Guo B, Guo J, Hao M, Wu YC, Lin YA, La T, Yao PT, Mei YA, Feng Y, Xue L (2016) Extremely Low Frequency Electromagnetic Fields Facilitate Vesicle Endocytosis by Increasing Presynaptic Calcium Channel Expression at a Central Synapse. Scientific Reports 6:21774.

Suo Y, Wang Z, Zubcevic L, Hsu AL, He Q, Borgnia MJ, Ji RR, Lee SY (2020) Structural Insights into Electrophile Irritant Sensing by the Human TRPA1 Channel. Neuron 105:882-894 e885.

Sura L, Zima V, Marsakova L, Hynkova A, Barvik I, Vlachova V (2012) C-terminal acidic cluster is involved in Ca2+-induced regulation of human transient receptor potential ankyrin 1 channel. Journal of Biological Chemistry 287:18067-18077.

Survery S, Moparthi L, Kjellbom P, Hogestatt ED, Zygmunt PM, Johanson U (2016) The N-terminal Ankyrin Repeat Domain Is Not Required for Electrophile and Heat Activation of the Purified Mosquito TRPA1 Receptor. Journal of Biological Chemistry 291:26899-26912.

Takahashi N, Kuwaki T, Kiyonaka S, Numata T, Kozai D, Mizuno Y, Yamamoto S, Naito S, Knevels E, Carmeliet P, Oga T, Kaneko S, Suga S, Nokami T, Yoshida J, Mori Y (2011) TRPA1 underlies a sensing mechanism for O2. Nature Chemical Biology 7:701-711.

Takaya J, Mio K, Shiraishi T, Kurokawa T, Otsuka S, Mori Y, Uesugi M (2015) A Potent and Site-Selective Agonist of TRPA1. Journal of the American Chemical Society 137:15859-15864.

Talavera K, Gees M, Karashima Y, Meseguer VM, Vanoirbeek JA, Damann N, Everaerts W, Benoit M, Janssens A, Vennekens R, Viana F, Nemery B, Nilius B, Voets T (2009) Nicotine activates the chemosensory cation channel TRPA1. Nature Neuroscience 12:1293-1299.

Talavera K, Startek JB, Alvarez-Collazo J, Boonen B, Alpizar YA, Sanchez A, Naert R, Nilius B (2020) Mammalian Transient Receptor Potential TRPA1 Channels: From Structure to Disease. Physiological Reviews 100:725-803.

Taylor-Clark TE, Undem BJ, Macglashan DW, Jr., Ghatta S, Carr MJ, McAlexander MA (2008) Prostaglandin-induced activation of nociceptive neurons via direct interaction with transient receptor potential A1 (TRPA1). Molecular Pharmacology 73:274-281.

Ton HT, Phan TX, Abramyan AM, Shi L, Ahern GP (2017) Identification of a putative binding site critical for general anesthetic activation of TRPA1. Proceedings of the National Academy of Sciences of the United States of America 114:3762-3767.

Touska F, Winter Z, Mueller A, Vlachova V, Larsen J, Zimmermann K (2016) Comprehensive thermal preference phenotyping in mice using a novel automated circular gradient assay. Temperature 3:77-91.

Trevisani M, Siemens J, Materazzi S, Bautista DM, Nassini R, Campi B, Imamachi N, Andre E, Patacchini R, Cottrell GS, Gatti R, Basbaum AI, Bunnett NW, Julius D, Geppetti P (2007) 4-Hydroxynonenal, an endogenous aldehyde, causes pain and neurogenic inflammation through activation of the irritant receptor TRPA1. Proceedings of the National Academy of Sciences of the United States of America 104:13519-13524.

Tsai LH, Delalle I, Caviness VS, Chae T, Harlow E (1994) P35 Is a Neural-Specific Regulatory Subunit of Cyclin-Dependent Kinase-5. Nature 371:419-423.

Tsutsumi T, Kajiya H, Fukawa T, Sasaki M, Nemoto T, Tsuzuki T, Takahashi Y, Fujii S, Maeda H, Okabe K (2013) The potential role of transient receptor potential type A1 as a mechanoreceptor in human periodontal ligament cells. European Journal of Oral Sciences 121:538-544.

Vandewauw I, De Clercq K, Mulier M, Held K, Pinto S, Van Ranst N, Segal A, Voet T, Vennekens R, Zimmermann K, Vriens J, Voets T (2018) A TRP channel trio mediates acute noxious heat sensing. Nature 555:662-666.

Vandewauw I, Owsianik G, Voets T (2013) Systematic and quantitative mRNA expression analysis of TRP channel genes at the single trigeminal and dorsal root ganglion level in mouse. BMC Neuroscience 14:21.

Venkatachalam K, Montell C (2007) TRP channels. Annu Rev Biochem 76:387-417.

Vilceanu D, Stucky CL (2010) TRPA1 mediates mechanical currents in the plasma membrane of mouse sensory neurons. PLoS One 5:e12177.

Vlachova V, Teisinger J, Sušánková K, Lyfenko A, Ettrich R, Vyklicky L (2003) Functional role of C-terminal cytoplasmic tail of rat vanilloid receptor 1. Journal of Neuroscience 23:1340-1350.

Voets T (2014) TRP channels and thermosensation. Handbook of Experimental Pharmacology 223:729-741.

Wan X, Lu Y, Chen X, Xiong J, Zhou Y, Li P, Xia B, Li M, Zhu MX, Gao Z (2014) Bimodal voltage dependence of TRPA1: mutations of a key pore helix residue reveal strong intrinsic voltage-dependent inactivation. Pflügers Archiv: European Journal of Physiology 466:1273-1287.

Wang H, Schupp M, Zurborg S, Heppenstall PA (2013) Residues in the pore region of Drosophila transient receptor potential A1 dictate sensitivity to thermal stimuli. The Journal of Physiology 591:185-201.

Wang L, Fu TM, Zhou Y, Xia S, Greka A, Wu H (2018a) Structures and gating mechanism of human TRPM2. Science 362(6421):eaav4809.

Wang S, Kobayashi K, Kogure Y, Yamanaka H, Yamamoto S, Yagi H, Noguchi K, Dai Y (2018b) Negative Regulation of TRPA1 by AMPK in Primary Sensory Neurons as a Potential Mechanism of Painful Diabetic Neuropathy. Diabetes 67:98-109.

Wang S, Lee J, Ro JY, Chung MK (2012) Warmth suppresses and desensitizes damage-sensing ion channel TRPA1. Molecular Pain 8:22.

Wang YY, Chang RB, Allgood SD, Silver WL, Liman ER (2011) A TRPA1-dependent mechanism for the pungent sensation of weak acids. Journal of General Physiology 137:493-505.

Wang YY, Chang RB, Waters HN, McKemy DD, Liman ER (2008) The Nociceptor Ion Channel TRPA1 Is Potentiated and Inactivated by Permeating Calcium Ions. Journal of Biological Chemistry 283:32691-32703.

Wei H, Chapman H, Saarnilehto M, Kuokkanen K, Koivisto A, Pertovaara A (2010) Roles of cutaneous versus spinal TRPA1 channels in mechanical hypersensitivity in the diabetic or mustard oil-treated non-diabetic rat. Neuropharmacology 58:578-584.

Weng HJ, Patel KN, Jeske NA, Bierbower SM, Zou W, Tiwari V, Zheng Q, Tang Z, Mo GC, Wang Y, Geng Y, Zhang J, Guan Y, Akopian AN, Dong X (2015) Tmem100 Is a Regulator of TRPA1-TRPV1 Complex and Contributes to Persistent Pain. Neuron 85:833-846.

Wilkes M, Madej MG, Kreuter L, Rhinow D, Heinz V, De Sanctis S, Ruppel S, Richter RM, Joos F, Grieben M, Pike AC, Huiskonen JT, Carpenter EP, Kuhlbrandt W, Witzgall R, Ziegler C (2017) Molecular insights into lipid-assisted Ca(2+) regulation of the TRP channel Polycystin-2. Nature Structural & Molecular Biology 24:123-130.

Wilson SR, Nelson AM, Batia L, Morita T, Estandian D, Owens DM, Lumpkin EA, Bautista DM (2013) The ion channel TRPA1 is required for chronic itch. Journal of Neuroscience 33:9283-9294.

Winter Z, Gruschwitz P, Eger S, Touska F, Zimmermann K (2017) Cold Temperature Encoding by Cutaneous TRPA1 and TRPM8-Carrying Fibers in the Mouse. Frontiers of Molecular Neuroscience 10:209.

Witschas K, Jobin ML, Korkut DN, Vladan MM, Salgado G, Lecomte S, Vlachova V, Alves ID (2015) Interaction of a peptide derived from C-terminus of human TRPA1 channel with model membranes mimicking the inner leaflet of the plasma membrane. Biochimica et Biophysica Acta 1848:1147-1156.

Wu X, Indzhykulian AA, Niksch PD, Webber RM, Garcia-Gonzalez M, Watnick T, Zhou J, Vollrath MA, Corey DP (2016) Hair-Cell Mechanotransduction Persists in TRP Channel Knockout Mice. PLoS One 11:e0155577.

Xiao B, Dubin AE, Bursulaya B, Viswanath V, Jegla TJ, Patapoutian A (2008) Identification of transmembrane domain 5 as a critical molecular determinant of menthol sensitivity in mammalian TRPA1 channels. Journal of Neuroscience 28:9640-9651.

Xu H, Blair NT, Clapham DE (2005) Camphor activates and strongly desensitizes the transient receptor potential vanilloid subtype 1 channel in a vanilloid-independent mechanism. Journal of Neuroscience 25:8924-8937.

Xu H, Delling M, Jun JC, Clapham DE (2006) Oregano, thyme and clove-derived flavors and skin sensitizers activate specific TRP channels. Nature Neuroscience 9:628-635.

Yamaki S, Chau A, Gonzales L, McKemy DD (2020) Nociceptive afferent phenotyping reveals that transient receptor potential ankyrin 1 promotes cold pain through neurogenic inflammation upstream of the neurotrophic factor receptor GFRalpha3 and the menthol receptor transient receptor potential melastatin 8. Pain 162:609-618.

Yao J, Liu B, Qin F (2011) Modular thermal sensors in temperature-gated transient receptor potential (TRP) channels. Proceedings of the National Academy of Sciences of the United States of America 108:11109-11114.

Yin K, Baillie GJ, Vetter I (2016) Neuronal cell lines as model dorsal root ganglion neurons: A transcriptomic comparison. Molecular Pain 12:1744806916646111.

Yin Y, Le SC, Hsu AL, Borgnia MJ, Yang H, Lee SY (2019) Structural basis of cooling agent and lipid sensing by the cold-activated TRPM8 channel. Science 363:eaav9334.

Zayats V, Samad A, Minofar B, Roelofs KE, Stockner T, Ettrich R (2013) Regulation of the transient receptor potential channel TRPA1 by its N-terminal ankyrin repeat domain. Journal of Molecular Modeling 19:4689-4700.

Zhang W, Cheng LE, Kittelmann M, Li J, Petkovic M, Cheng T, Jin P, Guo Z, Gopfert MC, Jan LY, Jan YN (2015) Ankyrin Repeats Convey Force to Gate the NOMPC Mechanotransduction Channel. Cell 162:1391-1403.

Zhang X, Li L, McNaughton PA (2008) Proinflammatory mediators modulate the heat-activated ion channel TRPV1 via the scaffolding protein AKAP79/150. Neuron 59:450-461.

Zhang Z, Toth B, Szollosi A, Chen J, Csanady L (2018) Structure of a TRPM2 channel in complex with Ca(2+) explains unique gating regulation. eLife 7:e36409.

Zhao J, Lin King JV, Paulsen CE, Cheng Y, Julius D (2020) Irritant-evoked activation and calcium modulation of the TRPA1 receptor. Nature 585:141-145.

Zhong L, Bellemer A, Yan H, Ken H, Jessica R, Hwang RY, Pitt GS, Tracey WD (2012) Thermosensory and nonthermosensory isoforms of Drosophila melanogaster TRPA1 reveal heat-sensor domains of a thermoTRP Channel. Cell Reports 1:43-55.

Zimova L, Barvikova K, Macikova L, Vyklicka L, Sinica V, Barvik I, Vlachova V (2020) Proximal C-Terminus Serves as a Signaling Hub for TRPA1 Channel Regulation via Its Interacting Molecules and Supramolecular Complexes. Frontiers in Physiology 11:189.

Zimova L, Sinica V, Kadkova A, Vyklicka L, Zima V, Barvik I, Vlachova V (2018) Intracellular cavity of sensor domain controls allosteric gating of TRPA1 channel. Science Signaling 11:eaan8621.

Zubcevic L (2020) TRP Channels, Conformational Flexibility, and the Lipid Membrane. Journal of Membrane Biology 253:299-308.

Zubcevic L, Herzik MA, Jr., Chung BC, Liu Z, Lander GC, Lee SY (2016) Cryo-electron microscopy structure of the TRPV2 ion channel. Nature Structural & Molecular Biology 23:180-186.

Zubcevic L, Lee SY (2019) The role of pi-helices in TRP channel gating. Current Opinion in Structural Biology 58:314-323.

Zurborg S, Yurgionas B, Jira JA, Caspani O, Heppenstall PA (2007) Direct activation of the ion channel TRPA1 by Ca2+. Nature Neuroscience 10:277-279.

10. Appendix

Publication I	Acute exposure to high-induction electromagnetic field affects activity of model peripheral sensory neurons
Publication II	Molecular basis of TRPA1 regulation in nociceptive neurons. A review
Publication III	Phospho-Mimetic Mutation at Ser602 Inactivates Human TRPA1 Channel
Publication IV	Intracellular cavity of sensor domain controls allosteric gating of TRPA1 channel
Publication V	Putative interaction site for membrane phospholipids controls activation of TRPA1 channel at physiological membrane potentials
Publication VI	Proximal C-terminus serves as a signaling hub for TRPA1 channel regulation via its interacting molecules and supramolecular complexes
Publication VII	Human and mouse TRPA1 are heat and cold sensors differentially tuned by voltage
Publication VIII	Odontoblast TRPC5 channels signal cold pain in teeth